

# **Enzymes involved in biosynthesis and degradation of poly- $\alpha$ 2,8-sialic acid: structure-function relationships**

Vom Fachbereich Chemie der Universität Hannover  
zur Erlangung des Grades  
Doktorin der Naturwissenschaften  
(Dr. rer. nat.)  
genehmigte Dissertation

von

Dipl.-Biochem. Katharina Stummeyer  
geboren am 20. Dezember 1975 in Stadthagen

2004

Referentin: Prof. Dr. Rita Gerardy-Schahn  
Korreferent: Prof. Dr. Walter Müller  
Tag der Promotion: 08. Juni 2004

Schlagworte: Polysialinsäure, Polysialyltransferase, Endosialidase

Key words: polysialic acid, polysialyltransferase, endosialidase

---

<b>1</b>	<b>Zusammenfassung</b> .....	<b>1</b>
<b>2</b>	<b>Abstract</b> .....	<b>3</b>
<b>3</b>	<b>Introduction</b> .....	<b>4</b>
3.1	Polysialic acid .....	4
3.2	Polysialic acid in mammals.....	5
3.2.1	The Neural Cell Adhesion Molecule (NCAM) .....	5
3.2.2	Eukaryotic polysialyltransferases .....	8
3.3	Endoneuraminidases.....	11
3.4	Aims of the present study.....	15
<b>4</b>	<b>Materials and methods</b> .....	<b>16</b>
4.1	Materials.....	16
4.1.1	Cell lines.....	16
4.1.2	Bacterial strains .....	16
4.1.3	Plasmids.....	16
4.1.4	Oligonucleotides.....	18
4.1.5	Chromatography columns and media.....	18
4.1.6	Antibodies.....	19
4.1.7	Molecular weight markers.....	19
4.1.8	Chemicals .....	20
4.1.9	Culture media and additives .....	22
4.1.10	Standardbuffer and media.....	22
4.1.11	Enzymes .....	23
4.1.12	Laboratory equipment .....	23
4.1.13	Consumables and Kits .....	24
4.2	Molecular biological techniques .....	24
4.2.1	Analytical plasmid preparation.....	24
4.2.2	Preparative plasmid preparation .....	25
4.2.3	Agarose gel electrophoresis of DNA.....	25
4.2.4	Determination of DNA concentrations.....	26
4.2.5	Restriction digest of DNA.....	26
4.2.6	Dephosphorylation of DNA .....	26
4.2.7	Isolation of DNA fragments form agarose gels.....	26
4.2.8	Ligation of DNA.....	27
4.2.9	Preparation of CaCl <sub>2</sub> -competent <i>E. coli</i> .....	27
4.2.10	Transformation of competent <i>E. coli</i> .....	27
4.2.11	Polymerase chain reaction (PCR).....	28
4.2.12	Site-directed mutagenesis .....	28
4.3	Cell biological techniques .....	28

---

4.3.1	Cultivation of CHO cells.....	28
4.3.2	Transfection of CHO cells.....	29
4.3.3	Cultivation of <i>Sf9</i> cells .....	29
4.3.4	Generation of recombinant baculoviruses .....	30
4.3.5	Baculoviral expression of ST8SiaIV $\Delta$ 25 in <i>Sf9</i> cells.....	31
4.4	Biochemical techniques.....	32
4.4.1	Protein estimation.....	32
4.4.2	Polyacrylamide gelelectrophoresis (SDS-PAGE) .....	32
4.4.3	Coomassie staining of polyacrylamide gels .....	32
4.4.4	Silver staining of polyacrylamide gels .....	33
4.4.5	Western Blotting.....	33
4.4.6	Immunostaining of Western Blots.....	33
4.4.7	Covalent coupling of mAb 9E10 to protein G-sepharose .....	34
4.4.8	Expression of recombinant proteins in <i>E. coli</i> .....	34
4.4.9	Preparation of soluble and insoluble <i>E. coli</i> fractions.....	34
4.4.10	Purification of mAb 9E10 .....	35
4.4.11	Purification of protein A-NCAM .....	35
4.4.12	Purification of ST8SiaIV $\Delta$ 25 .....	36
4.4.13	Purification of the N- and C-terminal fragment of endoNF .....	37
4.4.14	Expression and purification of selenomethionine derivatised endoNF .....	39
4.4.15	ELISA-based polysialyltransferase assay.....	39
4.4.16	Radioactive polysialyltransferase activity assay .....	41
4.4.17	Quantitative endosialidase activity assay (TBA-assay) .....	42
4.4.18	ELISA-based endosialidase activity assay .....	43
4.4.19	Crystallization procedure.....	43
<b>5</b>	<b>Results .....</b>	<b>44</b>
5.1	The eukaryotic polysialyltransferase ST8SiaIV: Large scale expression, purification and crystallization trials.....	44
5.1.1	Expression of the polysialyltransferase ST8SiaIV in insect cells .....	44
5.1.2	Purification of ST8SiaIV from the culture supernatant of baculovirus infected <i>Sf9</i> cells.....	47
5.1.3	Crystallization trials.....	55
5.2	Crystal structure of the polysialic acid degrading endoneuraminidase cloned from bacteriophage K1F.....	56
5.2.1	N-terminal truncations of endoNF.....	56
5.2.2	Expression and purification of recombinant endoNF.....	59
5.2.3	Crystallization and data collection .....	66
5.2.4	Phasing, density improvement, and model building .....	68
5.2.5	Structure description.....	70
5.2.6	Site directed mutagenesis of conserved active site residues of endoNF .....	78



---

<b>6</b>	<b><i>Discussion</i></b> .....	<b>80</b>
6.1	The eukaryotic polysialyltransferase ST8SiaIV: Large scale expression, purification and crystallisation trials .....	80
6.2	Crystal structure of the polysialic acid degrading endosialidase cloned from bacteriophage K1F .....	85
<b>7</b>	<b><i>References</i></b> .....	<b>95</b>
<b>8</b>	<b><i>Abbreviations</i></b> .....	<b>107</b>
<b>9</b>	<b><i>Curriculum vitae and publications</i></b> .....	<b>108</b>

# 1 Zusammenfassung

Polysialinsäure (polySia, poly- $\alpha$ 2,8-*N*-acetylneuraminic acid) ist eine dynamisch regulierte posttranslationale Modifikation des Neuralen Zelladhäsionsmoleküls NCAM. Polysialyliertes NCAM ist ein wichtiger Promotor zellulärer Plastizität im sich entwickelnden embryonalen und im adulten Gehirn. PolySia ist an der Steuerung zahlreicher neuronaler Prozesse wie Migration, axonalem Wachstum und Wegfindung, synaptischer Aktivität bis hin zu Lern- und Gedächtnisleistungen und schließlich an der Neurogenese beteiligt. Darüber hinaus ist polySia ein Marker für verschiedene aggressive Tumore neuroectodermalen Ursprungs und ein bedeutender Virulenzfaktor neuroinvasiver Bakterien, die Sepsis und Meningitis verursachen. Es wird postuliert, dass die antiadhäsiven Eigenschaften der polySia, resultierend aus Größe und Ladung des Polysaccharids, für die zahlreichen Funktionen verantwortlich sind.

Die Expression von polySia in Tumoren korreliert mit hohem Metastasierungspotential und einer schlechten Prognose. Man nimmt heute an, dass polySia die Ablösung einzelner Zellen vom Primärtumor erleichtert und die Halbwertszeit der Tumorzellen in der Zirkulation erhöht, da tumorspezifische Antigene durch die immunologisch inerte polySia abgeschirmt werden.

Mit Blick auf das Ziel, steuernd in die polySia Expression einzugreifen, stellen die Schlüsselenzyme der NCAM-Polysialylierung, die Polysialyltransferasen ST8SiaII und ST8SiaIV, vielversprechende Zielstrukturen dar. Eine für die Entwicklung therapeutisch wirksamer Substanzen zwingend notwendige biochemische und strukturelle Charakterisierung dieser Enzyme steht jedoch noch weitgehend aus. Der wichtigste Grund hierfür ist die begrenzte Verfügbarkeit der Polysialyltransferasen. Polysialyltransferasen sind Glykoproteine und die Funktion der Enzyme ist essentiell an die Integrität der Glykosylierung gebunden. Somit ist die rekombinante Herstellung aktiver Polysialyltransferasen nur in glycosylierungskompetenten Zellsystemen möglich. Im Verlauf dieser Arbeit wurde ein System zur Expression und Aufreinigung von eukaryotischen Polysialyltransferasen in einem Insektenzellsystem (*Sf9*) etabliert. Die Studien wurden modellhaft für die Polysialyltransferase ST8SiaIV durchgeführt. Über diverse Optimierungsschritte wurde die Expression und homogene Darstellung des aktiven Proteins im Milligrammbereich erreicht. Mit dem gereinigten Enzymool wurden ausgedehnte Versuchsreihen zur Kristallisation des Proteins durchgeführt. Allerdings konnten bislang keine Proteinkristalle erhalten werden.

In einem zweiten Projekt wurden Studien zur Aufklärung von Struktur- und Funktionszusammenhängen polySia degradierender Enzyme, der Endoneuraminidasen, unternommen. Endoneuraminidasen sind Bakteriophagenproteine und die einzigen bisher bekannten Enzyme, die hoch spezifisch polySia abbauen. Sie sind im Zusammenhang mit Diagnose und Therapie polySia positiver Tumore von großem Interesse. Im Rahmen dieser Arbeit gelang erstmals die Kristallisation und strukturelle Analyse einer Endoneuraminidase. Die katalytisch aktive Einheit der Endoneuraminidase des Phagen K1F wurde bestimmt und im Komplex mit oligomerer Sialinsäure

---

kristallisiert. Das Enzym setzt sich aus vier klar unterscheidbaren Domänen zusammen. Die aktive Einheit ist das Trimer, das eine Pilz-ähnliche Struktur ausbildet. Dabei enthält der „Schirm“ Strukturelemente die auch in Exosialidasen gefunden werden, während das dominierende Strukturmotiv des „Stiels“ eine Tripel- $\beta$ -Helix ist. Die erhaltenen Kristallstrukturdaten zeigen klar, dass pro Trimer drei polySia Ketten binden, wobei die Bindung jeder einzelnen polySia Kette alle drei im funktionellen Komplex vorhandenen Untereinheiten verlangt. Die Struktur des aktiven Zentrums und der Bindungsmodus des Substrates lassen auf einen substratvermittelten Katalysemechanismus als molekulare Basis für die hohe Substratspezifität der Endoneuraminidasen schließen.

## 2 Abstract

Polysialic acid (polySia, poly- $\alpha$ 2,8-*N*-acetylneuraminic acid) is a dynamically regulated posttranslational modification of the neural cell adhesion molecule (NCAM). Polysialylated NCAM is an important mediator of cellular plasticity in the developing and in the adult brain. PolySia has been implicated in many neuronal processes like neurogenesis, cell migration, axonal growth and pathfinding and synaptic activity including learning and memory. Moreover, polySia is an oncodevelopmental marker expressed by several aggressive tumours of neuroectodermal origin and an important virulence factor of pathogenic bacteria causing sepsis and meningitis. It is proposed that many of the biological functions of polySia result from its anti-adhesive properties caused by size and charge of the polysaccharide.

The expression of polySia in tumours directly correlates with poor prognosis and high metastatic potential. PolySia is believed to facilitate the shedding of cells from primary tumours and to protect metastatic cells in the circulation by hiding tumour specific antigens from the immune system. Main targets to interfere with polySia expression are the key enzymes of the polysialylation pathway, the eukaryotic polysialyltransferases ST8SiaII and ST8SiaIV. However, detailed structural and biochemical characterisations of the enzymes, essential for the development of therapeutic substances, were heretofore prevented mainly by very limited protein supply. Polysialyltransferases are glycoproteins and the integrity of the glycosylation is pivotal for enzymatic activity. Therefore recombinant production of polysialyltransferases requires glycosylation competent cell systems. In the course of this study an expression and purification procedure was established using an insect cell system (*Sf9* cells). The studies were exemplarily carried out with the polysialyltransferase ST8SiaIV. After careful optimisation of expression and purification conditions several milligrams of homogeneously purified enzyme were obtained. The purified enzyme was used for extensive screenings in crystallisation experiments, however, no protein crystals were observed so far.

The second project of this study concentrated on delineating the structure-function relationships of polySia degrading enzymes, the endoneuraminidases. These phage born proteins are the only known enzymes that specifically degrade polySia. They are of particular interest with respect to diagnosis or therapy of polySia bearing human tumours. This study describes the first crystal structure of an endoneuraminidase. Crystals were obtained of the catalytic domain of endoneuraminidase of bacteriophage K1F (amino acids 246-911) in complex with oligomeric sialic acid. The enzyme folds into four distinct domains and assembles into a catalytic trimer with an overall mushroom like outline. The 'cap' domain contains structural elements also found in exosialidases while the dominant structural feature of the 'stem' region is a triple  $\beta$ -helix. The obtained data clearly show, that each trimer can bind and hydrolyse three polySia chains, whereby the binding of each polySia chain requires all three subunits of the functional complex. The structure of the active site and the mode of polySia binding suggest a substrate assisted catalytic mechanism as molecular basis for the high substrate specificity of endoneuraminidases.

### 3 Introduction

#### 3.1 Polysialic acid

Linear homopolymers of sialic acids represent unique carbohydrate structures that have been identified in a broad evolutionary range of species from bacteria to humans. Polysialic acid has been detected in neuroinvasive bacteria, fish and sea urchin eggs, *Drosophila* embryos as well as in vertebrate tissues (Mühlenhoff *et al.*, 1998). Although more than 50 distinct sialic acid derivatives have been described, in polysialic acids mainly 5-*N*-acetylneuraminic acid (Neu5Ac), 5-*N*-glycolylneuraminic acid and 2-keto-3-deoxynonulosonic acid (Kdn) are found (Figure 1).

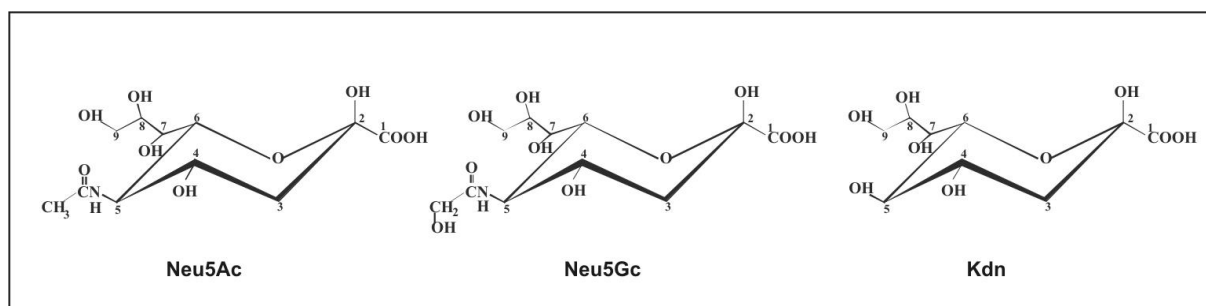


**Figure 1: Three major building blocks of polysialic acid: 5-*N*-acetylneuraminic acid (Neu5Ac), 5-*N*-glycolylneuraminic acid and 2-keto-3-deoxynonulosonic acid (Kdn)**

Already the unusual binding properties of polySia specific antibodies and enzymes, requiring at least an octamer of  $\alpha$ 2,8-linked sialic acid residues for efficient binding, have led to the postulation of an extended binding epitope formed by the polysaccharide chains (Finne and Makela, 1985; Jennings *et al.*, 1985; Evans *et al.*, 1995) and NMR studies with polySia derived from encapsulated bacteria provided evidence for high-order local helices with an extended conformation of approximately nine residues per turn (Brisson *et al.*, 1992). A most recent NMR study, however, was unable to confirm the helical conformation (Henderson *et al.*, 2003). It may be that the polySia concentration used in these studies provides a crucial factor for the secondary organisation of the chain.

Due to the carboxylate function in position C2 sialic acids are negatively charged under physiological conditions. The polyanionic polySia has been shown to possess a high water binding capacity and thus a large hydrodynamic volume (Yang *et al.*, 1992). Experiments have been carried out to define the length of the polySia chains in bacteria and vertebrates.

Although no precise numbers are available, the obtained data demonstrate that polySia chains in bacteria reach up to 200 residues (Rohr and Troy, 1980) while the degree of polymerisation (dp) is significantly smaller in vertebrates (dp  $\leq$  60; (Inoue *et al.*, 2000; Angata *et al.*, 2002)).

Expression of the bulky, space filling polySia in vertebrate tissues has been suggested to attenuate cellular interactions and plays a critical role in many developmental processes. Of particular interest is also the reexpression of polySia on human tumours including Wilms' tumour (Roth *et al.*, 1988), small cell lung carcinoma (Kibbelaar *et al.*, 1989; Komminoth *et al.*, 1991), neuroblastoma (Livingston *et al.*, 1988; Figarella-Branger *et al.*, 1990) and rhabdomyosarcoma (Soler *et al.*, 1993). In these tumours polySia expression has been correlated with poor prognosis and was shown to increase metastatic potential and tumour growth (Scheidegger *et al.*, 1994; Glüer *et al.*, 1998; Tanaka *et al.*, 2000; Daniel *et al.*, 2001).

Moreover, polySia capsules provide important virulence factors of neuroinvasive bacteria causing sepsis and meningitis in humans.

## **3.2 Polysialic acid in mammals**

To date, a total of three polysialylated proteins have been identified in mammals. By far the major carrier of polySia is thereby the neural cell adhesion molecule (NCAM). Knock out mice lacking NCAM (Cremer *et al.*, 1994), have been described to be devoid of polySia. However, polySia has also been identified on the  $\alpha$ -subunit of the voltage depended sodium channel (Zuber *et al.*, 1992) and the CD36 scavenger receptor in milk (Yabe *et al.*, 2003).

### **3.2.1 The Neural Cell Adhesion Molecule (NCAM)**

NCAM is a membrane bound glycoprotein that belongs to the family of immunoglobuline-like proteins. NCAM contains five immunoglobuline (Ig)-like domains and two fibronectin type III repeats. NCAM is schematically shown in Figure 2.

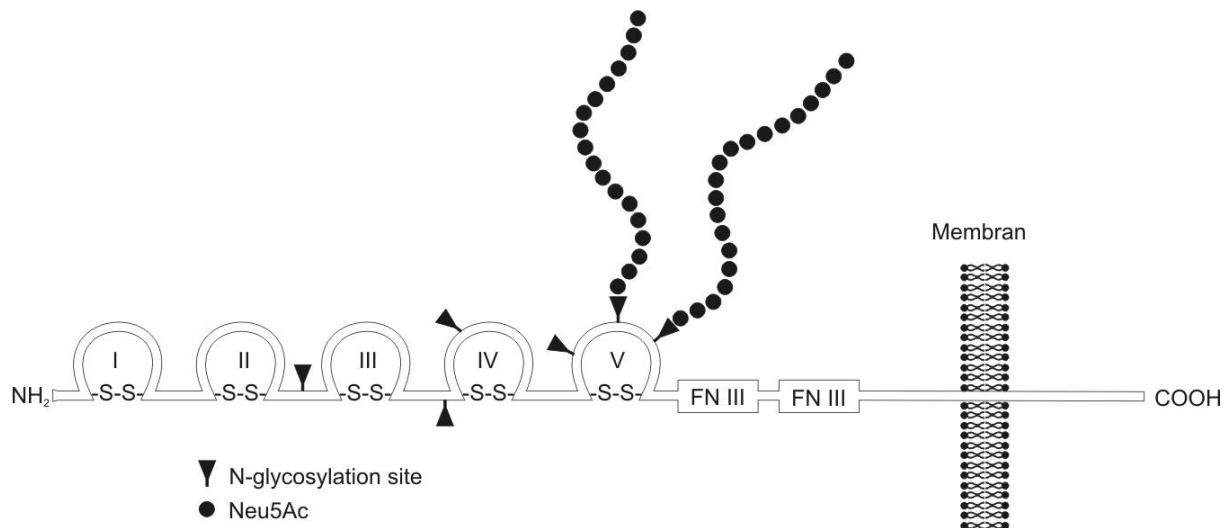


**Figure 2: Schematic representation of the neural cell adhesion molecule (NCAM)** The N-terminal part contains five immunoglobuline-like domains indicated with latin numbers (I-V) and two fibronectin type III repeats (FNIII). Out of six N-glycosylation sites present in the NCAM only two (sites five and six) can be modified with polySia.

NCAM exists in three major isoforms of 180, 140 and 120 kDa that arise from alternative splicing of a single gene located on human chromosome 11 (Hirn *et al.*, 1983; Walsh *et al.*, 1986; Cunningham *et al.*, 1987; Santoni *et al.*, 1987; Barthels *et al.*, 1987; Santoni *et al.*, 1989). The three isoforms have identical N-terminal domains but differ with respect to their cytoplasmic tails and their association to the membrane. NCAM 180 and 140 both are membrane spanning proteins with C-terminal cytosolic domains of differing size while NCAM 120 is linked to the membrane by a glycosyl-phosphatidylinositol anchor (He *et al.*, 1987). Six N-glycosylation sites are present in NCAM, but polySia is selectively added to sites 5 and 6 of the fifth immunoglobulin-like domain (Nelson *et al.*, 1995; Liedtke *et al.*, 2001; Von der Ohe *et al.*, 2002). Recent analysis of the polysialylated N-glycans of murine NCAM revealed bi-, tri- and tetraantennary complex-type core structures that were partially sulphated (Liedtke *et al.*, 2001).

NCAM is an important mediator of cellular interactions and was first characterised as calcium independent homophilic adhesion molecule. The third Ig-like domain of NCAM was assigned to mediate the *trans*-binding interactions between NCAM molecules of adjacent cells (Rao *et al.*, 1992). Furthermore interactions with extracellular matrix proteoglycans via the second Ig-like domain were reported (Cole *et al.*, 1986) and heterophilic *cis*-interactions of NCAM with the cell adhesion molecule L1 were described. Here the fourth Ig-like domain of NCAM was proposed to bind to oligomannosidic structures expressed by L1 (Kadmon *et*

*al.*, 1990a; Kadmon *et al.*, 1990b; Horstkorte *et al.*, 1993). In addition, the largest isoform NCAM 180, but not the smaller isoforms (NCAM 120 and NCAM 140), was shown to make contacts to the cytoskeleton by binding to brain spectrin (Pollerberg *et al.*, 1986; Pollerberg *et al.*, 1987).

Like other adhesion molecules also NCAM directly participates in cell signalling pathways. Most recently NCAM 140 was shown to be an alternative signalling receptor for glial cell line-derived neurotrophic factor (GDNF) family ligands (Paratcha *et al.*, 2003). Association of NCAM with GFR $\alpha$ 1 as coreceptor was shown to enhance GDNF binding and result in a rapid activation of *fyn* (Paratcha *et al.*, 2003). Constitutive association of NCAM 140 with the cytoplasmic tyrosine kinase *fyn* had already been described in earlier studies to recruit the focal adhesion kinase FAK (Beggs *et al.*, 1997). In other studies NCAM was reported to transactivate the fibroblast growth factor receptor (FGFR) (Williams *et al.*, 1994; Saffell *et al.*, 1997).

PolySia is a prominent posttranslational modification of NCAM and strongly influences the functions of the protein. The negatively charged and highly hydrated polysaccharide is supposed to exhibit a strong anti-adhesive effect and thus interfere with the overall formation of tight cell-cell contacts. In the neural system, the presence of polySia strictly correlates with stages of cellular motility and/or functional plasticity (Rutishauser and Landmesser, 1996).

The expression of polySia is developmentally regulated and found at highest levels in embryonic and neonatal stages where it is not only restricted to neural tissues but also expressed in developing kidney, heart or skeletal muscles (Finne *et al.*, 1983; Sunshine *et al.*, 1987). Polysialylated NCAM is involved in a number of developmental events such as cell migration (Ono *et al.*, 1994) or axonal growth and fasciculation (Doherty *et al.*, 1990; Zhang *et al.*, 1992). In the adult, expression of polySia is restricted to brain areas with ongoing neurogenesis and plasticity including the olfactory bulb (Miragall *et al.*, 1990), the hypothalamus (Theodosis *et al.*, 1991) and the hippocampus (Seki and Arai, 1991; Bonfanti *et al.*, 1992). PolySia found in the suprachiasmatic nuclei (SCN) of the hypothalamus was shown to impair circadian rhythm stability and attenuate photic signalling events (Shen *et al.*, 1997; Glass *et al.*, 2000). Presence of polySia in the hippocampus was found to be required for the induction of long-term potentiation (LTP) (Muller *et al.*, 1996) and was associated with learning and memory processes (Becker *et al.*, 1996). As the hippocampal expression of polySia is regulated by neuronal activity (Muller *et al.*, 1996) polySia was proposed to function as activity-induced modulator of synaptic plasticity (Kiss and Rougon, 1997).



The model introduced by Rutishauser (Rutishauser, 1996) explains the broad range of biological effects of polySia with impeding sterical influences of the bulky structure on *cis*- and *trans*- binding interactions. According to this model, polySia does not only influence NCAM-mediated binding functions, but has a general effect on cellular contact formation. There is, however, growing evidence that besides the mode of action by sterical hindrance, polySia has other biological activities. It has for instance been shown that polySia is required to obtain sensitivity of neurons towards the brain-derived neurotrophic factor (BDNF) (Vutskits *et al.*, 2001).

### 3.2.2 Eukaryotic polysialyltransferases

Two polysialyltransferases, ST8SiaII and ST8SiaIV, that add polysialic acid to NCAM have been cloned from several vertebrate species (Livingston and Paulson, 1993; Eckhardt *et al.*, 1995; Yoshida *et al.*, 1995; Nakayama *et al.*, 1995; Scheidegger *et al.*, 1995). Both enzymes are typ-II transmembrane proteins and with 59% identity at amino acid level highly homologous to each other (Figure 3). They contain three sequence motifs known as sialylmotifs L (large), S (short) and VS (very short) that are conserved in all eukaryotic sialyltransferases (Livingston *et al.*, 1993; Drickamer, 1993; Geremia *et al.*, 1997). Mutagenesis studies of the  $\alpha$ 2,6-sialyltransferase ST6GalI provided convincing evidence that the L-motif is involved in binding of the sugar donor CMP-Neu5Ac, while the S-motif participates in the binding of both, donor and acceptor substrate (Datta and Paulson, 1995; Datta *et al.*, 1998). Mutations of the two conserved VS-motif residues (HxxxxE) resulted in inactive but secreted ST8SiaIV mutants illustrating the functional importance of this short motif (Windfuhr *et al.*, 2000; Kitazume-Kawaguchi *et al.*, 2001)

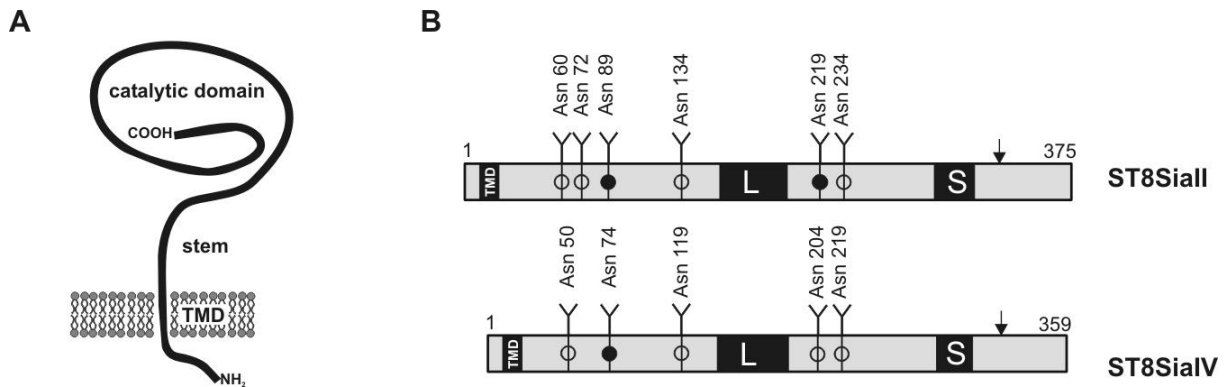


**Figure 3: Schematic representation of polysialyltransferases** (A) Cartoon illustrating the type II membrane topology; transmembrane domain (TMD), stem region and globular catalytic domain are indicated. (B) Schematic representations of ST8SiaII and ST8SiaIV. The large (L) and the small (S) sialylmotifs are highlighted as black boxes, the position of the very short sialylmotifs (VS) is indicated by arrows. Asparagine residues involved in N-glycosylation are indicated. N-glycans important for polysialyltransferase activity are marked with filled circles.

ST8SiaII and ST8SiaIV are both individually able to polysialylate all NCAM-isoforms by adding polySia to complex  $\alpha$ 2,3- or  $\alpha$ 2,6- sialylated N-glycans (Mühlenhoff *et al.*, 1996b; Angata *et al.*, 1998; Franceschini *et al.*, 2001). Both polysialyltransferases prefer the sixth (membrane proximal) N-glycosylation site of NCAM (Figure 2); although this effect is less pronounced in the case of ST8SiaII (Angata *et al.*, 1998). Both enzymes polysialylate glycan structures attached to NCAM with much greater efficiency than N-glycans released from NCAM (Angata *et al.*, 2000), suggesting that the polysialylation reaction is protein specific. Recent *in vivo* cell culture studies with NCAM deletion mutants showed, that the fifth Ig-like domain and the adjacent fibronectin type III (FN) repeat are sufficient for polysialylation by both enzymes. Thereby, the FN repeat seems to act as polysialyltransferase recognition and docking site (Close *et al.*, 2003). This finding contrasts earlier *in vitro* data where also the fourth Ig-like domain of NCAM was found to be crucial for polysialylation (Angata *et al.*, 2002).

*In vitro* ST8SiaIV was shown to produce longer polySia chains than ST8SiaII (Angata *et al.*, 1998; Windfuhr *et al.*, 2000; Mühlenhoff *et al.*, 2001; Angata *et al.*, 2002) and to exhibit a wider acceptor spectrum. In contrast to ST8SiaII, it was able to extend oligosialylated monoantennary structures and to polysialylate more than one antenna of multiantennary core structures (Angata *et al.*, 2002). The same authors also reported that the concerted action of both enzymes resulted in more and longer polySia chains than seen with either enzyme alone

(Angata *et al.*, 2002) and proposed that ST8SiaII and IV act cooperatively in NCAM polysialylation.

Besides the polysialylation of NCAM the protein specific polysialyltransferases were shown to modify themselves by adding polySia onto their own N-glycans. This self modification, referred to as autopolsialylation, was described for both enzymes *in vitro* and *in vivo* (Mühlenhoff *et al.*, 1996a; Close and Colley, 1998; Mühlenhoff *et al.*, 2001). The polysialyltransferases contain six (ST8SiaII) and five (ST8SiaIV) N-glycan attachment sites, respectively. Autopolsialylation is predominantly involving the N-glycan attached to asparagine 74 in ST8SiaIV and the N-glycans attached to asparagines 89 and 219 in ST8SiaII (Mühlenhoff *et al.*, 2001). In contrast to NCAM-polysialylation, where priming sialylation in  $\alpha$ 2,3- or an  $\alpha$ 2,6- glycosidic linkage is the minimal requirement for polySia synthesis (Mühlenhoff *et al.*, 1996b; Angata *et al.*, 1998), autopolsialylation can occur on asialoglycans but was shown to require terminal galactose. Agalacto forms of ST8SiaIV are unable to perform auto- and NCAM-polysialylation (Mühlenhoff *et al.*, 1996a). This argues for a tight functional link between NCAM- and autopolsialylation, however, the hypothesis that an *en bloc* transfer of autocatalytically synthesized polySia chains to the acceptor NCAM occurs, could be ruled out (Mühlenhoff *et al.*, 1996a). Whether the self-modification process is in fact a prerequisite for functional polysialyltransferases or whether autopolsialylation has only enhancing influence on NCAM-polysialylation is controversially discussed and the reported data are partly contradicting (Close *et al.*, 2000; Windfuhr *et al.*, 2000; Angata *et al.*, 2001; Mühlenhoff *et al.*, 2001; Close *et al.*, 2001)

Transcript analyses revealed that both polysialyltransferases are expressed in early developmental stages, but ST8SiaII is the prominent enzyme in embryonic tissue and its transcript level decreases substantially after birth. In the adult brain ST8SiaIV is the dominant enzyme (Angata *et al.*, 1997; Hildebrandt *et al.*, 1998; Ong *et al.*, 1998). Consequently very low polySia levels were detected in adult ST8SiaIV-deficient mice and an age-dependent impairment of learning and memory was shown via reduced long-term potentiation and long-term depression (Eckhardt *et al.*, 2000).

### 3.3 Endoneuraminidases

Bacteriophage-born endoneuraminidases (endoN) have been essential and widely used tools in polySia research and to a large extent enabled the recent progress made in understanding the physiological and pathological functions of polySia. Endoneuraminidases are the only enzymes known so far that efficiently degrade polySia. As they are highly specific for polysialic acid, the enzymes can be used to exclusively degrade polySia on cultured cells or even in living animals without interfering with abundant monosialylated structures.

Endoneuraminidases have been isolated from bacteriophages capable to infect polySia encapsulated *E. coli* K1. This neuroinvasive pathogen, which causes sepsis and meningitis in neonates wears a thick layer of  $\alpha$ 2,8-linked sialic acid residues (Figure 4) composed of up to 200 residues per chain (Rohr *et al.*, 1980). The polySia capsule is an important virulence factor of the pathogenic bacterium. It is structurally and immunochemically identical to polySia found in the human host, enabling the bacterium to escape the human immune system by ‘antigenic mimicry’. Identical capsules are also found in the human pathogen *Neisseria meningitidis* serogroup B, in *Moraxella nonliquefaciens* and in *Pasteurella haemolytica* A2 infecting ruminants (Troy, 1992). Capsules composed of alternating  $\alpha$ 2,8/ $\alpha$ 2,9-linked sialic acid residues are described for *E. coli* K92 and Bos-12 strains while *Neisseria meningitidis* serogroup C capsules consists of  $\alpha$ 2,9-linked sialic acids. In accordance with the ‘antigenic mimicry’ concept,  $\alpha$ 2,8-linked capsular polysaccharides are poorly immunogenic, while the capsules containing also  $\alpha$ 2,9-linkages induce massive immune reactions in the host.

Though polysaccharide capsules generally protect bacteria from hostile environmental influences, many encapsulated bacterial are infected by specialized bacteriophages that carry host-capsule degrading hydrolases. These enzymatic activities enable the phages to penetrate the protective capsular layer and access the bacterial membrane (Figure 4). The hydrolases are usually tailspike associated and important determinants of the bacteriophage host range.

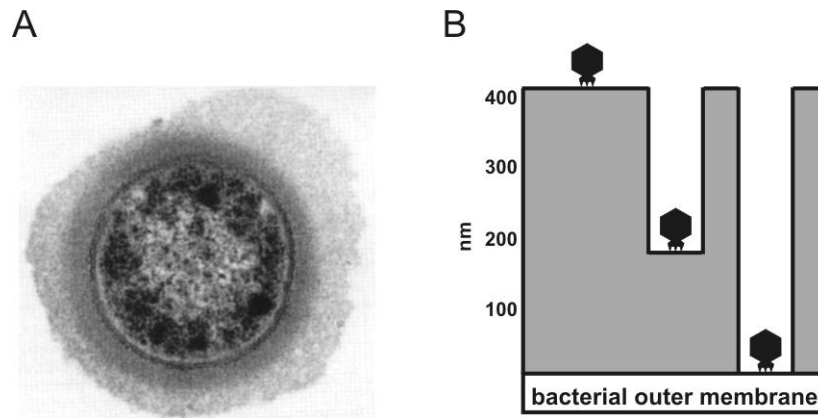


**Figure 4: PolySia encapsulated *E. coli* K1** (A) Electron microscopy of an *E. coli* K1 bacterium encapsulated in polysialic acid (Roth et al., 1993). The thick polySia capsule is seen as amorphous grey layer surrounding the bacterium. (B) Schematic representation of bacteriophages penetrating the polySia capsule of *E. coli* K1.

More than 20 bacteriophages have so far been isolated mainly from sewage that specifically infect *E. coli* K1 (Table 1). The K1-specific phages are lytic linear double-stranded DNA viruses of different morphology. Though most of the phages belong to the group of *podoviridae* with short noncontractile tails, some were shown to be *myoviridae* exhibiting a long and contractile tail apparatus (Miyake *et al.*, 1997). Common to all K1-phages are polySia degrading tailspikes, the endoneuraminidases, that were shown to be associated with the bacteriophage baseplate (Petter and Vimr, 1993; Miyake *et al.*, 1997).

phage	host strain	phage isolation	endosialidase gene	enzyme
ΦK1A, ΦK1B, ΦK1C, ΦK1D,	<i>E. coli</i> K1	(Gross <i>et al.</i> , 1977)	-	
ΦK1E	<i>E. coli</i> K1	(Gross <i>et al.</i> , 1977)	(Gerardy-Schahn <i>et al.</i> , 1995) (Long <i>et al.</i> , 1995)	endoNE
ΦK1F	<i>E. coli</i> K1	(Vimr <i>et al.</i> , 1984)	(Petter <i>et al.</i> , 1993) (Mühlenhoff <i>et al.</i> , 2003)	endoNF
Φ 1.2	<i>E. coli</i> K1	(Kwiatkowski <i>et al.</i> , 1982)	-	
B, C, D, F, G, K, L, P, R	<i>E. coli</i> K1	(Smith and Huggins, 1982)	-	
3, 9, a, d, A, E	<i>E. coli</i> K1	(Miyake <i>et al.</i> , 1997)	-	
63D	<i>E. coli</i> K1	(Machida <i>et al.</i> , 2000)	Accession Nr. AB015437	endoN63D
ΦK1-5	<i>E. coli</i> K1 <i>E. coli</i> K5	(Scholl <i>et al.</i> , 2001)	(Scholl <i>et al.</i> , 2001)	
Φ 92	<i>E. coli</i> K1 <i>E. coli</i> K92	(Kwiatkowski <i>et al.</i> , 1983)	-	

**Table 1: Overview of isolated *E. coli* K1 specific phages and cloned endoneuraminidase genes**

A common cleavage pattern was reported for the endosialidases of  $\Phi$ K1A – E and  $\Phi$ 92 by analysing the purified phages. For moderate enzyme and high substrate concentrations the minimum substrate size was found to be an octamer of sialic acid residues that was cleaved five residues from the reducing end (Pelkonen *et al.*, 1989). However, the same study reported under exhaustive conditions (high enzyme concentrations) further enzyme specific break down of the substrate. Similar studies performed with endoN purified from  $\Phi$ K1F reported a minimum of five sialic acid residues for cleavage yielding mainly tetrameric and monomeric sialic acid (Hallenbeck *et al.*, 1987). All endoneuraminidases purified from phage lysates were shown to oligomerise. EndoNF forms SDS-resistant homotrimers composed of 103 kDa subunits (Hallenbeck *et al.*, 1987; Mühlenhoff *et al.*, 2003), while for endoNE an SDS-resistant heterotrimeric complex with a not further characterised 38 kDa protein was described (Tomlinson and Taylor, 1985; Gerardy-Schahn *et al.*, 1995). EndoN63D was reported to form tetrameric complexes composed of 90 kDa subunits linked by disulfide bridges.

Meanwhile endoneuraminidases have been cloned from the phages K1E, K1F, 63D and K1-5 (Petter *et al.*, 1993; Gerardy-Schahn *et al.*, 1995; Long *et al.*, 1995; Machida *et al.*, 2000; Scholl *et al.*, 2001; Mühlenhoff *et al.*, 2003), whereby the enzymes cloned from  $\Phi$ K1E and  $\Phi$ K1-5 are almost identical (>97% amino acid identity). All enzymes share a common endoN core domain of about 650 amino acids with high sequence identity (50-81 %) that was proposed to harbour the catalytic domain. In contrast to endoNE, the significantly larger endosialidases cloned from  $\Phi$ K1F and  $\Phi$ 63D are N-terminally extended by 200 and 120 amino acids, respectively. The extended regions exhibit homology to the N-terminal part of the tail fibre protein gp17 of coliphages T3 and T7 and of yersiniophage YeO3-12 (Pajunen *et al.*, 2000). For coliphage T7 was shown that complexes of gp17 form the phage tail fibres and that the fibres are attached to the phage capsid by the N-terminal domain of gp17 (Steven *et al.*, 1988). Thus a similar function of the homologous region in endoNF and endoN63D has been suggested (Petter *et al.*, 1993).

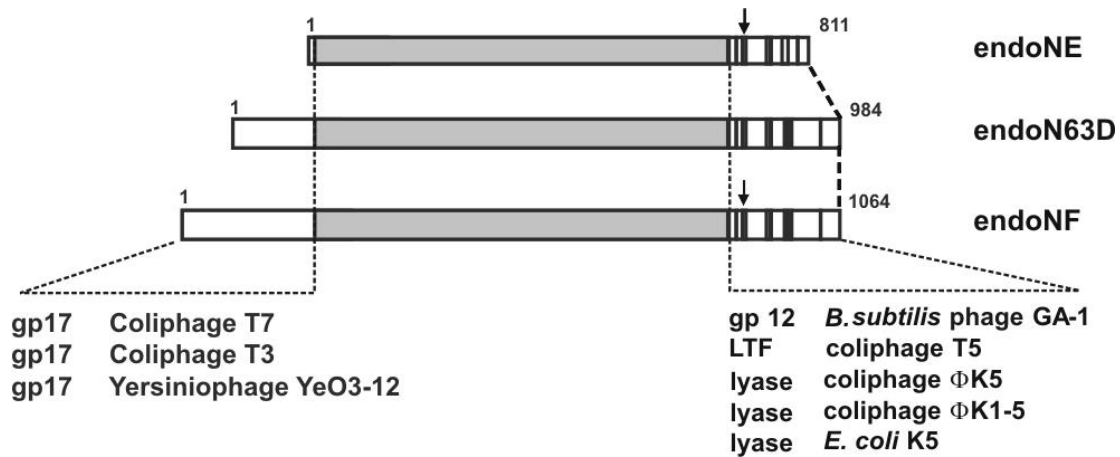


**Figure 5: Schematic representation of the cloned endoneuraminidases** The highly homologous endoN core domain is highlighted in grey. The sites of proteolytic cleavage are indicated by arrows while homologous stretches within the C-terminal domain are shown as black bars. The C-terminal domain exhibits sequence similarity to the C-terminal parts of the neck appendage protein gp12 of *Bacillus subtilis* phage GA-1, the L-shaped tail fiber protein (LTF) of coliphage T5 and to K5-specific lyases of coliphages K5 and K1-5 as well as to the *E. coli* K5 lyase. The N-domains of endoN63D and endoNF exhibit homology to parts of the tail fibre protein gp17 of coliphages T3 and T7 and of yersiniophage YeO3-12.

Recently it was shown, that the C-terminal domain of endoNE and endoNF is proteolytically cleaved off during maturation of the enzymes (Leggate *et al.*, 2002; Mühlenhoff *et al.*, 2003). The conserved cleavage site is indicated by arrows in Figure 5. Cleavage is not essential for activity and the cleaved off domain is not part of the active enzyme complex (Mühlenhoff *et al.*, 2003). However, the presence of this domain in the primary translation product was demonstrated to be a prerequisite for the formation of active endosialidases suggesting that the C-terminal domain facilitates proper folding or complex formation of the enzymes (Mühlenhoff *et al.*, 2003). Database searches revealed significant homology between the C-terminal part of the endosialidases and other phage tail proteins (see Figure 5) (Mühlenhoff *et al.*, 2003). Whether these domains have a similar function and the presence of an intramolecular ‘chaperone’ or ‘oligomerisation platform’ is a more common concept in tail associated bacteriophage proteins remains to be elucidated.

### 3.4 Aims of the present study

Polysialic acid is an important modulator of cellular interactions essentially involved in ontogenic development and integrity of neuronal functions. Ectopic expression of polySia has been associated with severe human diseases, e.g. neuroendocrine tumours. In addition, polySia is an important virulence factor of pathogenic bacteria causing sepsis and meningitides. The key enzymes in polySia synthesis are the polysialyltransferases. Genes encoding polysialyltransferases have been cloned from different vertebrate sources and from the neuroinvasive bacteria *E. coli* K1 and *Neisseria meningitides*. Because polysialyltransferases are the main targets to interfere with the cellular polysialylation machinery, the goal of the study was to delineate molecular details on structure-function-relationships in this enzyme group. Towards this aim my studies concentrated on the large scale expression and purification of eukaryotic polysialyltransferases to enable structural analyses by protein crystallization

My second project concentrated on polySia degrading enzymes, the endoneuraminidases. Endoneuraminidases are the only known enzymes that specifically bind and degrade polysialic acid and therefore are widely used tools in polySia research. Most recent studies in animal model systems highlighted the therapeutic potential of these enzymes by demonstrating that endoneuraminidase activity interfered with the pathomechanism of neuroinvasive bacteria and limited the metastatic potential of polySia encapsulated tumour cells. Because no information was available on the functional mechanisms of endosialidases when this study was started, my second goal pointed towards the molecular characterisation of endoneuraminidases by crystal structure analysis.



## 4 Materials and methods

### 4.1 Materials

#### 4.1.1 Cell lines

- Sf9* cells : *Spodoptera frugiperda* insect cell line (Invitrogen)
- CHO-2A10 : Chinese hamster ovary cell line with defect ST8SiaIV gene (Eckhardt *et al.*, 1995)
- CHO-6B2 : Chinese hamster ovary cell line with defect CMP-sialic acid transporter gene (Eckhardt *et al.*, 1996)

#### 4.1.2 Bacterial strains

- E. coli* JM109 : Genotype: e14-(McrA-) *recA1 endA1 gyrA96 thi-1 hsdR17*(r<sub>k</sub><sup>-</sup> m<sub>k</sub><sup>+</sup>) *supE44 relA1 Δ(lac-proAB)* [F<sup>c</sup> *traD36 proAB lacI*<sup>q</sup>ZΔM15] (Stratagene)
- E. coli* DH10Bac : Genotype: F- *mcrA (mrr-hsdRMS-mcrBC) 80dlacZM15 lacX74 deoR recA1 endA1 araD139 (ara-leu)7697 galU galK rpsL nupG /bMON14272 /pMON7124* (Invitrogen)
- E. coli* BL21(DE3) : Genotype: F<sup>-</sup> *ompT hsdS<sub>B</sub> (r<sub>B</sub><sup>-</sup> m<sub>B</sub><sup>-</sup>) gal dcm* (DE3) (Novagen)
- E. coli* B834(DE3) : Genotype: F<sup>-</sup> *ompT hsdS6 (r<sub>B</sub><sup>-</sup> m<sub>B</sub><sup>-</sup>) gal dcm met* (DE3) (Novagen)

#### 4.1.3 Plasmids

- pProtA-PST : Eukaryotic expression vector for expression of soluble and secreted N-terminally by 25 amino acids truncated ST8SiaIV as protein A fusion protein (Mühlenhoff *et al.*, 2001).
- pMyc-ST8SiaIV : Eukaryotic expression vector for expression of soluble and secreted N-terminally by 25 amino acids truncated ST8SiaIV with C-terminal myc-His<sub>6</sub>-epitope (Windfuhr *et al.*, 2000).
- pFastBac-HBM : Baculovirus transfer vector based on pFastBac (Invitrogen) including a honey-Bee melittin (HMB) secretion signal (obtained from Y.Strandberg, IMB, Brisbane, Australia).
- pFastBac-HT : Baculovirus transfer vector of the Bac-To-Bac system (Invitrogen). Includes His<sub>6</sub>-tag and rTev-protease site.

- pHBM $\Delta$ 25-ST8SiaIV : Transfer vector used to generate recombinant baculovirus for expression of C-terminally myc-His<sub>6</sub>-tagged ST8SiaIV secreted to the culture medium of *Sf9* cells. The N-terminally by 25 amino acids truncated ST8SiaIV was amplified from pMyc-ST8SiaIV (including the myc-His<sub>6</sub>-sequence) using the primer pair KS1f/KS1r and inserted between restriction sites *XhoI* and *HindIII* of pFastBac-HBM.
- pFB $\Delta$ 25-ST8SiaIV : Transfer vector used to generate recombinant baculovirus for expression of N-terminally His<sub>6</sub>-tagged ST8SiaIV in *Sf9* cells. The N-terminally by 25 amino acids truncated ST8SiaIV was amplified from pMyc-ST8SiaIV (without myc-His<sub>6</sub>-sequence) using the primer pair MM35/KS9r and inserted between restriction sites *NcoI* and *HindIII* of pFastBac-HT.
- pHBM<sub>HT</sub> $\Delta$ 25-ST8SiaIV: Transfer vector used to generate recombinant baculovirus for expression of N-terminally His<sub>6</sub>-tagged ST8SiaIV secreted to the culture medium of *Sf9* cells. The ST8SiaIV-insert of pFB $\Delta$ 25-ST8SiaIV (including His<sub>6</sub>-rTev-sequence) was amplified using the primer pair KS15/KS9r and inserted between restriction sites *SacI* and *HindIII* of pFastBac-HBM.
- pET22b-Strep : Prokaryotic expression vector based on pET22b (Novagen) including an N-terminal StrepII-sequence (WSHPQFEK) instead of the pelB-sequence. The StrepII-adaptor was inserted between the restriction sites *NheI* und *BamH I*.
- pEndoNF : Eukaryotic expression vector based on pET22b-Strep for expression of N-terminally StrepII- tagged and C-terminally His<sub>6</sub>-tagged endoNF. EndoNF was inserted using the restriction sites *BamHI* and *XhoI*.
- p $\Delta$ 245-EndoNF : Eukaryotic expression vector based on pET22b-Strep for expression of N-terminally by 245 amino acids truncated endoNF with N-terminal StrepII- tag and C-terminal His<sub>6</sub>-tag. The truncated endoNF was inserted using the restriction sites *BamHI* and *XhoI*.
- p $\Delta$ 245-EndoNF-E<sup>525</sup>A : Eukaryotic expression vector similar to p $\Delta$ 245-EndoNF for expression of mutant endoNF. The glutamic acid in position 525 was mutated to alanine by site directed mutagenesis using the primer pair KS61/KS62.
- p $\Delta$ 245-EndoNF-E<sup>581</sup>A : Eukaryotic expression vector similar to p $\Delta$ 245-EndoNF for expression of mutant endoNF. The glutamic acid in position 581 was mutated to alanine by site directed mutagenesis using the primer pair KS63/KS64.
- p $\Delta$ 245-EndoNF-R<sup>596</sup>A : Eukaryotic expression vector similar to p $\Delta$ 245-EndoNF for expression of mutant endoNF. The arginine in position 581 was mutated to alanine by site directed mutagenesis using the primer pair KS65/KS66.
- p $\Delta$ 245-EndoNF-R<sup>647</sup>A : Eukaryotic expression vector similar to p $\Delta$ 245-EndoNF for expression of mutant endoNF. The arginine in position 647 was mutated to alanine by site directed mutagenesis using the primer pair KS67/KS68.

#### 4.1.4 Oligonucleotides

##### Sequencing primers (5' → 3')

KS2f	TGTAATCAGGTGCAAT	Target sequence	ST8SiaIV
KS7f	TATCCGGATTATTCA		pFastBac
T7	TAATACGACTCACTATA		pET22b
T7term	GCTAGTTATTTGCTCAGCGG		pET22b
MM104	GTCAGAGCCGTGCATCAA		endoNF

##### PCR amplification primers (5' → 3')

KS1f	GACTCGAGAGCCAGAAGTGGAGGAGCAC	Target sequence	ST8SiaIV	<i>XhoI</i>
KS1r	CTAAGCTTTCAATGATGATGATGATGATG		pMyc-ST8SiaIV	<i>HindIII</i>
MM35	ATGCCATGGCCAGAAGTGGAGGAGCAC		ST8SiaIV	<i>NcoI</i>
Ks9r	TGAAGCTTTTATTGCATTCATGCACTCCCTGT		ST8SiaIV	<i>HindIII</i>
KS15	GAGAGCTCGCATCACCATCACCATCACGAT		pFastBac-HT	<i>SacI</i>

##### Mutagenesis primers (5' → 3')

KS61	TCCCTAGTGTCACAGCTGTGCATAGCTTT	Target sequence	endoNF	E525A
KS62	GCAAAGCTATGCACAGCTGTGACACTAGGGA -		endoNF	E525A
KS63	CCAGATGCGTCAGCGCCGTGCATCAAG		endoNF	E581A
KS64	CTTGATGCACGGCGCTGACGCATCTGG		endoNF	E581A
KS65	GGTGTATTATACCTTATCACTGCAGGCACTCGTGGTGATAGACT		endoNF	R596A
KS66	AGTCTATCACCACGAGTGCCTGCAGTGATAAGGTATAATACACC		endoNF	R596A
KS67	CCTTATTATGTTTGGTTCAGAAGCTGCAGAAAATGAATGGGAAGC		endoNF	R647A
KS68	GCTTCCCATTCATTTTCTGCAGCTTCTGAACCAAACATAATAAGG		endoNF	R647A

#### 4.1.5 Chromatography columns and media

Superdex 200 HR 10/30	Amersham Biosciences
HiPrep 26/10 Desalting	Amersham Biosciences
StrepTactin affinity matrix	IBA
ProBond Ni <sup>2+</sup> affinity matrix	Invitrogen
HiTrap Chelating (5ml)	Amersham Biosciences
Protein G-sepharose	Amersham Biosciences
IgG-Sepharose	Amersham Biosciences

#### 4.1.6 Antibodies

anti-T7 mAb	: monoclonal antibody (mouse IgG 2b) directed against the T7-epitope (MTGGQQM) (Novagen)
anti-penta His mAb	: monoclonal antibody (mouse IgG) directed against the His <sub>6</sub> -epitope (HHHHHH) (Qiagen)
anti-myc mAb (9E10)	: monoclonal antibody (mouse IgG 1) directed against the myc-epitope (EQKLISEEDL) (Roche)
735 mAb	: monoclonal antibody (mouse IgG 2a) directed against poly- $\alpha$ 2,8- <i>N</i> -acetylneuraminic acid with a minimum chain length of eight residues (Frosch <i>et al.</i> , 1985)
735-bio-fab	: Fab'2 fragments of mAb 735 conjugated with biotin
anti-mouse-AP	: polyclonal goat anti mouse IgG conjugated with alkaline phosphatase (Dianova)
anti-mouse-POX	: polyclonal goat anti mouse IgG conjugated with horseradish peroxidase (Southern)
mouse IgG	: mouse IgG (Pierce)
streptavidine-POX	: streptavidine horseradish peroxidase conjugate (Roche)

#### 4.1.7 Molecular weight markers

'1 kb DNA ladder' (Invitrogen)

[kb]: 0.08; 0.13; 0.15; 0.20; 0.2; 0.30; 0.34; 0.40; 0.51; 0.52; 1.0; 1.6; 2.1; 3.1; 4.1; 5.0; 6.1; 7.1; 8.1; 9.2; 10.2; 11.2; 12.2

' $\lambda$ -DNA / HindIII-Fragments' (Invitrogen)

[kb]: 0.14; 0.56; 2.03; 2.23; 4.63; 6.68; 9.41; 23.13

'SDS-PAGE molecular weight standards high range' (BioRad)

[kDa]: 45; 66; 97; 116; 200

'SDS-PAGE molecular weight standards low range' (BioRad)

[kDa]: 14; 22; 31; 45; 66; 97

'Unstained Precision Protein Standards' (BioRad)

[kDa]: 10; 15; 20; 25; 37; 50; 75; 100; 150; 250

'[<sup>14</sup>C]-Methylated Proteins' [5  $\mu$ Ci/ml]' (Amersham Biosciences)

[kDa]: 14,3; 30; 46; 66; 97,4; 100; 220

### 4.1.8 Chemicals

ABTS	Roche
Acetic acid (100 %)	Merck
Aceton	Baker
Acrylamide 40% 4 K-Mix (37,5:1)	Serva
Agarose	Serva
Ammonium chloride	Merck
Ammonium persulphate (APS)	Serva
Ampicillin, sodium salt	Serva
Aprotinin	Bayer
Avidin	Sigma
BCA <i>Protein Assay Reagent</i>	Pierce
BCIP (5-Brom-4-chlor-3-indolyl-phosphat)	Fluka
Bestatin	Sigma
Beta-Mercaptoethanol	Sigma
Bluo-gal	Invitrogen
Borate, sodium salt	Merck
Bromphenol Blue, sodium salt	Applichem
BSA (Fraktion V)	Applichem
BSA protein standard	Pierce
Carbenicillin, disodium salt	Fluka
CELLfectin transfection reagent	Invitrogen
Chloroform	Baker
Citric acid	Merck
Colominic acid	Sigma
Cytidine 5'-monophosphat [ <sup>14</sup> C]sialic acid	Amersham Biosciences
Cytidine 5'-monophosphat sialic acid	Sigma
Desthiobiotin	Sigma
Dimethylformamide (DMF)	Fluka
Dimethylpimelimidate	Sigma
Dimethylsulfoxide (DMSO)	Merck
Dipotassium hydrogenphosphate	Merck
Disodium hydrogenphosphate	Merck
Disodium hydrogenphosphate	Merck
Dithiothreitol (DTT)	Sigma
dNTPs (100 mM each)	Pharmacia
Dry milk	Applichem
EDTA, Disodium salt (Titriplex III)	Merck
Ethanol, abs.	Baker
Ethidium Bromide	USB Corporation
Formaldehyde	Sigma
Gentamicin	Sigma
D-glucose	Sigma
Glycerine (99%)	KMF
Glycine	Sigma
Hydrochloric acid (38%)	Baker
Imidazole	Fluka
IPTG (Isopropyl-beta-D-thiogalactopyranoside)	Merck
Isopropanol (2-Propanol)	Merck
Kanamycin	Sigma

Korsolex plus	Roche
LipofectAMINE transfection reagent	Invitrogen
Lithium sulphate	Sigma
Magnesium chloride hexahydrate	Merck
Magnesium sulphate	Baker
Manganese chloride	Merck
MES (2-(N-Morpholino)ethanesulphonic acid)	Merck
Methanol	Baker
L-methionine	Sigma
NBT (Nitrotetrazolium bluechloride)	Fluka
Pepstatin	Roche
Phenylmethylsulfonyl fluorid (PMSF)	Sigma
Polyethyleneglycol, various from PEG300 to PEG 20000	Sigma
Ponceau S, sodium salt	Sigma
Potassium dihydrogenphosphate	Merck
Roti-Blue Coomassie-stain (5x)	Roth
D/L-selenomethionine	Sigma
Sialic acid (5- <i>N</i> -acetylneuraminic acid)	Serva
Sialic acid pentamer $\alpha$ 2,8-linked	Calbiochem
Sodium acetate	Merck
Sodium azide	Merck
Sodium cacodylate ('Dimethylarsinic acid')	Sigma
Sodium chloride	Merck
Sodium dihydrogenphosphate	Merck
Sodium dodecylsulphate (SDS)	Merck
Sodium hydroxide	Merck
Sodium meta-arsenite	Merck
Sodium periodate	Sigma
Streptavidine Horseradish peroxidase conjugate	Roche
TEMED (N,N,N',N'-Tetramethyl-ethylendiamin)	Serva
Tetracycline	Sigma
Tetramethyl benzidine (TMB)	Sigma
Thiamin	Sigma
Thiobarbituric acid (TBA)	Sigma
Tricine (N-Tris(hydroxymethyl)-methylglycine)	Serva
TRIS (Tris(hydroxymethyl)-aminomethan)	Merck

All chemicals not explicitly listed above were purchased in p.a. quality from either Merck or Sigma.

### 4.1.9 Culture media and additives

DMEM/Hams F12	Biochrom
OptiMEM	Invitrogen
Fetal calf serum	Invitrogen
Sf-900 II SFM	Invitrogen
L-Glutamine	Biochrom
LB-medium	Becton Dickinson
LB-agar	Becton Dickinson

### 4.1.10 Standardbuffer and media

2xGEBS	20% glycerol, 50 mM EDTA 0,05% bromephenol Blue, 0,5% sarcosyl
2xLaemmli	200 mM Tris-HCl pH 6,8, 30% (v/v) glycerol, 3% (w/v) SDS, 0,1% (w/v) bromephenol Blue
BCIP	25 mg/ml BCIP in 100% DMF
M9- medium	42 mM Na <sub>2</sub> HPO <sub>4</sub> , pH 7.4 22 mM KH <sub>2</sub> PO <sub>4</sub> 0.05% (w/w) NaCl 19 mM NH <sub>4</sub> Cl 2 mM MgSO <sub>4</sub> 0.4% (w/w) glucose 0.1 mM CaCl <sub>2</sub> 2 mg/l thiamin, 2 mg/l biotin
NBT	50 mg/ml NBT in 70% (v/v) DMF
PBS	10 mM sodium phosphate pH 7,4 150 mM NaCl
PBS/EDTA	10 mM sodium phosphate, pH 7,4 150 mM NaCl 2 mM EDTA
TBE	100 mM Tris-HCl, pH 8,0 100 mM Borate 2,5 mM EDTA
TE	10 mM Tris-HCl, pH 8,0 1 mM EDTA

### 4.1.11 Enzymes

Alkaline calf intestine phosphatase	New England Biolabs
T4-DNA-Ligase	New England Biolabs
<i>cloned Pfu</i> -DNA-Polymerase	Stratagene
<i>Taq</i> -DNA-Polymerase	Sigma
Lysozyme	Serva
Restriction enzymes: <i>Bam</i> HI, <i>Dpn</i> I, <i>Hind</i> III, <i>Nhe</i> I, <i>Nco</i> I, <i>Sac</i> I, <i>Xho</i> I,	New England Biolabs

### 4.1.12 Laboratory equipment

Blotting chamber Fast-Blot B44	Biometra
Easy Enhanced Analysis System (E.A.S.Y RH-3, Videokamera 429K)	Herolab
Elektrophoresis chamber for agarose-gels	peqlab
Elektrophoresis chamber for SDS-PAGE	BioMetra
ELISA-Reader: DigiScan	Asys Hitech
FPLC-system ÄKTA	Amersham Biosciences
Heatingblock TB1	BioMetra
HeraSafe Hood	Heraeus
Incubators	Heraeus
Peristaltikpump P-1	Amersham Biosciences
Scales CP 224S ( $\mu$ g) / CP 3202 (g)	Sartorius
Sonifier 450	Branson
Spectrophotometer Ultrospec 2100 pro	Amersham Biosciences
Speedvac RVC 2-18	Christ
Standard Power Pack P25	Biometra
Thermocycler T1 und T Gradient	Biometra
Thermomixer compact	Eppendorf
Centrifuges :	Heraeus
- Biofuge fresco	Heraeus
- Biofuge pico	Heraeus
- Multifuge 3 S-R	Eppendorf
- Centrifuge 5415C	Beckman
- Coulter Avanti J-30I	Kontron
- Centrikon T-1170	Beckman
Rotors:	Beckman
- JA 25.50	Beckman
- JLA 10.500	Beckman
- JS-24.15	Rigaku msc
X-ray generators:	
- MicroMax-007	
- RU-H3R	
Detektor:	MARresearch
- mar345 DTB	



### 4.1.13 Consumables and Kits

Cell culture bottles and dishes	Sarstedt
Concert High Purity Plasmid MiniPrep System	Invitrogen
Crychem plates, polystyrene (24 wells)	Hampton Research
Crystal Clear sealing tape	Hampton Research
Culture dishes (92 x 16 mm, PS)	Sarstedt
Filterpaper 3MM	Whatman
Hyperfilm MP	Amersham Biosciences
Microtiterplates 96-well polystyrol (U-bottom)	Greiner
Microtiterplates MicroTest III Flexible Assay Plate	Becton Dickinson
Nitrocellulose membrane (0,45 µm)	Schleicher & Schuell
PCR-tubes (0,2 ml)	Biozym
Plastic disposable pipettes (5 ml, 10 ml, 25 ml)	Sarstedt
Polypropylentubes (14 ml, 50 ml)	Greiner
QIAGEN Plasmid Mini und Midi Kit	QIAGEN
QIAquick Gel Extraction Kit	QIAGEN
Reaction tubes (0.5 ml, 1.5 ml)	Sarstedt
Reaction tubes safelock (1.5 ml, 2 ml)	Eppendorf
Sterile filters Millex GP (0,22 µM)	Milipore
Syringes (1 ml, 5 ml, 10 ml)	Braun
VivaFlow50 crossflow filtration units (PES membrane, 10 kDa MWCO)	Vivascience
Vivaspin concentrator 20 ml	Vivascience

## 4.2 Molecular biological techniques

### 4.2.1 Analytical plasmid preparation

3 ml LB medium containing the appropriate antibiotic were inoculated with a single bacterial colony from a selective agar plate and incubated for 12-16 h at 37°C and 250 rpm. 1.5 ml of the culture were pelleted by centrifugation (20 sec, 14500xg, RT) and resuspended in 100 µl buffer P1 (50 mM Tris/HCl pH 8.0, 10 mM EDTA, 100 µg/ml RnaseA). 100 µl of buffer P2 (1 % SDS, 0.2 M NaOH) and 100 µl of chilled buffer P3 (3,0 M potassium acetate, pH 5.5) were added, each buffer addition followed by a cautious mixing step. The samples were centrifuged (5 min, 14500xg, RT) and 300 µl of isopropanol were added to the supernatant followed by 5 min incubation at room temperature. The plasmid DNA was then pelleted by centrifugation (10 min, 14500xg, RT), washed in 500 µl ethanol (70 %) and again centrifuged (5 min, 14500xg, RT). The dried pellet was dissolved in 20 µl TE buffer.

### 4.2.2 Preparative plasmid preparation

For plasmid isolation in preparative scale the 'Qiagen plasmid Kit Midi' was used according to the manufacturers instructions.

A starter culture was generated by incubating 3 ml LB medium (200 µg/ml carbenicillin) inoculated with single bacterial colony from a selective agar plate for 12-16 h at 37°C and 250 rpm. 200 µl of the starter culture were diluted in 100 ml LB medium (200 µg/ml carbenicillin) and again incubated for 12-16 h at 37°C and 250 rpm. The culture was centrifuged (15 min, 6000xg, 4°C) and the bacterial pellet resuspended in 4 ml buffer P1 (50 mM Tris/HCl pH 8.0, 10 mM EDTA, 100 µg/ml RnaseA). After the addition of 4 ml buffer P2 (1 % SDS, 0.2 M NaOH) and cautious mixing the bacterial lysis was allowed to proceed for 5 min at room temperature. Then 4 ml of chilled buffer P3 (3,0 M potassium acetate, pH 5.5) were added, the sample was again cautiously mixed, incubated on ice for 15 min and centrifuged (30 min, 20000xg, 4°C). The supernatant instantly was applied to a QIAGEN-Tip 100 column equilibrated in buffer QBT (750 mM NaCl, 50 mM MOPS pH 7.0, 15% isopropanol, 0.15% (v/v) TritonX-100). After two washing steps with 10 ml buffer QC (1 M NaCl, 50 mM MOPS pH 7.0, 15% isopropanol) the bound plasmid DNA was eluted in 5 ml buffer QF (1.25 M NaCl, 50 mM Tris-HCl pH 8,5, 15% isopropanol) and 3.5 ml isopropanol were added to the eluent. After centrifugation (30 min, 20000xg, 4°C) the pelleted DNA was washed in 2 ml ethanol (70 %) and recentrifuged (15 min, 20000xg, 4°C). The dried DNA pellet was dissolved in 200 µl TE buffer and stored at -20°C. The DNA concentration was determined as described in 4.2.4.

### 4.2.3 Agarose gel electrophoresis of DNA

DNA samples were diluted in 2xGEBS and separated on horizontal agarose gels (0.6 to 1.5 % agarose in TBE buffer). Electrophoresis was performed at 5 V/cm in TBE buffer. The DNA was detected after staining in ethidium bromide (50 µg/ml) at 302 nm. For documentation the 'Easy Enhanced Analysis System' (Herolab) was used.

#### 4.2.4 Determination of DNA concentrations

DNA concentrations were determined photometrically and calculated from the absorbance measured at 260 nm:  $c(\text{DNA}) = \text{absorbance}(260 \text{ nm}) \times 50 \mu\text{g/ml}$ . Very low DNA concentrations were estimated by comparing the signal intensity obtained on ethidium bromide stained agarose gels with known concentrations of  $\lambda$ -HindIII-marker.

#### 4.2.5 Restriction digest of DNA

Restriction enzymes and reaction buffers were used according to the manufacturers instructions. For preparative digests 2-5  $\mu\text{g}$  of DNA were incubated with 5-20 U of enzyme for 60-120 min at 37°C while the added volume of enzyme solution never exceeded 10 % of the total sample volume. For analytical digests 5  $\mu\text{l}$  of plasmid DNA (4.2.1) were incubated for 30 min at 37°C with 2-5 U of enzyme.

#### 4.2.6 Dephosphorylation of DNA

The 5'-phosphate groups of linearised vector DNA were removed to avoid self-ligation of the vector fragments. Per  $\mu\text{g}$  of vector DNA 1 U of calf intestine alkaline phosphatase (NEB) was directly added to the restriction mix.

#### 4.2.7 Isolation of DNA fragments form agarose gels

To isolate DNA fragments after restriction digest, DNA was separated on an agarose gel (4.2.3) and the desired fragments were excised from the gel. For further DNA purification the 'Qiaquick PCR Purification Kit' (Qiagen) was used according to the manufacturers instructions. The gel slice was completely dissolved in 300  $\mu\text{l}$  buffer QG per 100 mg gel at 50°C and applied to a Qiaquick column. After one washing step with 500  $\mu\text{l}$  buffer PE bound DNA was eluted in 30  $\mu\text{l}$  EBC (10 mM Tris-Cl pH 8,5). Sample and buffer applications were mediated by centrifugation (60 sec, 14500xg, RT) of the column.

#### 4.2.8 Ligation of DNA

20 fmol of digested and dephosphorylated vector DNA and 100 fmol of the respective insert were incubated with 1 Weiss-U of T4-DNA-Ligase (NEB) in 20  $\mu$ l ligation buffer (50 mM Tris-HCl pH 7.8, 10 mM MgCl<sub>2</sub>, 1 mM ATP, 10 mM DTT, 25  $\mu$ g/ml BSA). The ligation mix was either incubated for 2 h at RT or overnight at 16°C and transformed into competent *E. coli* cells.

#### 4.2.9 Preparation of CaCl<sub>2</sub>-competent *E. coli*

100 ml SOB medium were inoculated with 5 ml of an overnight starter culture and grown at 37°C and 250 rpm to an optical density of OD<sub>600</sub> = 0.5. The culture was incubated on ice for 10 min and centrifuged (10 min, 4000xg, 4°C). The bacterial pellet was carefully resuspended in 30 ml of ice-cold TB (10 mM MES pH 6.7, 15 mM CaCl<sub>2</sub>, 250 mM KCl, 55 mM MnCl<sub>2</sub>), incubated for 10 min on ice and centrifuged (10 min, 4000xg, 4°C). The pellet was again carefully resuspended in 8.6 ml TB including 0.6 ml DMSO and aliquots of 200  $\mu$ l were flash frozen in liquid nitrogen and stored at -80°C. This protocol was used to prepare competent *E. coli* of the strains DH5 $\alpha$ , JM109, XL1Blue, BL21(DE3) and BL834(DE3). To prepare competent *E. coli* DH10Bac, 50  $\mu$ g/ml kanamycin and 10  $\mu$ g/ml tetracycline were added to the SOB-medium.

#### 4.2.10 Transformation of competent *E. coli*

50-200  $\mu$ l of competent *E. coli* were thawed on ice and 10 ng of plasmid DNA or 10  $\mu$ l of ligation mix (4.2.8) were added. The mix was left on ice for 15 min, subjected to a 45 sec heat shock at 42°C and incubated on ice for another 15 min. 500  $\mu$ l of LB-medium was added, the cell suspension was incubated at 37°C for 30 min and plated on selective LB-agar plates containing the appropriate antibiotics.

### 4.2.11 Polymerase chain reaction (PCR)

To amplify DNA-fragments by PCR reaction, 10-50 ng of plasmid DNA, sense and antisense primer (100 pmol each), 5 U *Pfu*-polymerase (Stratagene) and dNTP's (20  $\mu$ M each) were mixed in a total volume of 100  $\mu$ l 1xPCR buffer (Stratagene). The PCR-mix was incubated in a Thermocycler for 25-30 of the following cycles: 45 sec at 94°C to denature double stranded DNA, 60 sec to anneal the oligonucleotide primers (5°C below their calculated melting point) and elongation at 72°C for 120 sec per kb of synthesis product. In the last cycle the elongation step was extended to 10 min. PCR reaction were either performed using the 'GeneAmp System 2400' (Perkin Elmer) or the 'T1-Thermocycler' (Biometra).

### 4.2.12 Site-directed mutagenesis

To generate mutant recombinant proteins by site-directed mutagenesis a protocol derived from the 'QuikChange<sup>TM</sup> Site-Directed Mutagenesis Kit' (Stratagene) was used. Mutations are site-specifically introduced by a mutant sense/antisense primer pair that is used to amplify the complete plasmid in a PCR-reaction. Methylated template DNA is then digested by *DpnI* and the mutated synthesis product is transformed in competent *E. coli* cells.

50 ng of template DNA, mutant sense and antisense primer (10 pM each), 5 U *Pfu*-polymerase (Stratagene) and dNTP's (20  $\mu$ M each) were mixed in a total volume of 50  $\mu$ l 1xPCR buffer (Stratagene). The PCR-reaction was performed as described in 4.2.11 for a total of 16 cycles. 10 U of *DpnI* were added and the sample was incubated for 1 h at 37°C. 2  $\mu$ l of the sample were transformed in competent *E. coli* cells as described in 4.2.10. Introduction of the correct mutations was confirmed by DNA sequencing.

## 4.3 Cell biological techniques

### 4.3.1 Cultivation of CHO cells

Chinese hamster ovary (CHO) cells were kept in a humidified incubator at 37°C and 5 % CO<sub>2</sub>. Cells were cultured in DMEM/HAM's F12 medium (Biochrom) supplemented with 1 mM sodium pyruvate and 5 % fetal calf serum (FCS). Confluent cell layers were treated with PBS/EDTA to detach the cells from the culture vessel and diluted 1:10 in fresh medium.

For long term storage in liquid nitrogen, cells were pelleted by centrifugation (5 min, 200xg, RT) and resuspended in culture medium containing 20 % FCS and 10 % DMSO at a concentration of  $1 \times 10^7$  cells/ml. Aliquots of 1 ml were filled in cyro vials, stored overnight at  $-80^\circ\text{C}$  and then transferred to liquid nitrogen.

To recover frozen cell pellets, they were kept on dry ice for 5-10 min, thawed in a water bath at  $37^\circ\text{C}$  and diluted by drop wise addition of culture medium containing 10 % FCS. After centrifugation (5 min, 200xg, RT) the cell pellet was again resuspended in culture medium (10 % FCS) and transferred to culture vessels.

### 4.3.2 Transfection of CHO cells

For transient transfection of CHO cells  $2 \times 10^6$  cells were seeded in 90-mm culture vessels and cultivated over night as described in 4.3.1. A transfection mix was prepared by diluting 4  $\mu\text{g}$  of plasmid DNA and 24  $\mu\text{l}$  of Lipofectamine in 400  $\mu\text{l}$  OptiMEM (Invitrogen) each. Both dilutions were combined and incubated for 15-30 min at RT.

The CHO cell layer (70-80 % confluent) was washed twice in PBS and incubated with freshly prepared transfection mix diluted with 3.2 ml OptiMEM for 6 h. The transfection was stopped by the addition of 4 ml DMEM/HAM's F12 medium (Biochrom) supplemented with 1 mM sodium pyruvate and 10 % fetal calf serum (FCS). The medium was replaced 24 h after begin of the transfection with 8 ml culture medium containing 5 % FCS and cells were cultivated for another 48 h.

### 4.3.3 Cultivation of *Sf9* cells

Suspension cultures of *Spodoptera frugiperda* (*Sf9*) cells were cultivated at  $27^\circ\text{C}$  and 100 rpm in Sf900-II SFM medium (Invitrogen). Cell density was maintained between  $0.5 \times 10^6$  and  $8 \times 10^6$  cells per millilitre by diluting dense cultures in fresh medium.

For long term storage in liquid nitrogen, cells were pelleted by centrifugation (5 min, 200xg, RT) and resuspended in the conditioned culture medium containing 10 % DMSO at a concentration of  $1 \times 10^7$  cells/ml. Aliquots of 1 ml were filled in cyro vials and cooled down by

subsequent incubations at 4°C and -20°C for 1 h each. Cells were stored overnight at -80°C and then transferred to liquid nitrogen.

To recover frozen cell pellets, they were kept on dry ice for 5-10 min, thawed in a water bath at 37°C and directly added to 30 ml culture medium in a culture vessel.

#### **4.3.4 Generation of recombinant baculoviruses**

Recombinant baculoviruses were generated on basis of transposon-mediated recombination (Luckow *et al.*, 1993) in *E. coli* DH10Bac cells (Invitrogen) using pFastBac baculovirus transfer vectors.

##### **4.3.4.1 Preparation of recombinant bacmid DNA**

100 µl of competent *E. coli* DH10Bac were thawed on ice and incubated for 30 min with 20 ng of the respective pFastBac vector construct. The transformation mix was subjected to a heat shock at 42°C for 45 sec and incubated on ice for another 2 min. 900 µl of SOC-medium were added, the cell suspension was incubated at 37°C for 4 h and plated on selective LB-agar plates containing 50 µg/ml kanamycin, 7 µg/ml gentamicin, 10 µg/ml tetracycline and 40 µg/ml IPTG. For blue-white screening additionally 30 µl of BlueGal solution (20 mg/ml in DMSO) was spread on the plates prior to plating. Positive transformants were identified after 48 h incubation at 37°C as purely white colonies and restreaked on fresh plates to confirm the white phenotype. 5 ml LB-medium containing 50 µg/ml kanamycin, 7 µg/ml gentamicin and 10 µg/ml tetracycline was inoculated with a positive colony and incubated overnight at 37°C and 250 rpm. Bacmid DNA was isolated using the ‘Concert High Purity Pasmid Kit’ (Invitrogen) according to the manufacturers instructions. Briefly, 3 ml of bacterial culture were pelleted (1 min, 14500xg, RT), resuspended in 0.4 ml buffer ‘E1’ and lysed for 5 min at RT after addition of 0.4 ml buffer ‘E2’. 0.4 ml neutralisation buffer ‘E3’ was added, the samples were centrifuged (10 min, 14500xg, RT) and the supernatant was applied to ‘Concert HP’ columns equilibrated in buffer ‘E4’. After two washings steps with 2.5 ml buffer E5 bound bacmid DNA was eluted in 0.9 ml buffer ‘E6’. 0.63 ml isopropanol were added to the eluent and the pelleted DNA (30 min, 14500xg, 4°C) was washed in 1 ml ethanol (70 %) and recentrifuged (15 min, 20000xg, 4°C). The bacmid DNA pellet was airdried for 10 min, dissolved in 50 µl TE and used for transient transfections of *Sf9* cells (4.3.4.2).

#### 4.3.4.2 Production of recombinant baculoviruses and high-titer virus stocks

Baculoviruses were produced by transfecting the prepared recombinant bacmid DNA (4.3.4.1) into *Sf9* cells.  $1 \times 10^6$  log-phase *Sf9* cells were seeded in 2 ml culture medium per well of a 6-well tissue culture plate. The cells were allowed to attach to the culture plate for 1 h at 27°C. In the meantime a transfection mix was prepared by diluting 5 µl of the bacmid DNA prep and 6 µl of Cellfectin in 100 µl Sf900-II medium (Invitrogen) each. Both dilutions were combined and incubated for 30 min at RT.

The medium was aspirated from the adhered *Sf9* cells and replaced with transfection mix diluted in 1 ml Sf900-II medium. The transfection mix was removed after 12 h and replaced with 2 ml culture medium. The transfected cells were incubated at 27°C for 4-8 days until signs of viral infection like enlarged cell diameters and a granular appearance of the cells were clearly visible.

The supernatant (low-titer P1-stock) was harvested and stored at -80°C. For virus amplification  $2 \times 10^6$  *Sf9* cells were seeded in 4 ml in a 25 cm<sup>2</sup> cell culture bottle and infected with 40 µl of the P1-stock. The P2-stock was harvested after 4 days, sterile filtered and stored at -80°C. Large P3-stocks were obtained by infecting 50 ml suspension cultures ( $2 \times 10^6$  cells/ml) with 100 µl of the P2-stock. The virus stock was harvested after 48 h. Cells were pelleted by centrifugation (5 min, 500xg, RT), the supernatant was sterile filtered and stored at 4°C.

#### 4.3.5 Baculoviral expression of ST8SiaIVΔ25 in *Sf9* cells

For baculoviral expression of recombinant ST8SiaIVΔ25 log-phase *Sf9* cells at a density of  $2 \times 10^6$  cells/ml were infected with the respective high titer virus stock and grown for 72 h at 27°C and 150 rpm before the culture supernatant was harvested (700xg, 10 min, 4°C). The dose of baculovirus required for optimal expression was tested for each lot of high titer stocks in small scale test expressions. 30 ml suspension cultures of *Sf9* cells at a density of  $2 \times 10^6$  cells/ml were infected with different amounts of the viral stock (from 30 µl to 300 µl). Culture supernatants were assayed for protein expression by SDS-PAGE (4.4.2) and Western blot analysis (4.4.5) 72 h after infection and the optimal of dose viral stock per millilitre of expression culture was used for further large scale expressions.



## **4.4 Biochemical techniques**

### **4.4.1 Protein estimation**

Protein concentrations were estimated using the 'BCA Protein Assay Reagent' (Pierce) according to the manufacturers instructions. Briefly, reagents A and B were mixed 50:1 immediately before use. 200 µl of the mixture were added to 10 µl sample and incubated at 55°C for 30 min in 96-well microtiter plates. As reference, samples with known BSA concentrations were included. The absorbance of all samples was measured at 540 nm using the ELISA-Reader 'DigiScan' (Asys Hitech) and protein concentrations were calculated from the BSA standard curve.

### **4.4.2 Polyacrylamide gelelectrophoresis (SDS-PAGE)**

SDS-PAGE was performed according to Laemmli (Laemmli, 1970). Protein samples were separated on SDS-polyacrylamide gels composed of a 3 % stacking gel (125 mM Tris/HCl pH 6.8, 0.1 % SDS, 3 % polyacrylamide) and a 7-14 % separating gel (375 mM Tris/HCl pH 8.8, 0.1 % SDS, 7-14 % polyacrylamide). Gels were prepared by mixing buffer, SDS and the acrylamide stock solution (37,5 % acrylamide, 1 % bisacrylamide) and polymerisation was initiated by adding 0,1 % TEMED and 1 % ammonium persulphate. Samples were mixed with 2xLaemmli-buffer and either heated to 95 °C for 5 min or to 60 °C for 20 min if they contained heat-labile polysialic acid. Electrophoresis was performed in SDS-electrophoresis buffer (50 mM Tris, 350 mM glycine, 0.1 % SDS) at 70 V (stacking gel) and 140 V (separating gel), respectively.

### **4.4.3 Coomassie staining of polyacrylamide gels**

For Coomassie staining of protein gels, the colloidal staining solution Roti<sup>®</sup>-Blue (Roth) was used. The gels were directly after electrophoresis (4.4.2) incubated overnight in 50 ml 1xRoti<sup>®</sup>-Blue in 20 % methanol, destained for 1 h in 25 % methanol and dried after 1 h incubation in drying-buffer (20 % ethanol, 10 % glycerol).

#### 4.4.4 Silver staining of polyacrylamide gels

For silver staining the gels were directly after electrophoresis incubated for 1 h or overnight in fixing solution (30 % ethanol, 10 % acetic acid, 1.85 % formaldehyde). After two washing steps (20 min, 50 % ethanol) the gels were incubated for exactly 1 min in thiosulphate solution (20 mg/100 ml), washed three times for 20 sec in deionised water and incubated for 20 min in staining solution (0.2 % (w/w) AgNO<sub>3</sub>, 2.8 % formaldehyde). After two washing steps in deionised water for 20 sec, the gels were incubated in freshly prepared developer solution (6 % (w/w) NaCO<sub>3</sub>, 2 % (v/v) thiosulphate solution, 1.85 % formaldehyde) until protein bands were lighting up. The reaction was stopped by transferring the gels to stop solution (30 % ethanol, 10 % acetic acid) and gels were dried after 1 h incubation in drying-buffer (20 % ethanol, 10 % glycerol).

#### 4.4.5 Western Blotting

By SDS-PAGE separated proteins were transferred to nitrocellulose membranes using a *semidry* blotting chamber (Biometra) at 2 mA/cm<sup>2</sup> for 1 h. Gel and membrane were placed between two layers of *Whatman* filter paper soaked in blotting buffer (48 mM Tris, 39 mM glycine). To check the transfer efficiency and to label the bands of the molecular weight standard, the membrane was reversibly stained in Ponceau S-solution (0.2 % (w/v) Ponceau S in 3 % TCA) and destained in deionised water and PBS.

#### 4.4.6 Immunostaining of Western Blots

The nitrocellulose membranes were incubated for 1 h at RT or at 4°C overnight in blocking solution (2 % drymilk in PBS, 0.02 % NaN<sub>3</sub>). After two washing steps for 5 min in PBS the membranes were incubated for 1 h with the primary antibodies in blocking solution (9E10: 5 g/ml, anti-T7 (Novagen): 1 µg/ml), washed again twice for 5 min in PBS and were finally incubated for 30 min with alkaline phosphatase-conjugated secondary antibody (1:2000, Dianova) in blocking solution. For colour development membranes were rinsed twice in PBS, once in AP-buffer (100 mM Tris-HCl pH 9.5, 100 mM NaCl, 5 mM MgCl<sub>2</sub>) and stained with BCIP/NBT solution (0.3 mg/ml NBT, 0.15 mg/ml BCIP in AP-buffer).

#### 4.4.7 Covalent coupling of mAb 9E10 to protein G-sepharose

For covalent coupling 20 mg of purified mAb 9E10 (4.4.10) were incubated for one hour at RT with 5 ml protein G-sepharose matrix. The bead were washed twice in 50 ml sodium borate (0.2 M, pH 9.0) by centrifugation (5 min, 10.000xg, 4 °C), resuspended in 50 ml sodium borate (0.2 M, pH 9.0) and the coupling reaction was started by addition of 5.184 mg/ml dimethylpimelimidate (solid). The reaction was stopped after 30 min by washing the beads once in 50 ml ethanolamine (0.2 M, pH 8.0) by centrifugation (5 min, 10.000xg, 4 °C). The beads were resuspended in 50 ml ethanolamine (0.2 M, pH 8.0), incubated at RT for 2 h and after a final washing step resuspended in 10 ml PBS (0.02 % NaN<sub>3</sub>). The efficiency of the coupling reaction was checked by Coomassie stained SDS-PAGE.

#### 4.4.8 Expression of recombinant proteins in *E. coli*

For bacterial expression of recombinant proteins the pET-vector system (Novagen) was used. 30 – 1000 ml cultures of *E. coli* BL21(DE3) transformed with the respective expression plasmids (4.2.10) were grown in LB medium (200 µg/ml carbenicillin) at 37 °C and 250 rpm to an optical density of OD<sub>600</sub>=0.6. The cultures were induced with 1 mM IPTG and harvested after 2 h by centrifugation (15 min, 6000xg, 4 °C). The bacterial pellet was stored at –20 °C.

#### 4.4.9 Preparation of soluble and insoluble *E. coli* fractions

For analytical preparations bacterial pellets obtained from 1 ml of expression culture (...) were resuspended in 100 µl TE buffer, 10 µg of lysozyme was added and the samples were incubated at 37 °C for 15 min. After sonification in a beaker resonator (Branson, 50 % duty cycle, level 5) for 2 min at 4 °C the soluble (supernatant) and insoluble fractions (pellet) were separated by centrifugation (15 min, 14500xg, 4 °C).

For large scale preparative set-ups the bacterial pellets obtained from 0.5 l expression culture were resuspended in 5 ml buffer A (10 mM Tris/HCl pH 8.0, 300 mM NaCl) and the protease inhibitors bestatin (40 µg/ml), PMSF (1 mM) and pepstatin (4 µg/ml) were added. The bacteria were lysed by sonification (Branson sonifier, 100% duty cycle, level 5) for 30 sec on

ice. The procedure was repeated 6 times with a break of 30 sec between the repeats. After centrifugation (15 min, 14500xg, 4 °C) the supernatant was filtered (Millex-GP, 0.22 µm) and applied to subsequent purification steps (4.4.13)

#### **4.4.10 Purification of mAb 9E10**

The monoclonal antibody 9E10 was purified from the culture supernatant of hybridoma cells by protein G-affinity chromatography. 500 ml of cell culture supernatant stored at -20 °C were thawed at 4 °C, filtered (cellulose acetate filter, 0.8 µm) and applied with a flow-rate of 2 ml/min to a protein G-sepharose affinity column (5 ml column volume) at 4 °C. The column was washed with 10 column volumes of PBS and 10 column volumes of wash buffer (20 mM sodium phosphate pH 7.0). Bound antibody was eluted in an acid step (100 mM glycine, pH 2.7), immediately supplemented with 300 mM NaCl and adjusted to pH 7.5 with neutralising buffer (1 M Tris/HCl pH 9.0). All buffers were filtered (cellulose acetate filter, 0.8 µm) prior to use.

#### **4.4.11 Purification of protein A-NCAM**

Recombinant protein A-NCAM was purified from the culture supernatant of stably transfected CHO-2A10 cells by IgG-affinity chromatography. 55 ml of cell culture supernatant stored at -20 °C were thawed at 4 °C, filtered (cellulose acetate filter, 0.8 µm) and applied at 4 °C with a flow-rate of 1 ml/min to an IgG-sepharose affinity column (column volume: 1 ml). The column was washed with 15 ml buffer A (10 mM MES pH 6.8, 100 mM NaCl) and bound protein A-NCAM was eluted in an acid step (100 mM glycine, pH 2.7). The eluent was immediately supplemented with 200 mM NaCl and adjusted to pH 7.5 with neutralising buffer (1 M Tris/HCl pH 9.0). All buffers were filtered (cellulose acetate filter, 0.8 µm) prior to use. The protein solution was concentrated to 80 µg/ml using a 'VivaSpin' centrifugal device (Vivascience, 3000xg, 4 °C) and stored at 4 °C.

## 4.4.12 Purification of ST8SiaIV $\Delta$ 25

### 4.4.12.1 Myc-affinity chromatography

Recombinant ST8SiaIV carrying a myc-His<sub>6</sub>-epitope at the C-terminal end was purified from the culture supernatant of baculovirus infected *Sf9* cells by myc-affinity chromatography. The affinity matrix was generated as described in 4.4.7 by covalent coupling of mAb9E10 to protein G-sepharose (Amersham Biosciences). 500 ml of harvested *Sf9* cell culture supernatant (4.3.5) were centrifuged (25 min, 7000xg, 4 °C), filtered (cellulose acetate filter, 0.8  $\mu$ m) and applied to the myc- affinity column (column volume: 2 ml) with a flow-rate of 1 ml/min at 4 °C. The column was washed with 45 ml buffer A (20 mM sodium phosphate pH 7.5, 500 mM NaCl) and 25 ml buffer B (20 mM sodium phosphate pH 7.5). Bound enzyme was eluted in an acid step with elution buffer and immediately or stepwise adjusted to pH 7.5 with neutralising buffer (1 M Tris/HCl pH 9.0). As elution buffers 100 mM glycine (pH 2.7-4) and 100 mM citric acid (pH 3-5) were tested. All buffers were filtered (cellulose acetate filter, 0.8  $\mu$ m) prior to use.

### 4.4.12.2 Ni<sup>2+</sup>-chelating chromatography

As the acidic elution conditions required for myc-affinity purification of ST8SiaIV $\Delta$ 25 (4.4.12.1) resulted in partially denatured protein, a procedure for purification by Ni<sup>2+</sup>-chelating chromatography was established and carefully optimised. 1000 ml culture supernatant of baculovirus infected *Sf9* cells (4.3.5) were centrifuged (25 min, 7000xg, 4 °C), filtered (Millipore, 0.22  $\mu$ m) and concentrated to 100 ml using VivaFlow50 crossflow filtration units (PES membrane, 10 kDa MWCO) at 4 °C. To exchange the buffer and remove small molecular binding inhibitors, the concentrate was refilled with buffer A (20 mM MES pH 6.8, 75 mM NaCl) to 400 ml, concentrated again to 100 ml, once more refilled to 300 ml with buffer A (20 mM MES pH 6.8, 75 mM NaCl) and finally concentrated to 80 ml. The concentrated sample was filtered (Millipore, 0.22  $\mu$ m) and after addition of 10 % glycerol incubated overnight at 4°C with 1 ml 'ProBond' Ni<sup>2+</sup>-matrix (Invitrogen). The following washing and elution steps were performed at room temperature using an 'Äkta FPLC system' (Amersham Biosciences) at a flow rate of 2 ml/min if not otherwise indicated. All buffers were filtered (cellulose acetate filter, 0.8  $\mu$ m) and degassed prior to use. The resin was subsequently washed with 15 ml buffer B (20 mM MES pH 6.8, 750 mM NaCl, 10 % glycerol, 20 mM imidazole) and 10 ml buffer C (20 mM MES pH 6.8, 75 mM NaCl, 10 % glycerol, 20 mM imidazole). The histidine-tagged protein was eluted in a linear imidazole

gradient (20-400 mM) composed of buffer C and buffer D (20 mM MES pH 6.8, 75 mM NaCl, 10 % glycerol, 400 mM imidazole). 1 ml fractions were collected throughout the purification. Peak fractions were pooled and immediately subjected to a desalting column (HiPrep 26/10, Amersham Biosciences) equilibrated in buffer A (20 mM MES pH 6.8, 75 mM NaCl), to remove the imidazole from the protein samples. The column was eluted with buffer A at a flow rate of 3 ml/min. Protein fractions were pooled, concentrated to 3 mg/ml using 'VivaSpin' centrifugal devices (Vivascience, 3000xg, 4 °C) and either flash frozen in liquid nitrogen or further purified by gel filtration.

#### 4.4.12.3 Size exclusion chromatography

Recombinant ST8SiaIV $\Delta$ 25 purified by Ni<sup>2+</sup>-chelating chromatography (4.4.12.2) was subjected to size exclusion chromatography for further purification. 300  $\mu$ l of protein sample (3 mg/ml) were applied to a Superdex 200 HR 10/30 gel filtration column (Amersham Biosciences) equilibrated in buffer A (10 mM MES pH 6.8, 100 mM NaCl) and eluted at a flow rate of 0.75 ml/min (Äkta FPLC, Amersham Biosciences). The buffer was filtered (cellulose acetate filter, 0.22  $\mu$ m) and degassed prior to use. Fractions of 1 ml were collected throughout the purification and analysed by silver stained SDS-PAGE. ST8SiaIV $\Delta$ 25 containing fractions were pooled and concentrated to 2 mg/ml in 'VivaSpin' centrifugal devices (Vivascience, 3000xg, 4 °C). The concentrated samples were flash frozen in liquid nitrogen and stored at -80 °C.

### 4.4.13 Purification of the N- and C-terminal fragment of endoNF

#### 4.4.13.1 Ni<sup>2+</sup>-chelating chromatography

Recombinant endoNF carrying a StrepII-tag at the N-terminus and a His<sub>6</sub>-tag at the C-terminus was expressed in *E. coli* BL21(DE3). The lysate (4.4.9) obtained from 1 l expression culture (4.4.8) was applied to a 5 ml HiTrap Chelating column (Amersham Biosciences, 2 ml/min). The following washing and elution steps were performed at room temperature at a flow rate of 2 ml/min (Äkta FPLC, Amersham Biosciences) with filtered (cellulose acetate filter, 0.8  $\mu$ m) and degassed buffers. The column was washed with 15 ml buffer A (10 mM Tris/HCl pH 8.0, 300 mM NaCl) and eluted in two subsequent linear imidazole gradients from 0-100 mM and from 100-500 mM imidazole. 1 ml fractions were collected throughout the purification. The peak fractions of the first elution step containing the N-

terminal fragment were pooled and further purified by StrepII-affinity. The pooled fractions of the second elution step containing the His<sub>6</sub>-tagged C-terminal fragment were subjected to gelfiltration for further purification.

#### 4.4.13.2 StrepII-affinity chromatography

After separation of N- and C-terminal fragment of endoNF by Ni<sup>2+</sup>-chelating chromatography (4.4.13.1), the pool containing the N-terminal fragment was applied to a 5 ml StrepTactin affinity column (IBA) at a flow rate of 2 ml/min. The column was connected to the FPLC system (Äkta, Pharmacia), washed with 30 ml buffer W (100 mM Tris/HCl pH 8.0, 150 mM NaCl, 1 mM EDTA) and bound protein was eluted in a desthiobiotin step with buffer E (100 mM Tris/HCl pH 8.0, 150 mM NaCl, 1 mM EDTA, 2.5 mM desthiobiotin). Washing and elution step were performed at a flow rate of 2 ml/min. Protein containing fractions were pooled, subjected to a desalting column (HiPrep 26/10, Amersham Biosciences) equilibrated in buffer K (10 mM Tris/HCl pH 7.5, 100 mM NaCl) and eluted at a flow rate of 3 ml/min. Protein fractions were pooled, concentrated to 7 mg/ml using 'VivaSpin' centrifugal devices (Vivascience, 3000xg, 4 °C) and flash frozen in liquid nitrogen for storage at -80 °C. All elution and washing buffers were filtered (cellulose acetate filter, 0.8 µm) and degassed. The StrepTactin column was regenerated in two subsequent steps with buffer R (100 mM Tris/HCl pH 8.0, 150 mM NaCl, 1 mM EDTA, 1 mM hydroxyl-azophenyl-benzoic acid) and buffer W. Purifications from more than 500 ml expression culture exceeded the binding capacity of the StrepTactin column and the procedure was repeated with the flow through of the first run.

#### 4.4.13.3 Size exclusion chromatography

The pool containing the C-terminal fragment after Ni<sup>2+</sup>-chelating chromatography (4.4.13.1) was concentrated to 8 mg/ml in 'VivaSpin' centrifugal devices (Vivascience, 3000xg, 4°C). Half of the sample (250 µl) was subjected to a Superdex 200 HR 10/30 gelfiltration column (Amersham Biosciences) equilibrated in filtered (cellulose acetate filter, 0.22 µm) and degassed buffer A (10 mM MES pH6.8, 100 mM NaCl) and eluted at a flow rate of 0.5 ml/min (Äkta FPLC, Amersham Biosciences). The procedure was repeated with the second half of the sample. Fractions of 1 ml were collected throughout the purification and analysed by Coomassie stained SDS-PAGE. Fractions of the main peak were concentrated to 12 mg/ml ('VivaSpin', 3000xg, 4°C), flash frozen in liquid nitrogen and stored at -80°C.

#### 4.4.14 Expression and purification of selenomethionine derivatised endoNF

For the expression of selenomethionine derivatives the methionine auxotroph *E. coli* strain B834(DE3) was used. A 5 ml starter culture of *E. coli* B834(DE3) transformed with the respective expression plasmid (4.2.10) was grown over night in LB medium (200 µg/ml carbenicillin, 37 °C, 250 rpm). The bacteria were pelleted (10 min, 3000xg, 4 °C) and resuspended in 500 ml M9-medium (200 µg/ml carbenicillin) supplemented with 50 mg/l L-methionine. The culture was grown at 37 °C and 250 rpm to an optical density of OD<sub>600</sub> = 0.5 and centrifuged (15 min, 3000xg, 4 °C). The bacterial pellet was resuspended in 500 ml M9-medium (200 µg/ml carbenicillin) without methionine supplementation and the culture was incubated at 37 °C and 250 rpm for 20 min to exhaust intracellular methionine reservoirs. 50 mg/l D-/L-selenomethionine was added and expression was induced after 30 min with 1 mM IPTG. The bacteria were harvested after 3 h by centrifugation (10 min, 5000xg, 4 °C) and the pellet was stored at -20 °C.

For purification of the recombinant protein the bacteria were lysed as described in chapter 4.4.9. To avoid oxidation of the selenomethionine 10 mM DTT was added to buffer A. The N-terminal fragment of endoNF was then purified by StrepII-affinity chromatography as described in chapter 4.4.13.2 followed by Ni<sup>2+</sup>-chelating chromatography (4.4.13.1). After addition of 10 mM DTT the protein pool was applied to a desalting column (HiPrep 26/10, Amersham Biosciences) equilibrated in buffer K (10 mM Tris/HCl pH 7.5, 100 mM NaCl, 10 mM DTT) and eluted at a flow rate of 2 ml/min. Protein fractions were pooled, concentrated to 14 mg/ml using 'VivaSpin' centrifugal devices (Vivascience, 3000xg, 4 °C) and flash frozen in liquid nitrogen for storage at -80 °C.

#### 4.4.15 ELISA-based polysialyltransferase assay

The ELISA-based assay system (Stummeyer, 2000) schematically shown in Figure 6 is highly sensitive and reliable. The solid phase fixation of the enzymes allows the detection of polysialyltransferase activity directly from polysialyltransferase containing cell culture supernatants. Autopolysialylation can be measured separately, while the NCAM-polysialylation signal results from polySia synthesized on both NCAM and enzyme. If, however, purified enzymes are used as enzyme source, also separate detection of NCAM-polysialylation is enabled as the enzymes can be added in solution.



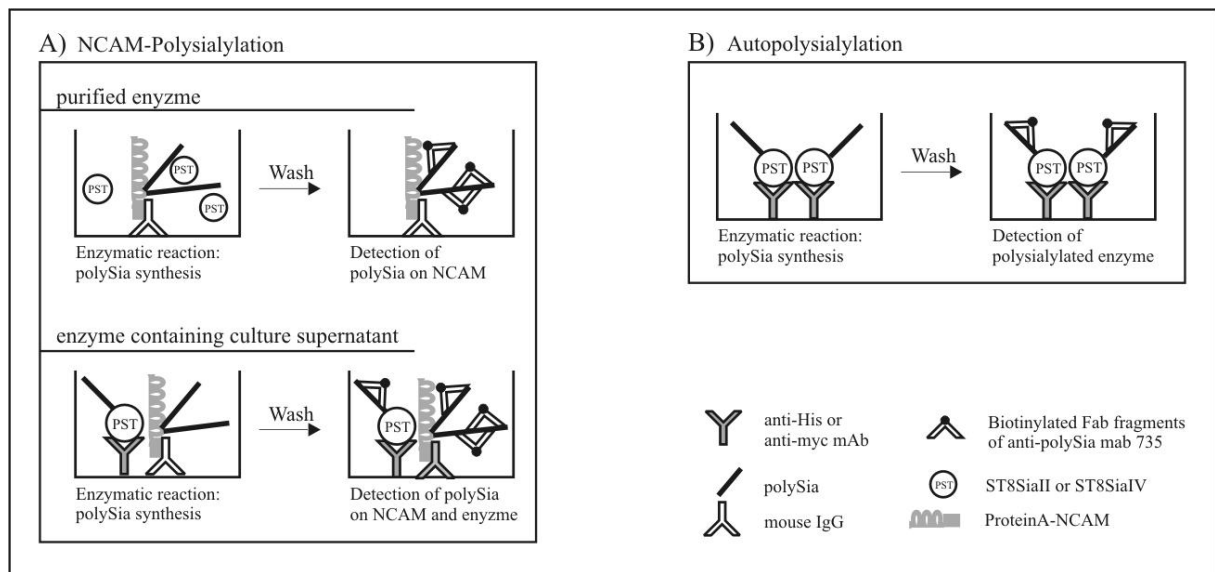


**Figure 6: Schematic representation of the ELISA-based polysialyltransferase assay**

For solid phase fixation of enzyme and the polySia acceptor NCAM, 96-well microtiter plates (Greiner) were coated with 20 µl/well of mAb 9E10 (5 µg/ml) diluted in PBS for 1 h at RT. Alternatively also the penta-His antibody (Qiagen) was used at 1 µg/ml. After blocking with 200 µl blocking solution (1 % BSA in PBS) for 1 h and two washing steps with PBS, the plates were incubated with 25 µl/well protein A-NCAM containing cell culture supernatant of transfected CHO-2A10 cells (4.3.2) for 1 h at RT. The plates were washed twice with PBS and the recombinant polysialyltransferase was adsorbed to the wells by incubation with enzyme containing culture supernatant of baculovirus infected *Sf9* cells (25 µl/well, 1 h, RT). To measure exclusively autopolysialylation the incubation step with protein A-NCAM was omitted. After washing twice with PBS and once with reaction buffer (10 mM sodium cacodylate pH 6.5, 10 mM MgCl<sub>2</sub>), the enzyme reactions were initiated by addition of 25 µl reaction buffer containing 2 mM CMP-Neu5Ac and allowed to proceed for 3 h at 37 °C. The reaction was stopped by washing the plates twice with PBS and synthesised polySia was detected by subsequent incubations with biotinylated Fab-fragments of the anti-polySia antibody mAb 735 (2 µg/ml, 1 h, RT) and streptavidine-conjugated peroxidase (0.3 µg/ml, 30 min, RT) in blocking solution, each followed by two washing steps with PBS. Colour development was performed by incubating each well with 50 µl TMB-solution (0.2 mM citrate buffer pH 4.9, 0.1 mg/ml TMB, 0.0045 % H<sub>2</sub>O<sub>2</sub>) and stopped after 15 min by addition

of 25  $\mu\text{l}$  1 M  $\text{H}_2\text{SO}_4$ . The absorbance of the samples was measured at 450 nm using the ELISA-Reader 'DigiScan' (Asys Hitech).

For separate detection of NCAM-Polysialylation with purified enzyme, the microtiter plates were instead coated with 20  $\mu\text{l}$ /well mouse IgG (Pierce) at a concentration of 10  $\mu\text{g}/\text{ml}$  in PBS. ProteinA-NCAM was adsorbed to the IgG coated plates as described above and the enzyme reactions were initiated by addition of 25  $\mu\text{l}$  reaction buffer containing 2 mM CMP-Neu5Ac and 5  $\mu\text{l}$  of purified soluble polysialyltransferase. Synthesized polySia was detected as described above.

#### 4.4.16 Radioactive polysialyltransferase activity assay

Enzymatic activity of recombinant polysialyltransferases was monitored by the incorporation of radiocarbon labelled Neu5Ac into polySia. Recombinant ST8SiaIV expressed in *Sf9* cells was purified (4.4.12) and assayed in a soluble assay system while recombinant ST8SiaIV expressed in CHO-cells was adsorbed to IgG-coated sepharose beads and assayed as described in previously (Mühlenhoff *et al.*, 1996a).

For the soluble polysialyltransferase assay purified protein A-NCAM (4.4.11) was used as acceptor. Assays were carried out in a final volume of 20  $\mu\text{l}$  in reaction buffer (10 mM sodium cacodylate buffer pH 6.5, 10 mM  $\text{MnCl}_2$ ) containing 500 ng soluble NCAM-acceptor and 50-250 ng recombinant enzyme. To analyse autopolysialylation, no acceptor was added to the samples, instead the amount of enzyme was increased at least 10 fold. The enzyme reactions were started by addition of 0.25  $\mu\text{Ci}$  CMP-[ $^{14}\text{C}$ ]Neu5Ac (10.4 GBq/mmol, Amersham Pharmacia Biotech) and allowed to proceed for 3 h at 37 °C. The samples were divided into two equal aliquots after the enzyme reaction and one aliquot was incubated with 1  $\mu\text{l}$  endoNE (56 $\mu\text{g}/\text{ml}$ ) for 30 min at 37 °C as specificity control. The reactions were stopped by the addition of 2x Laemmli buffer and samples were analysed by 8 % or 10 % SDS-PAGE (4.4.2) followed by autoradiography.

To analyse polysialyltransferases expressed in transiently transfected CHO cells as secreted protein A-fusionproteins (4.3.2), 1 ml of enzyme containing culture supernatant was incubated with 20  $\mu\text{l}$  IgG-sepharose beads for 1 h at 4 °C. After one washing step in PBS the beads were incubated with 1 ml protein A-NCAM containing cell culture supernatant of transfected CHO-2A10 cells. The beads were washed three times in reaction buffer (10 mM

sodium cacodylate buffer pH 6.5, 10 mM MnCl<sub>2</sub>) and the enzyme reactions were started by the addition of 0.25 µCi CMP-[<sup>14</sup>C]Neu5Ac (10.4 GBq/mmol, Amersham Pharmacia Biotech) in a final volume of 40 µl reaction buffer. All samples were set up as duplicates. After 2 h at 37°C, the reactions were stopped by washing twice with PBS and 20 µl 2xLaemmli buffer was directly added to half of the samples. As specificity control the second half of the samples was resuspended in 40 µl PBS, incubated with endoNE (60 ng, 30 min, 37 °C) and washed twice in PBS prior to the addition of 20 µl 2xLaemmli buffer. The samples were analysed as described for the soluble assay above.

#### **4.4.17 Quantitative endosialidase activity assay (TBA-assay)**

The TBA-assay (Skoza and Mohos, 1976) enables photometric quantification of vicinal OH-groups present only at the free non-reducing end of sialic acids. As the non-reducing termini are increased upon digestion of polySia by endoNF, this method can be used to assay endosialidase activity. As polySia substrate colominic acid (Sigma) with an average degree of polymerisation of 16 (given by the manufacturer) was used.

3.2 mg/ml colominic acid in sodium phosphate buffer (0.1 M, pH 5.1) was incubated with 1/10 of the appropriate enzyme dilutions at 37 °C. Aliquots of 20 µl were taken in regular 3 min intervals, mixed with 20 µl chilled 96 % ethanol and stored on ice. 140 µl of deionised water were added to the samples and the vicinal hydroxyl-groups were oxidized by incubation with 50 µl oxidising solution (23.5 mM HJO<sub>4</sub> in 62.5 mM H<sub>2</sub>SO<sub>4</sub>) at 37 °C for 30 min. The reaction was stopped by the addition of 50 µl reducing solution (2 % NaAsO<sub>2</sub> in 0.5 M HCl). Samples were mixed and incubated for 7.5 min at 95 °C after addition of 100 µl 6 % 2-thiobabaturic acid. 400 µl of DMSO were added and the absorbance of the samples was measured at 550 nm using the ELISA-Reader 'DigiScan' (Asys Hitech). Values were corrected for the amount of substrate associated non-reducing ends that were determined in the absence of enzyme. The amounts of free non-reducing ends in the samples were calculated from a standard curve with free sialic acid (0.5 – 5 µg).

#### 4.4.18 ELISA-based endosialidase activity assay

The ELISA-based endosialidase assay provides a rapid method to detect endosialidase activity. After incubation of polySia coated microplate wells with endoNF the remaining non-cleaved substrate is detected by immunostaining using the polySia specific mAb 735. By end-point dilution this assay allows to compare enzymatic activity of different endoNF samples.

96-well microtiter plates (Becton Dickinson) were coated for 1 h at RT with 20  $\mu$ l/well capsular polysaccharide purified from *E. coli* K1 (1  $\mu$ g/ml in 10 mM sodium phosphate pH 7.4). After three washing steps in PBS the plates were blocked with 1 % BSA in PBS (200  $\mu$ l/well, 1 h, RT). The plates were washed three times in PBS and incubated with 20  $\mu$ l of the appropriate endoNF dilutions (100 – 2.000.000 fold diluted in PBS) for 30 min at 37 °C. After three washing steps with PBS remaining polySia was detected by subsequent incubations with mAb 735 (5  $\mu$ g/ml, 1 h, RT) and peroxidase-conjugated secondary antibody (1:2000, 30 min, RT) in 1 % BSA in PBS, each followed by two washing steps with PBS. Colour development was performed by incubating each well with 20  $\mu$ l ABTS substrate solution (Roche). The absorbance of the samples was measured after 15 min at 405 nm using the ELISA-Reader 'DigiScan' (Asys Hitech).

#### 4.4.19 Crystallization procedure

Protein samples for crystallization were thawed on ice, centrifuged (14.500xg, 15 min, 4 °C) and kept on ice during the preparation of the crystallization droplets. Crystallisation experiments were performed using the sitting drop vapour diffusion method. A drop composed of a mixture of 1  $\mu$ l protein sample and 1  $\mu$ l crystallization reagent was placed in vapour equilibration with a 500  $\mu$ l reservoir of the crystallization reagent. The experiments were carried out in 24-well Cryschem plates (Hampton Research) sealed with Crystal Clear Sealing tape (Hampton Research) that were incubated at either 4 °C or 20 °C for crystal growth.

Initial crystallization conditions were identified in sparse matrix screens and optimised by variations in pH, concentration of salts and precipitants or the addition of various additives.

## 5 Results

### 5.1 The eukaryotic polysialyltransferase ST8SiaIV: Large scale expression, purification and crystallization trials

The biological functions of the eukaryotic polysialyltransferases ST8SiaII and ST8SiaIV and of polysialylated NCAM, their synthesis product, are subjects of extensive international research efforts. PolySia-NCAM has been implicated in many physiological and pathological processes including the development of the central nervous system, neural regeneration and maintenance of plasticity in the adult brain. In addition, recent studies in the field of tumour biology directly correlated polySia expression in tumours of neuroectodermal origin with high metastatic potential and poor prognosis. This makes the polysialyltransferases very promising drug targets for cancer therapy. Although extensively studied there is still limited knowledge about the biochemical properties of the polysialyltransferases and no structural data exist. The lack of structural information is mainly due to difficulties associated with the large scale production of recombinant polysialyltransferases. N-glycosylation was shown to be essential for the formation of active polysialyltransferases (Mühlenhoff *et al.*, 1996a; Close *et al.*, 2000; Mühlenhoff *et al.*, 2001) and when this study was started, the expression of active recombinant enzymes was only described for mammalian cell culture (CHO- and COS cells). The yields of recombinant protein obtained from the mammalian cell systems were, however, too small to enable protein characterisations by means of biophysical methods. Therefore, the first goal of this study was to evaluate the insect cell line *Spodoptera frugiperda* (*Sf9*) as an expression system for the vertebrate polysialyltransferases.

#### 5.1.1 Expression of the polysialyltransferase ST8SiaIV in insect cells

Insect cells like *Spodoptera frugiperda* (*Sf9*) provide in combination with baculovirus expression vectors efficient expression systems for eukaryotic proteins. They are capable of performing posttranslational modifications like phosphorylation and N- or O-linked glycosylation. From earlier studies was known that replacement of the N-terminal transmembrane domain (TMD; see Figure 7) by a secretion signal leads to the expression of active, soluble polysialyltransferases in mammalian cell culture. Using this information, the 5'-truncated cDNA (bp 76-1077) of the hamster ST8SiaIV was subcloned into the baculovirus shuttle vector downstream of a honeybee melittin secretion signal. The N-terminally truncated

recombinant protein (ST8SiaIV $\Delta$ 25) is schematically shown in Figure 7. It contains a myc-His<sub>6</sub>-tag at the C-terminal end to facilitate detection and purification.

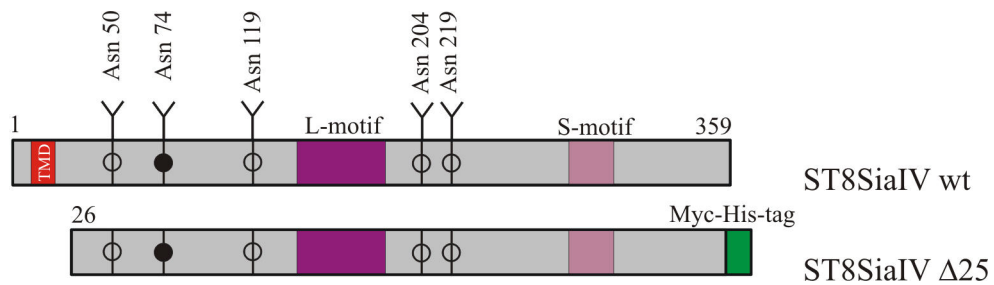


**Figure 7: Schematic representation of polysialyltransferase ST8SiaIV.** Full length ST8SiaIV(wt) and the N-terminally truncated ST8SiaIV( $\Delta$ 25). In the N-terminally truncated protein the transmembrane domain (TMD) is missing to allow expression of a secreted protein in *Sf9* cells. The large (L) and the small (S) sialylmotifs are highlighted as dark and light purple boxes, respectively. Asparagine residues involved in N-glycosylation are indicated. The N-glycan important for polysialyltransferase activity is marked with a filled circle. The myc-His<sub>6</sub>-tag is shown as a green box.

High titer stocks of recombinant baculovirus (BV-ST8SiaIV $\Delta$ 25) were generated as described in 4.3.4. For protein expression, *Sf9* cells were grown to a density of  $2 \times 10^6$  cells/ml and infected with the baculovirus stock (4.3.5). Expression of the recombinant proteins was analysed in a time-course over 96 hours by Western blot analysis. To test the enzymatic activity of ST8SiaIV in the harvested cell culture supernatants, a recently developed sensitive ELISA-based assay was used (Stummeyer, 2000). Polysialyltransferases are protein specific glycosyltransferases that accept two polySia acceptors, which are the neural cell adhesion molecule NCAM and the polysialyltransferases themselves (Mühlenhoff *et al.*, 1996a; Close *et al.*, 1998). The two polysialylation reactions are further on referred to as NCAM-polysialylation and autopolsialylation, respectively. The ELISA-based assay allows differential testing of either auto- or NCAM-polysialylation (Stummeyer, 2000). To assay autopolsialylation, the recombinant polysialyltransferase was immunoadsorbed to microtiter plates coated with anti-myc-tag antibodies. To assay NCAM-polysialylation, in a second step also Protein A-NCAM was adsorbed to the plates. PolySia-synthesis reactions were started by addition of CMP-Neu5Ac and polysialylated reaction products were detected with biotinylated Fab-fragments of the anti-polySia mAb 735 (for details see 4.4.15). The results are summarized in Figure 8.

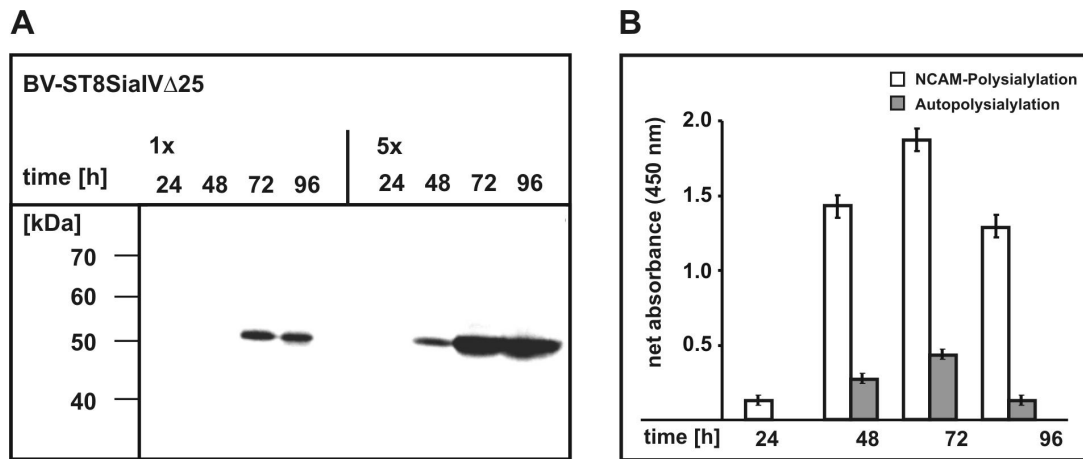


**Figure 8: Expression of catalytically active ST8SiaIV $\Delta$ 25 in *Sf9* insect cells** (A) Time course of the baculoviral expression of ST8SiaIV $\Delta$ 25 in *Sf9* cells. Culture supernatant of infected cells was assayed 24 h - 96 h after infection by 10% SDS-PAGE and Western blot developed with anti-myc antibody. The supernatant was either applied directly (1x) or after five fold concentration (5x) by TCA-precipitation. (B) Enzymatic activity of cell culture supernatants determined by an ELISA based activity assay. Samples were tested for NCAM- and autopolysialylation as shown by open and filled columns. Values are corrected by the negative control measured in the absence of CMP-Neu5Ac.

As shown in the Western blot (Figure 8A) recombinant ST8SiaIV $\Delta$ 25 was expressed and secreted to the cell culture supernatant of baculovirus infected *Sf9* cells. The protein was already detectable in the unconcentrated supernatant and reached a maximum expression level 72 h after infection. Furthermore the ELISA based activity assay confirmed the enzymatic activity of the recombinant enzyme. A clear signal for NCAM-polysialylation was obtained 48 h after infection that was maximal after 72 h but started to decrease 96 h after infection. Though the signals were not as high as for NCAM-polysialylation, also autopolysialylation was detectable. The course of the autopolysialylation activity corresponds to the course of NCAM-polysialylation. Because protein expression and activity peaked 72 h after infection, this time point was chosen to harvest the protein in subsequent experiments.

The finding of autopolysialylation was surprising since earlier experiments carried out in CHO-cells had shown that autopolysialylation activity in ST8SiaIV depends on the presence of terminal galactose residues within the recombinant protein (Mühlenhoff et al., 1996a). Yet *Sf9* cells are not believed to have the capacity to produce galactosylated N-glycans and lectin blot analysis carried out in this study with galactose specific lectins failed to identify galactosylated N-glycans on the insect cell expressed protein. However, it may be that a small proportion of enzyme in fact carries terminal galactose and a more detailed glycan analysis by e.g. mass spectrometry is necessary to answer the question. These kinds of experiments are planned for the near future.

In summary, these data demonstrate that the baculovirus mediated expression in *Sf9* insect cells provides a suitable system for the recombinant production of polysialyltransferases. The obtained proteins were capable to perform NCAM- and autopolysialylation and were expressed in good yields. Following experiments concentrated therefore on the optimisation of protein production and the establishment of protein purification procedures. In all these studies ST8SiaIV was used as a model protein.

## **5.1.2 Purification of ST8SiaIV from the culture supernatant of baculovirus infected *Sf9* cells**

### **5.1.2.1 Purification by myc-affinity chromatography**

To facilitate purification, recombinant ST8SiaIV $\Delta$ 25 was C-terminally tagged with myc- and His<sub>6</sub>-epitopes and in small scale pioneering studies at first purification by myc-affinity chromatography was tested. Anti-myc affinity matrix was generated by covalent coupling of the anti-myc antibody 9E10 to protein G-sepharose (4.4.7). The test purifications shown in Figure 9 were performed in batch format. 100  $\mu$ l of the anti-myc matrix was incubated for 1h with 50 ml ST8SiaIV $\Delta$ 25 containing cell culture supernatant. Beads were washed twice with PBS and bound protein was eluted under acidic conditions by resuspending the beads in 300  $\mu$ l elution buffer for 2 min. After centrifugation (1 min, 10000xg, 4 °C) the supernatant was adjusted to pH 7.0 with neutralizing buffer (1 M Tris/HCl pH 9.0).

As depicted in Figure 9A ST8SiaIV $\Delta$ 25 was efficiently purified from the culture supernatant and appeared as homogenous band in a Coomassie stained gel. The enzymatic activity of the purified protein was confirmed by ELISA-based activity assay that clearly showed NCAM- and autopolysialylation activity (Figure 9B).



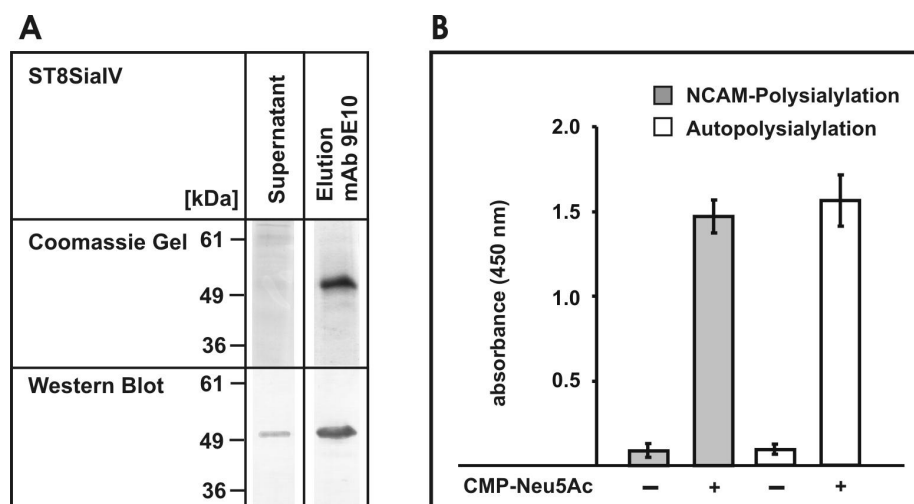


**Figure 9: Purification of ST8SiaIV $\Delta$ 25 by myc-affinity chromatography** (A) Analysis of the myc-affinity purification of ST8SiaIV $\Delta$ 25 from the culture supernatant of baculovirus infected *Sf9* cells by Coomassie stained 10% SDS-PAGE and Western blot developed with anti-myc antibody. (B) Enzymatic activity of the purified enzyme analysed by ELISA-based polysialyltransferase assay. To test for NCAM-polysialylation protein A-NCAM was adsorbed to IgG coated microtiter plates and the purified ST8SiaIV $\Delta$ 25 was added in solution. To test for autopolysialylation the purified ST8SiaIV $\Delta$ 25 was adsorbed to microtiter plates coated with anti-myc mAb. Control samples were tested in the absence of the substrate CMP-Neu5Ac.

Based on these results an anti-myc affinity column was prepared for larger scale purification of the recombinant protein. Therefore, 20 mg of anti-myc antibody 9E10 were purified from hybridoma cell culture supernatant by protein G-affinity chromatography (4.4.10) and covalently coupled to 5 ml protein G-sepharose (4.4.7). The resulting anti-myc affinity matrix was used to purify ST8SiaIV $\Delta$ 25 from 500 ml supernatant of baculovirus infected cell culture.

Although efficiently adsorbed to the affinity column, the recombinant protein precipitated shortly after elution and could not be re-dissolved. Because over-concentration of the protein sample was believed to cause the precipitation, the eluate was immediately diluted in the collection step. But precipitation occurred already for protein concentration below 100  $\mu$ g/ml and could neither be prevented by step-wise nor by rapid change to neutral pH. Therefore, different buffer systems (Citrate, Phosphate, Tris) were tested for elution in a pH-range from 2-8. Yet, they either failed to elute the protein or the eluted protein again precipitated. This systematic approach clearly demonstrated that buffer conditions required to break the high affinity binding between the monoclonal antibody 9E10 and the myc-tagged protein are not compatible with the stability of the recombinant enzyme.

Also trials to stabilize the protein by addition of divalent cations such as  $Mg^{2+}$  or  $Mn^{2+}$  (putative cofactors of the transferases that might have been washed out during the acidic elution), had no effect.

In summary these data allow to conclude that recombinant ST8SiaIV $\Delta$ 25 is at least partly denatured under the acidic pH-conditions needed to elute the enzyme from the myc-column. Myc-affinity chromatography is therefore not suitable to purify recombinant ST8SiaIV $\Delta$ 25 for structural analysis, in particular crystallography, where correctly folded protein is required at high concentrations.

#### 5.1.2.2 Purification by $Ni^{2+}$ -chelating chromatography

To avoid acidic elution steps during the purification of ST8SiaIV $\Delta$ 25 from the culture supernatant of baculovirus infected *Sf9* cells, purification by  $Ni^{2+}$ -chelating chromatography using the His<sub>6</sub>-affinity tag was tested. Initial studies were carried out with recombinant ST8SiaIV $\Delta$ 25 carrying the C-terminal myc-His<sub>6</sub>-tag as shown in Figure 7.

Binding of diluted protein samples to a  $Ni^{2+}$ -affinity column is in general not very efficient and was further hampered by the fact that media for insect cell culture are rich in components (e.g. amino acids) that compete for binding to  $Ni^{2+}$ -agarose. Careful optimisation steps were therefore necessary, to evaluate the conditions for binding of ST8SiaIV $\Delta$ 25 to the  $Ni^{2+}$ -matrix. Trials to harvest the recombinant protein from the medium by ammoniumsulphate or polyethylenglycole (PEG) precipitation were not successful, as the precipitated protein could not be re-dissolved. Instead the culture supernatant was concentrated using a tangential cross flow filtration system and small binding inhibitors were removed by buffer exchange. The final purification procedure is described in detail in chapter 4.4.12.

Parallel to the optimisation experiments a second baculovirus vector was generated that encoded the ST8SiaIV $\Delta$ 25 with an N-terminal His<sub>6</sub>-tag followed by an rTEV-protease site to facilitate removal of the affinity tag from the purified protein. This baculovirus was then used for the large-scale expression and purification of ST8SiaIV.

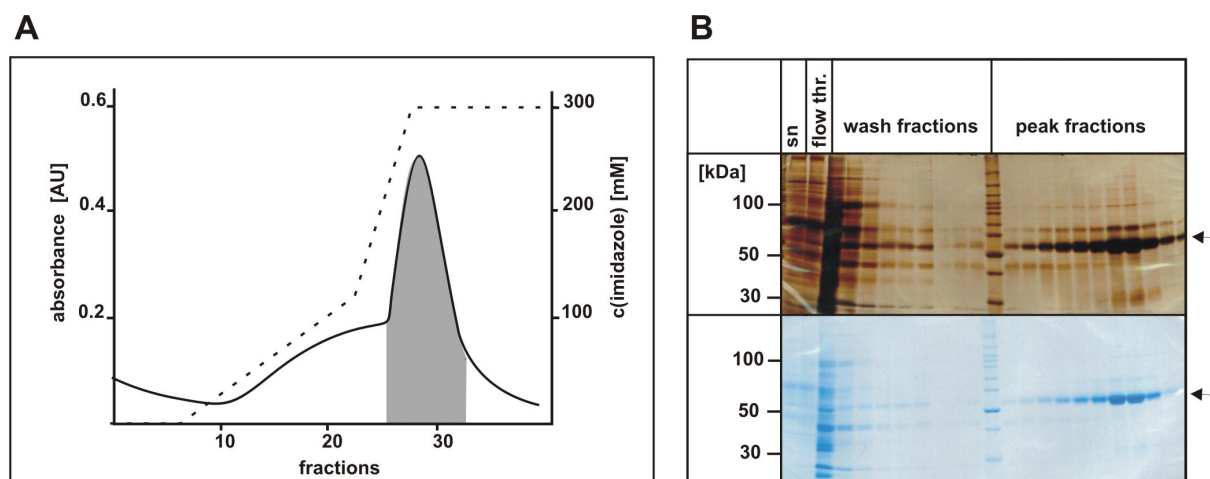


**Figure 10: Purification of ST8SiaIV $\Delta$ 25 by Ni<sup>2+</sup>-affinity chromatography** (A) Elution profile the of Ni<sup>2+</sup>-affinity purification of ST8SiaIV $\Delta$ 25 from culture supernatant of baculovirus infected *Sf9* cells. Absorbance at 280 nm is shown as solid line, the imidazole elution gradient as dotted line. Peak fractions containing ST8SiaIV $\Delta$ 25 are filled in grey. (B) Protein fractions obtained through the purification were analysed by Coomassie (lower panel) and silver (upper panel) stained 10% SDS-PAGE as indicated. Arrows indicate bands that correspond to ST8SiaIV $\Delta$ 25. (sn) ten fold concentrated supernatant applied to the column, (flow thr.) flowthrough of the column.

In Figure 10 the Ni<sup>2+</sup>-affinity purification ST8SiaIV $\Delta$ 25 from one litre of baculovirus infected *Sf9* cells is shown. The protein eluted at 100 mM imidazole and appeared as homogenous band on a Coomassie stained SDS-PAGE, though the more sensitive silver staining revealed some contaminating protein bands (Figure 10B). Following the Ni<sup>2+</sup>-column the pooled fractions were subjected to a desalting step to remove the imidazole (4.4.12.2).

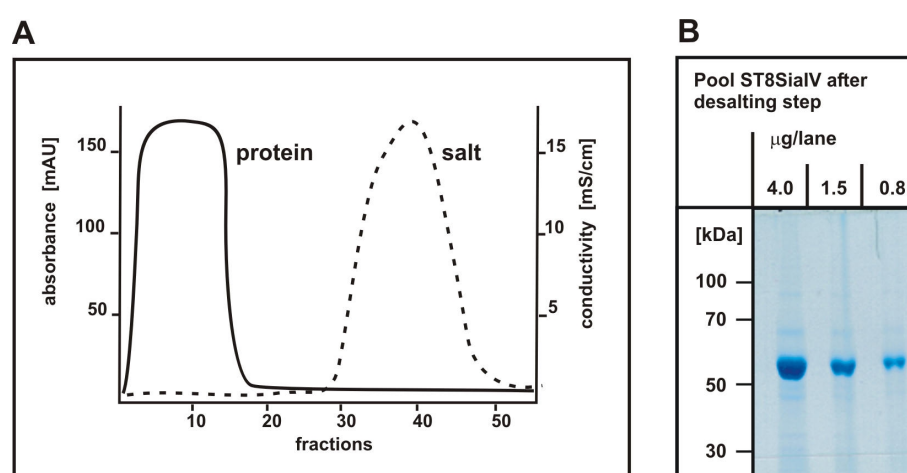


**Figure 11: Desalting of the ST8SiaIV $\Delta$ 25 pool after Ni<sup>2+</sup>-affinity chromatography** (A) Elution profile of the desalting step following the Ni<sup>2+</sup>-affinity purification of ST8SiaIV $\Delta$ 25. Absorbance at 280 nm is shown as solid line (protein), the conductivity as dotted line (salt). (B) Coomassie stained 10% SDS-PAGE of the concentrated ST8SiaIV $\Delta$ 25 pool after desalting. To analyse the purity of the sample 0.8, 1.5 and 4  $\mu$ g of protein were applied per lane as indicated.

As depicted in Figure 11A protein and imidazole containing salt peak were well separated and the purified ST8SiaIV $\Delta$ 25 appeared nearly homogenous in a Coomassie stained gel (Figure 11B). The protein sample was concentrated to 3 mg/ml and either further purified by size exclusion chromatography or flash frozen in liquid nitrogen and stored at  $-80^{\circ}\text{C}$  until used in crystallization trials. From a one-litre culture of baculovirus infected *Sf9* cells a total of 1.5 mg of purified ST8SiaIV was obtained.

### 5.1.2.3 Enzymatic activity of recombinant ST8SiaIV $\Delta$ 25 purified from *Sf9*-cell culture

The enzymatic activity of the ST8SiaIV $\Delta$ 25 containing fractions obtained during the purification by  $\text{Ni}^{2+}$ -affinity chromatography (5.1.2.2) was assayed using the ELISA-based assay (4.4.15). The detection principle of the assay, based on immunostaining of synthesised polySia, does not allow to determine the CMP-Neu5Ac incorporation into polySia as molar quantity. Therefore the specific enzyme activity is described as absorbance per mg protein. To stay within the linear range of the assay, samples were diluted up to 500 fold. As shown in Figure 12 the specific polysialyltransferase activity (NCAM- and autopolysialylation) can be enriched by more than factor 100 during the purification. In parallel the protein content decreased in a similar range indicating the stability of recombinant ST8SiaIV $\Delta$ 25 under the applied purification conditions.

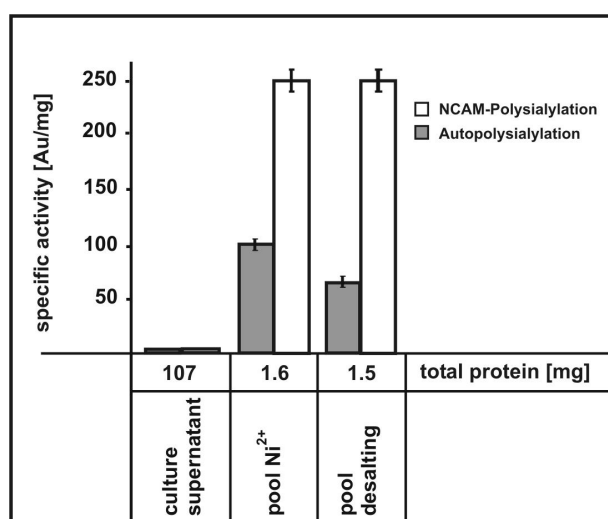


**Figure 12: Specific activity monitored throughout ST8SiaIV $\Delta$ 25 purification** ELISA based activity assay: The enzyme alone or together with Protein A-NCAM was adsorbed to ELISA-wells and incubated for 3 h at  $37^{\circ}\text{C}$  in the presence of CMP-Neu5Ac. Negative controls were incubated in the absence of CMP-Neu5Ac. Synthesised polySia was detected by immunostaining using ladled Fab fragments of the anti-polySia mAb 735. As enzyme source the fractions obtained throughout the purification of ST8SiaIV $\Delta$ 25 were used as indicated. Additionally the total protein content of the pools is given.

The purified enzyme was additionally assayed in a soluble system avoiding solid phase fixation of either enzyme or acceptor NCAM (4.4.16). In contrast to the ELISA-based assay, the soluble assay allows to visualize the length of the synthesized polySia chains. Due to the use of CMP-[C<sup>14</sup>]-Neu5Ac as sugar donor the synthesized chains are radioactively labelled and can be displayed by SDS-PAGE with following autoradiography.

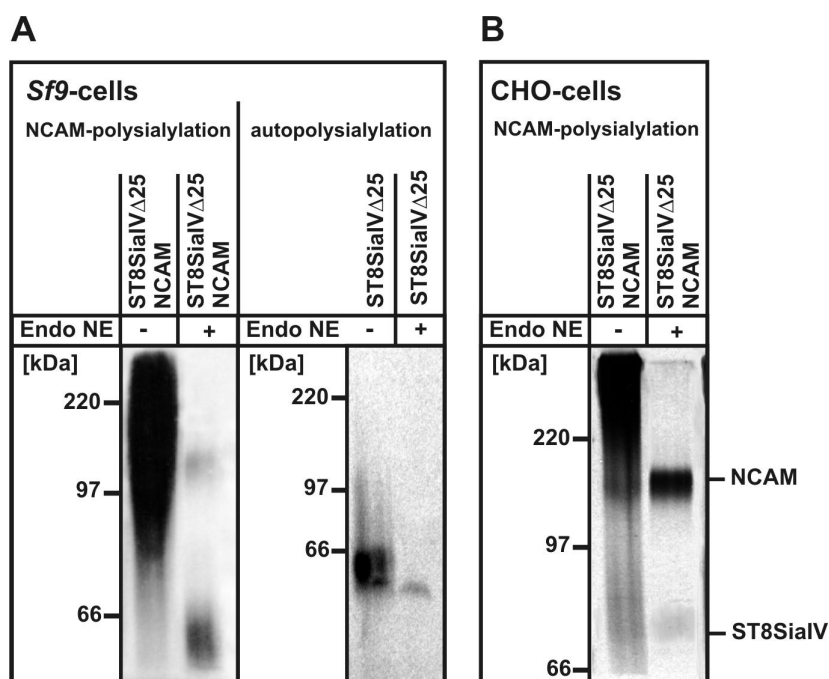


**Figure 13:** (A) Soluble activity assay using ST8SiaIVΔ25 purified from *Sf9* insect cells. The purified ST8SiaIVΔ25 (after desalting) was incubated for 16 h at 37 °C in the presence of CMP-[<sup>14</sup>C]Neu5Ac (autopolysialylation) and Protein A-NCAM (NCAM-polysialylation) as indicated. Half of the samples was treated with endoNE after the enzyme reaction. Polysialylated proteins were displayed by SDS-PAGE followed by autoradiography. (B) Polysialyltransferase assay with recombinant Protein A-ST8SiaIV expressed in CHO-cells. Enzyme and Protein A-NCAM were adsorbed to Ig-coated sepharose beads and further assayed as described in (A).

As shown in Figure 13A, a broad radioactive signal that indicates the presence of radiolabelled polySia was observed for purified ST8SiaIV when incubated with Protein A-NCAM and CMP-[C<sup>14</sup>]-Neu5Ac. Protein A-NCAM migrates in SDS-PAGE with an apparent molecular mass of 140 kDa. The addition of polySia chains by the polysialyltransferases influences the migration behaviour and causes a shift to higher apparent molecular masses. Thereby, the length of the synthesized polySia chains correlates with the extent of the shift. As specificity control, parts of the sample were treated with polySia-specific endoneuraminidase (endoNE) after the enzyme reaction (Figure 13A, lane2). Due to its

cleavage pattern endoNE leaves a residual stump of 5-7 sialic acid residues bound to the protein. Therefore the band at 140 kDa represents formerly polysialylated NCAM, whereas the second band at 55 kDa represents the enzyme itself. Trials to detect autopolsialylation in the absence of NCAM requested enzyme concentrations ten times higher (Figure 13A, lane3).

The data presented in Fig. 7A demonstrate that the recombinant ST8SiaIV $\Delta$ 25 expressed in *Sf9* cells is capable to perform NCAM- and autopolsialylation also in a soluble assay system.

In order to compare the properties of recombinant ST8SiaIV expressed in insect and mammalian cells a Protein A-fusion protein of ST8SiaIV $\Delta$ 25 was expressed in CHO-cells. Prior to incubation with CMP-[C<sup>14</sup>]-Neu5Ac, enzyme and Protein A-NCAM were adsorbed to Ig-coated sepharose. The assay was carried out as described in (4.4.16). Results are depicted in Figure 13B. The resulting radioactive signals were similar to the pattern observed for the insect cell expressed ST8SiaIV, indicating that both recombinant enzymes synthesize polySia chains of comparable length.

#### 5.1.2.4 Size exclusion chromatography of Ni<sup>2+</sup>-affinity purified ST8SiaIVΔ25

Though the recombinant ST8SiaIVΔ25 obtained after Ni<sup>2+</sup>-chelating chromatography and desalting appeared almost homogenous on a Coomassie stained SDS-PAGE (B), the more sensitive silver staining revealed contaminating protein bands (Figure 10B). For further purification, the protein sample obtained after Ni<sup>2+</sup>-affinity was concentrated to 3 mg/ml and subjected to size exclusion chromatography (4.4.12.3). The resulting elution profile is shown in Figure 14. Homogeneously purified ST8SiaIVΔ25 eluted in the main peak of the profile (fractions 14-18), well separated from contaminating proteins. However, significant amounts of ST8SiaIVΔ25 eluted already in earlier fractions, possibly due to oligomerisation of parts of the protein or due to the formation of heterocomplexes with the contaminants. The fractions of the two main peaks of the elution profile (11-13 and 14-18) were separately concentrated to 2 mg/ml, flash frozen in liquid nitrogen and stored at -80°C for later use in crystallization trials.

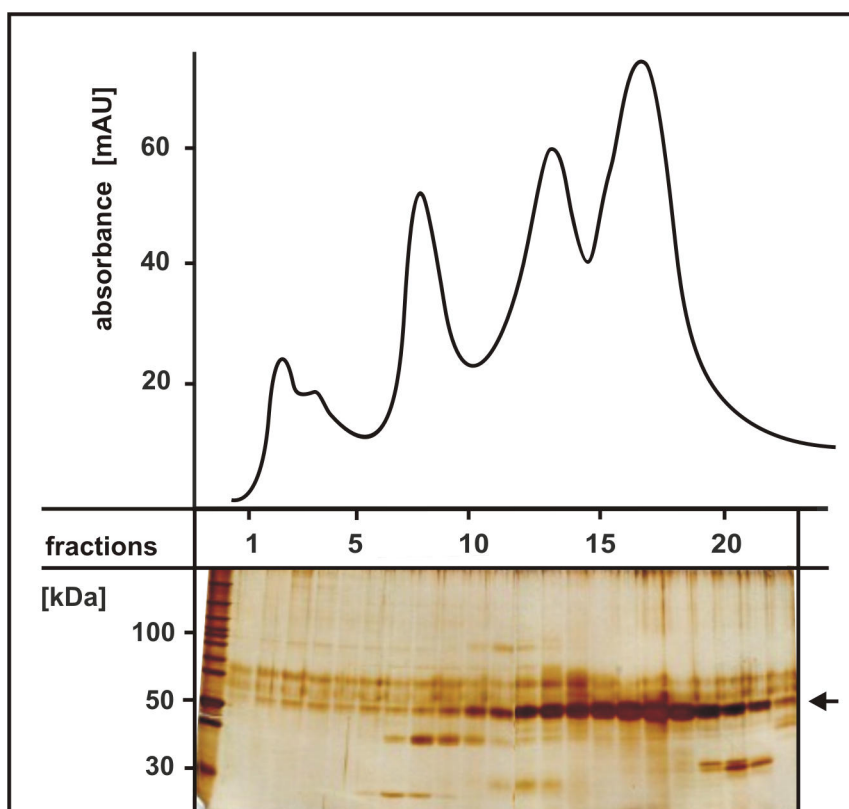


**Figure 14: Final purification of the ST8SiaIVΔ25 by size exclusion chromatography.** After Ni<sup>2+</sup>-affinity chromatography the ST8SiaΔ25 containing fraction was further purified by gelfiltration. Eluted fractions were analysed by silver stained 10% SDS-PAGE. Bands corresponding to ST8SiaIVΔ25 are indicated by an arrow.

### 5.1.3 Crystallization trials

Crystallization trials with ST8SiaIV were performed using either the sample obtained after Ni<sup>2+</sup>-chelating chromatography (5.1.2.2) or after size exclusion chromatography (5.1.2.4). The sitting drop vapour diffusion method as described in chapter 4.4.19 was applied. Equal volumes of protein sample and crystallization solution were mixed in a small droplet and equilibrated by vapour diffusion with a reservoir of the crystallisation solution.

Screenings at 20°C and at 4°C yielded finally small brownish coloured crystals for the Ni<sup>2+</sup>-affinity purified sample (Figure 15). The crystals did however not diffract and failed to grow from further purified protein samples obtained after gelfiltration. Therefore three crystals were dissolved in Laemmli-buffer after two washing steps in reservoir solution and analysed by silver stained 14% SDS-PAGE. As shown in Figure 15 the detectable protein bands at 30 and 25 kDa are too small to represent the polysialyltransferase. Instead two similar bands were identified in two fractions obtained after gelfiltration (Figure 15), corresponding to fractions 7 and 8 of the elution profile shown in Figure 14. As crystals grew from those fractions, the brownish crystals were clearly not ST8SiaIV $\Delta$ 25. Despite of extensive screenings in the course of this doctoral thesis no ST8SiaIV crystals have been obtained so far.

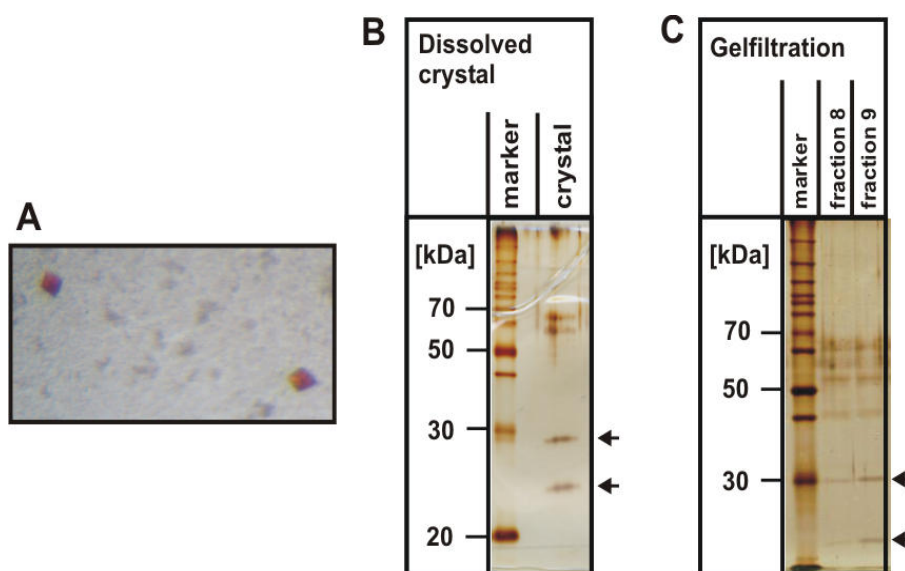


**Figure 15: SDS-PAGE of putative ST8SiaIV $\Delta$ 25 crystals** (A) Crystals obtained from the Ni<sup>2+</sup>-affinity purified ST8SiaIV $\Delta$ 25 sample. (B) Dissolved crystals analysed by silver stained 14 % SDS-PAGE. Protein bands are indicated by arrows. (C) Separation of the crystallizing contaminants from the Ni<sup>2+</sup>-affinity purified ST8SiaIV $\Delta$ 25 sample by gelfiltration and analysis by silver stained 14 % SDS-PAGE.



## 5.2 Crystal structure of the polysialic acid degrading endoneuraminidase cloned from bacteriophage K1F

In a second project efforts were focused on the structural analysis of polySia degrading enzymes, the endosialidases.

Due to their high specificity for polysialic acid (polySia), bacteriophage derived endosialidases (endo-N-acetylneuraminidases, endoN) are widely applied in neurosciences and may find use as diagnostic or therapeutic tools for polySia bearing tumours and meningitis caused by polySia encapsulated bacteria. For example, *E. coli* K1 specific bacteriophages have been found to efficiently treat septicaemia and meningitis in infected mice and chicken (Smith *et al.*, 1982; Barrow *et al.*, 1998) and the application of the enzyme in a mouse model system was demonstrated to significantly reduce the metastatic potential of polySia bearing tumour cells (Daniel *et al.*, 2001). Detailed understanding of the structure-function relationships in endosialidases is of major importance to exploit the bio-medical potencies of these enzymes. While crystal structures have been determined for several exosialidases (Varghese and Colman, 1991; Tulip *et al.*, 1991; Burmeister *et al.*, 1992; Crennell *et al.*, 1993; Crennell *et al.*, 1994; Gaskell *et al.*, 1995; Crennell *et al.*, 2000) and their catalytical mechanism is well described (Chong *et al.*, 1992), no structural data are available for endosialidases. Therefore the aim of this study was to determine the crystal structure of the polySia degrading endoNF.

### 5.2.1 N-terminal truncations of endoNF

Primary sequence alignments and BLAST searches (Altschul *et al.*, 1997) performed with endosialidases revealed a chimeric composition of the enzymes with three putative domains (Figure 16). Based on sequence homology to the tail fibre protein gp17 of coliphages T3 and T7 and the yersiniophage YeO3-12, the N-terminal part of endoNF was suggested to be the head-binding domain, attaching the endosialidase tailspike to the bacteriophage baseplate (Petter *et al.*, 1993; Pajunen *et al.*, 2000). The central part of the molecule is highly conserved in all endosialidases analysed so far and believed to comprise the catalytic domain. It is followed by a small C-terminal part (marked in red in Figure 16) that is cleaved off during

enzyme maturation and from our earlier work known to be essential for the formation of active endosialidases.

It was already known from the crystallisation of the P22 tailspike, which was shown to have a similar domain organisation (Chen and King, 1991) that the full-length protein failed to crystallize. Crystals of P22 could only be obtained from an N-terminally truncated protein lacking the head-binding domain (Steinbacher *et al.*, 1994). To identify the shortest catalytically active fragment of endoNF still capable to form SDS-resistant trimers, N-terminally truncated forms (see Figure 16) were generated, recombinantly expressed and analysed with respect to both complex formation and enzymatic activity.

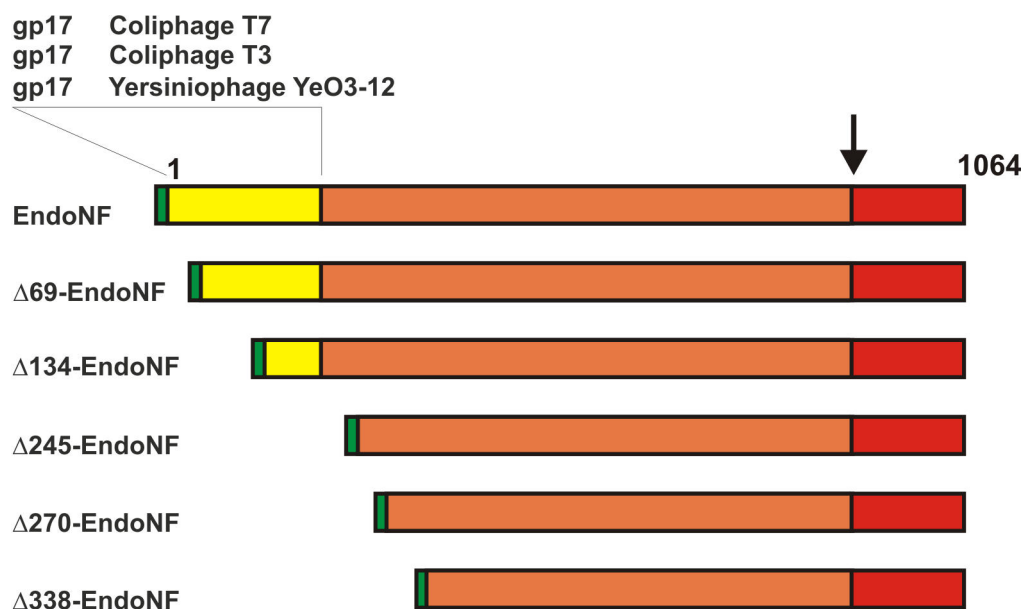


**Figure 16: Schematic representations of wild type (wt) and N-terminally truncated forms of endoNF.** The region homologous to the gp17 head binding domain of coliphages T7 and T3 and yersiniophage YeO3-12 is depicted in yellow. The small C-terminal fragment shown in red is proteolytically cleaved off during maturation of the enzyme; the cleavage site is indicated by an arrow. All proteins are epitope tagged with an N-terminal T7-tag (green box).

The N-terminal truncations depicted in Figure 16 were expressed in *E. coli* BL21(DE3) as described in chapter 4.4.8. Soluble fractions of the bacterial lysates were analysed by SDS-PAGE (4.4.2) and Western blot analysis (4.4.5). As shown in Figure 17A, N-terminal truncations of up to 245 amino acids resulted in the expression of soluble proteins and the observed molecular weights indicated that mutant proteins like the wild type protein were proteolytically processed. Further truncated proteins ( $\Delta 270$  and  $\Delta 338$ ) were still

proteolytically cleaved, but the expression level was dramatically decreased. Complex formation was tested by omitting the boiling step prior to SDS-PAGE analysis. As shown in Figure 17B an appearing high molecular mass band indicates the presence of trimeric endoNF complexes. No complexes were visible in the case of  $\Delta 338$ -EndoNF while up to 270 amino acids could be removed from the N-terminus without effecting trimer formation.

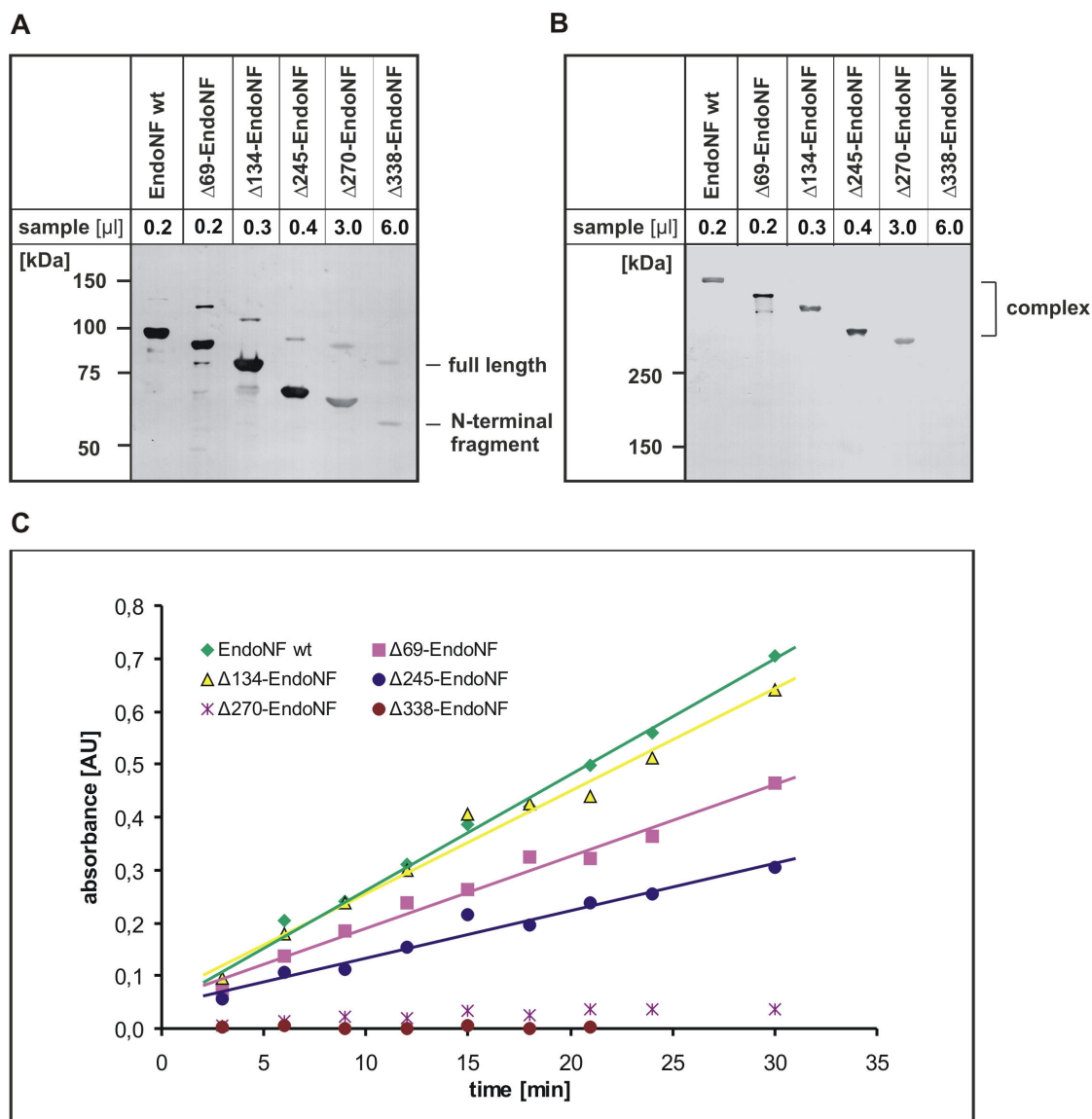


**Figure 17: Expression, complex formation and catalytic activity of wild type and N-terminally truncated endoNF forms.** (A) Wild type and N-terminally truncated forms of endoNF were expressed in *E. coli* BL21 (DE3). Soluble fractions of the bacterial lysates were analysed by 8% SDS-PAGE and Western blot that was developed with anti-T7 antibody. To compensate for differences in the expression rates, varying sample volumes were loaded as indicated. Bands corresponding to full length uncleaved endoNF and to the N-terminal fragment obtained after proteolytic processing are indicated. (B) Complex formation was analysed by 6% SDS-PAGE and Western blot as described in (A) but omitting the boiling step before electrophoresis. Bands corresponding to the SDS-resistant endoNF homotrimers are indicated. (C) Endosialidase activity of the soluble fractions (diluted 1:2 in assay buffer) was assayed using the thiobabutaric acid assay. Increasing absorbance at 550 nm corresponds to an increase of free non-reducing sialic acid moieties due to the enzymatic activity of endoNF.

Enzymatic activity of the truncated proteins was analysed by the thiobabituric acid (TBA) assay (4.4.17) using the soluble fractions as enzyme source. The TBA-assay (Skoza *et al.*, 1976) enables photometric quantification of vicinal OH-groups present only at the free non-reducing end of sialic acids. As digestion of polymeric sialic acid by endoNF increases the number of non-reducing ends the TBA-test can be used to quantitatively assay endoNF activity. As shown Figure 17C removal of up to 245 amino acids from the N-terminus of endoNF did not interfere with the catalytic activity. Variations visible for the enzymatic activity are most likely due to the reduced expression rates (see Figure 17A). In contrast the mutants  $\Delta 270$ - and  $\Delta 338$ -EndoNF were functionally inactive. In summary, the analysis of the N-terminal truncated forms of endoNF revealed, that the first 245 amino acids of endoNF are not required for efficient expression, proteolytic processing, the formation of SDS-resistant or enzymatic activity.

### 5.2.2 Expression and purification of recombinant endoNF

As the aim of this study was to investigate the structure and function relationships of endosialidases by crystal structure analysis, large quantities of pure proteins were needed. Therefore in a first step expression and purification procedures had to be established to ensure sufficient protein supply.

Endosialidases undergo proteolytic cleavage into a large N-terminal fragment harbouring the enzymatic activity and a small C-terminal fragment that is believed to function as an intramolecular chaperone (Mühlenhoff *et al.*, 2003). The C-terminal fragment is essential in the nascent protein chain but after proteolytic release not part of the active trimeric complex. To enable the purification of both fragments, N- and C-terminal ends of endoNF were epitope-labelled with two different affinity tags. As depicted in Figure 18A two constructs were generated encoding the full length (EndoNF-SH) and a truncated endoNF with deleted head binding domain ( $\Delta 245$ -EndoNF-SH). The purification procedure for both fragments is schematically shown in Figure 18B. The C-terminal fragment was purified by His<sub>6</sub>-affinity chromatography with subsequent size exclusion chromatography (gelfiltration) while the N-terminal fragment was affinity purified using the StrepII-tag followed by a desalting step.

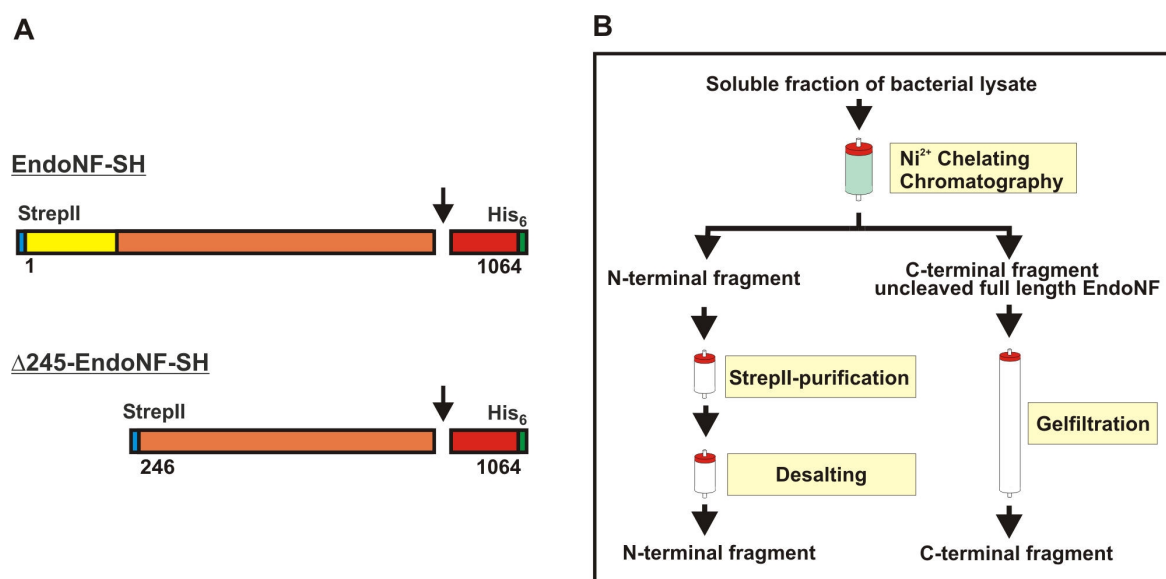


**Figure 18: The purification strategy** (A) Schematic representation of the full-length and N-terminally truncated endoNF constructs as overexpressed in *E. coli*. Recombinant proteins are epitope tagged. At the N-terminus a StrepII-tag (blue box) and at the C-terminus a His<sub>6</sub>-tag (green box) was added to allow the separate purification of the large N-terminal and the small C-terminal fragment, which are obtained after proteolytic cleavage of the full length proteins. The proteolytic cleavage site is indicated by an arrow. (B) Scheme of the purification procedures for the C- and the N-terminal fragments of endoNF.

### 5.2.2.1 Ni<sup>2+</sup>-chelating chromatography: Separation of N- and C-terminal endoNF fragments

Recombinant endoNF (EndoNF-SH) was overexpressed in *E. coli* (4.4.8). After bacterial lysis the soluble fraction was subjected to Ni<sup>2+</sup>-affinity purification as described in chapter 4.4.12.2. Proteins adsorbed to the Ni<sup>2+</sup>-chelating column were eluted in two linear imidazole gradient steps from 0-100 mM imidazole and from 100-500 mM imidazole. The small C-terminal fragment carrying a His<sub>6</sub>-tag eluted in a single peak at 300 mM imidazole (Figure 19A).

Because the bacterial lysates always contained a minor population of endoNF that was not proteolytically processed, the eluted fraction was not homogeneous. It contained contaminating full-length endoNF (carrying a His<sub>6</sub>-tag) and also detectable amounts of the large N-terminal fragment, that presumably co-purifies due to the formation of stable complexes with the full-length protein (Figure 19C).

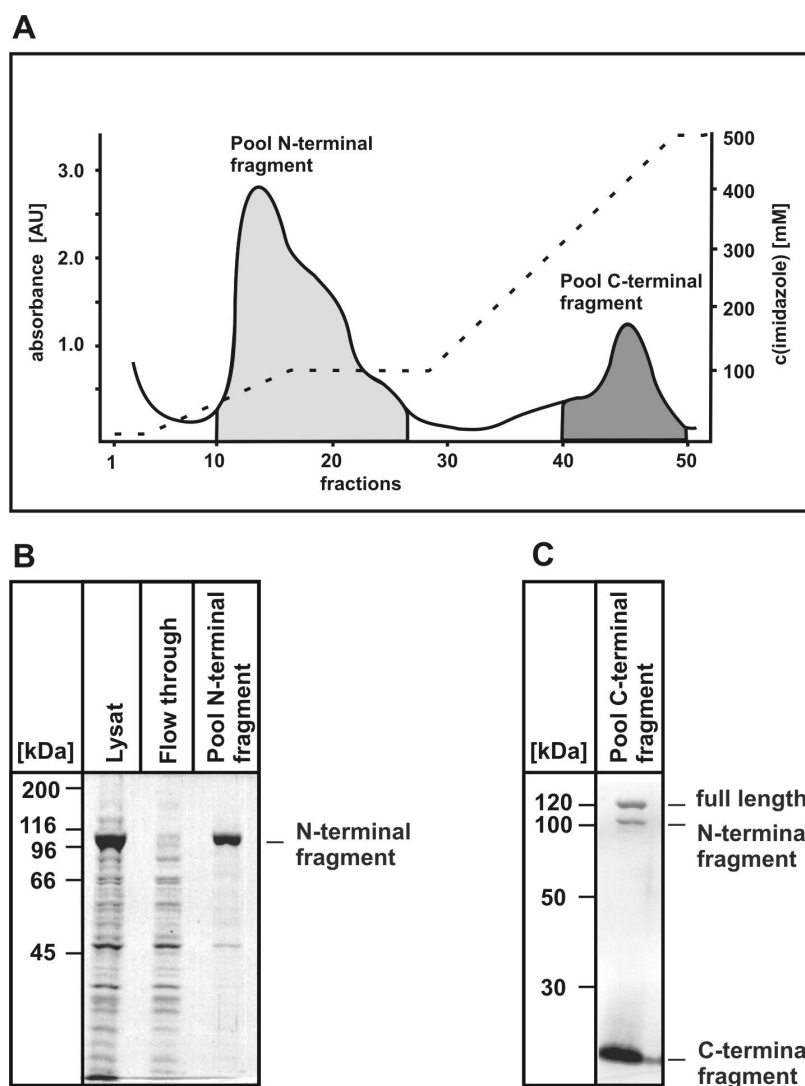


**Figure 19: Ni<sup>2+</sup>-affinity purification of endoNF** (A) Elution profile of Ni<sup>2+</sup>-affinity chromatography of C-terminally His<sub>6</sub>-tagged endoNF. Absorbance at 280 nm is shown as solid line, the imidazole elution gradient as dotted line. Peak fractions were analysed by Coomassie stained 10% SDS-PAGE (B) or 12% SDS-PAGE (C). Bands corresponding to full length uncleaved endoNF and to the N- and C-terminal fragments obtained after proteolytic processing are indicated.

Purification of recombinant endoNF by Ni<sup>2+</sup>-chelating chromatography resulted in efficient separation of N- and C-terminal fragments (Figure 19A-B). Although not carrying a His<sub>6</sub>-tag, the N-terminal fragment was bound quantitatively to the Ni<sup>2+</sup>-column and eluted almost homogeneously at low imidazole concentrations (peak fractions 10 – 27 in Fig. 13 A). The two isolated protein fractions were further purified by gelfiltration or StrepII-affinity, respectively.

### 5.2.2.2 Purification of the catalytically active N-terminal fragment of endoNF

The pool containing the N-terminal fragment of endoNF after Ni<sup>2+</sup>-chelating chromatography (5.2.2.1) was further purified by Strep-Tactin affinity chromatography as described in detail in chapter 4.4.13.2. The StrepII-tagged protein was adsorbed to the Strep-Tactin column and eluted in a desthiobiotin step gradient. As shown in Figure 20A the N-terminal fragment was purified to homogeneity after this second purification step. No contaminating bands were detectable on silver stained SDS-PAGE. As the N-terminal fragment is the catalytically active part of endoNF, the endosialidase activity was monitored during the purification procedure using the TBA-assay (4.4.17). As shown in Figure 20B, the specific activity of the enzyme pools increased 4.5 fold during the purification while in parallel the total amount of protein decreased 4.5 fold. This clearly indicates that the enzyme is stable under the selected purification conditions. It also illustrates the power of the chosen expression system as the recombinant endoNF amounts to more than 20 % of the soluble protein of the bacterial lysate.

Thus the subsequent purification of the catalytically active N-terminal fragment of endoNF by Ni<sup>2+</sup>-chelating and Strep-Tactin affinity chromatography resulted in homogeneously purified protein. From 1 l of bacterial expression culture 35 mg of catalytically active enzyme were obtained. After exchanging the buffer in a desalting step, the sample was concentrated to 7 mg/ml, flash frozen in liquid nitrogen and stored at -80 °C for crystallization trials.

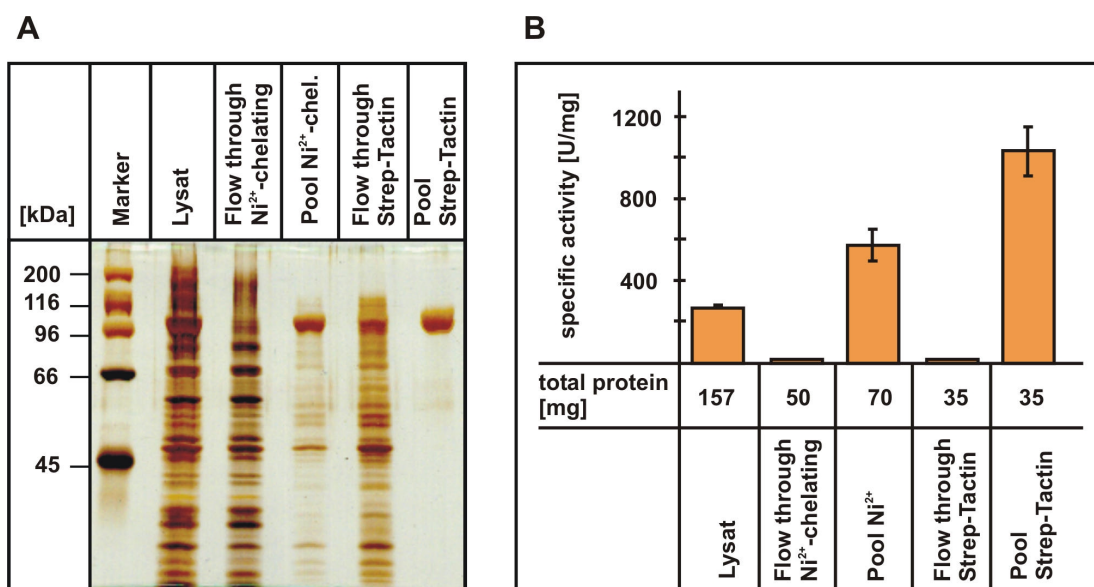


**Figure 20: Purification of the catalytically active N-terminal fragment of endoNF** (A) Subsequent purification the N-terminal fragment of endoNF (prominent band at 103 kDa) analysed by silver stained 10% SDS-PAGE. (B) The catalytic activity of the protein pools obtained during the purification was monitored using the TBA-assay. One unit was defined as the amount of endoNF that produces 1 nmol of reducing ends per minute at 37°C and pH 5.1. Additionally the total protein content of the pools is indicated.

### 5.2.2.3 Purification of the C-terminal fragment of endoNF

Purification of the C-terminal fragment of endoNF by Ni<sup>2+</sup>-chelating chromatography did not result in a homogeneous protein pool (5.2.2.1). It also contained full-length endoNF and parts of the N-terminal fragment. Therefore the pool was further purified by size exclusion chromatography as described in 4.4.13.3. As shown in Figure 15 efficient removal of the higher molecular weight forms could be achieved by this strategy. However, the separation of the small C-terminal fragment (22 kDa) from the significantly larger full length endoNF (125 kDa) or the N-terminal fragment (103 kDa), which additionally form stable trimers, was less pronounced than the huge differences in molecular mass suggested. Furthermore a minor fraction of the C-terminal fragment clearly co-eluted with the large fragments. Both facts suggest that also the C-terminal fragments aggregate to higher molecular mass oligomers.

From 1 litre of bacterial expression culture 2.5 mg of homogeneously purified C-terminal fragment were obtained. The sample was concentrated to 12 mg/ml, flash frozen in liquid nitrogen and stored at -80°C until used for crystallization trials.

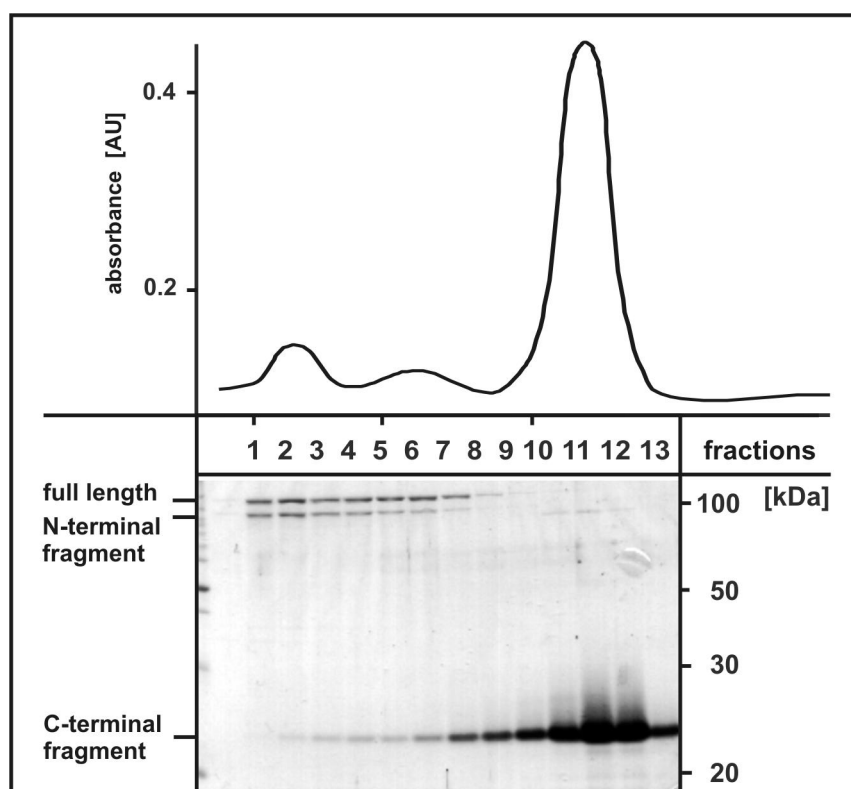


**Figure 21: Purification of the C-terminal fragment of endoNF by size exclusion chromatography** The pool containing the C-terminal fragment after Ni<sup>2+</sup>-affinity chromatography was further purified by gelfiltration. Eluted fractions were analysed by Coomassie stained 14% SDS-PAGE. Bands corresponding to full length uncleaved endoNF and to the N- and C-terminal fragments obtained after proteolytic processing are indicated.



### 5.2.2.4 Purification of $\Delta 245$ -EndoNF

Analysis of the N-terminal endoNF truncations (5.2.1) had revealed, that up to 245 amino acids could be deleted from the N-terminus without severely effecting expression rate, trimer stability or enzymatic activity. For crystallization trials therefore also truncated endoNF ( $\Delta 245$ -EndoNF-SH) was expressed and purified to homogeneity (Figure 21A) using the purification procedure described for the full-length protein (4.4.13). Like the full length endoNF also the truncated enzyme is highly stable under the purification conditions. The specific activity increased 6.6 fold during the purification while in parallel the total amount of protein decreased by the same factor. Considering the removal of 27% of the protein, the expression rates of full length and truncated endoNF and the specific activities of the purified samples are comparable. One litre of bacterial expression culture yielded 30 mg of the homogeneously purified  $\Delta 245$ -truncation. The protein was concentrated to 10 mg/ml, flash frozen in liquid nitrogen and stored at  $-80^{\circ}\text{C}$  for use in crystallization trials.

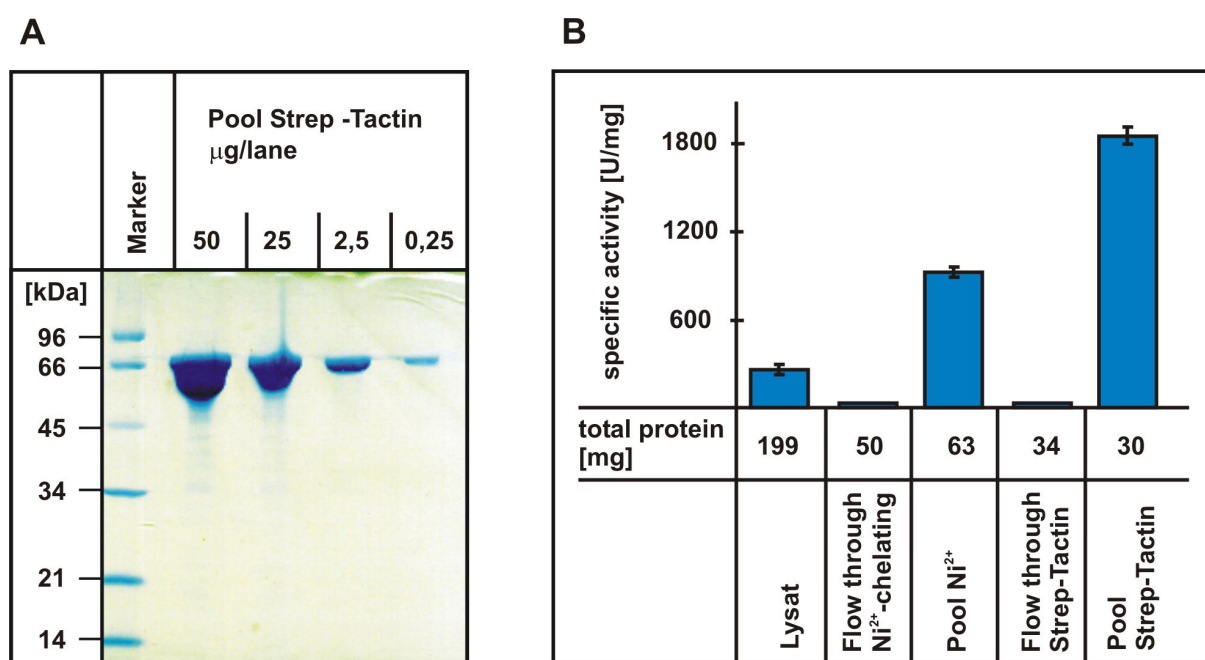


**Figure 22: Purification of  $\Delta 245$ -endoNF** (A) Coomassie stained 10% SDS-PAGE of  $\Delta 245$ -endoNF after the final purification step. To analyse the purity of the sample up to 50  $\mu\text{g}$  of protein were applied per lane as indicated. (B) The catalytic activity of the protein samples was monitored during the purification procedure using the TBA-assay. One unit was defined as the amount of endoNF that releases 1 nmol of reducing ends per minute at  $37^{\circ}\text{C}$  and pH 5.1. Additionally the total protein content of the samples is indicated.

### 5.2.2.5 Expression and purification of selenomethionine derivatised endoNF

The crystal structure of endoNF was solved by multiwavelength anomalous dispersion (MAD). For this method crystals were needed from selenomethionine derivatised endoNF. To obtain a protein, in which the methionine residues were quantitatively exchanged by selenomethionine residues, the methionine auxotroph *E. coli* strain B834(DE3) was used for protein expression. As described in 4.4.14 the bacteria were grown in M9 minimal medium that contained selenomethionine as the only methionine source. The protein was purified by Strep-Tactin affinity chromatography followed by Ni<sup>2+</sup>-chelating chromatography to remove residual uncleaved endoNF that co-purified in the first step (4.4.14). To avoid oxidation of the selenomethionine most steps of the purification were performed under reducing conditions. As depicted in Figure 23 the selenomethionine derivatised enzyme is functionally active and forms SDS-resistant complexes. However, the specific activity decreased after the second purification step, indicating that the derivative might be less stable than the native protein. 500 ml of bacterial expression culture yielded 7 mg of protein that was concentrated to 14 mg/ml, flash frozen in liquid nitrogen and stored at -80°C.

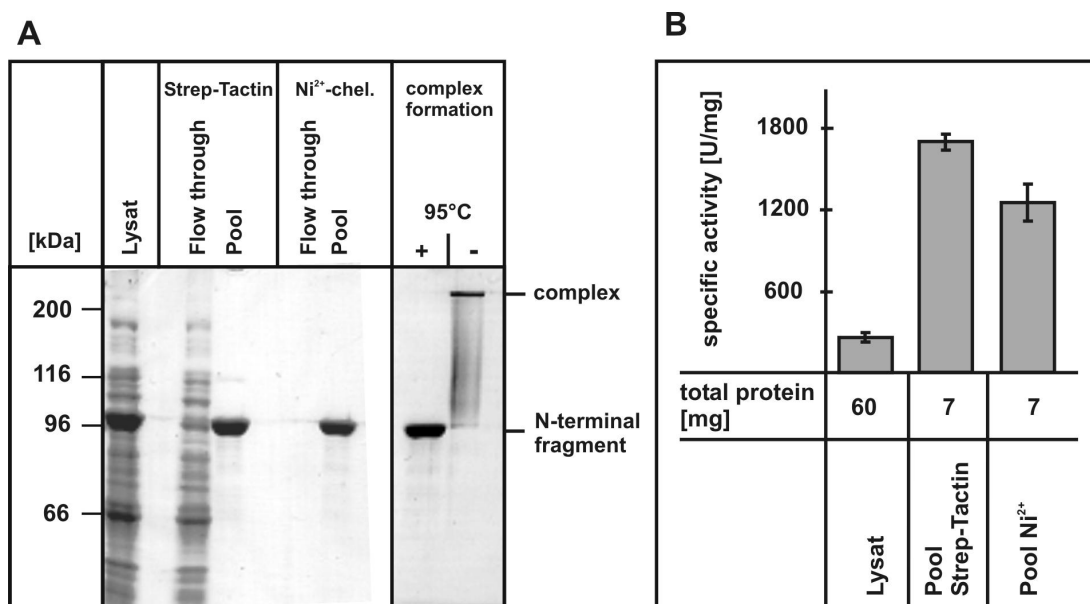


**Figure 23: Purification a selenomethionine derivative of  $\Delta 245$ -endoNF** (A) Coomassie stained 10% SDS-PAGE displaying the purification of the selenomethionine derivatised N-terminally truncated catalytic fragment of endoNF. The protein provides the major fraction in the bacterial lysate and binds quantitatively to the Strep-Tactin column. Homogeneously purified protein was obtained after Ni<sup>2+</sup>-chelating chromatography. Complex formation was analysed by omitting the boiling step before electrophoresis. Bands corresponding to monomeric endoNF and to the SDS-resistant trimeric complex are indicated. (B) The catalytic activity of the protein fractions analysed in (A) was monitored using the TBA-assay. One unit was defined as the amount of endoNF that produces 1 nmol of reducing ends per minute at 37°C and pH 5.1. Additionally the total protein content of the samples is indicated.

To check the incorporation of selenomethionine, the exact molecular mass of the recombinant protein was determined by ESI-TOF mass spectrometry. Each selenomethionine increases the molecular mass of the recombinant protein by 47 Da. The ESI-TOF analysis (cooperation with Dr. Detlev Suckau, Bruker Daltonik, Bremen) revealed a by 610 Da increased mass for the selenomethionine derivative (76514.2 Da; native protein 75904 Da). This mass difference is in perfect agreement with a complete replacement of the 13 methionine residues existing in endoNF with selenomethionine.

### 5.2.3 Crystallization and data collection

Crystallization trials were performed using the sitting drop vapour diffusion method described in chapter 4.4.19. Although extensively screened at 20 °C and at 4 °C no protein crystals were obtained for the full-length N-terminal fragment of endoNF (5.2.2.2). Also screenings with the C-terminal fragment (5.2.2.3) yielded no crystals. In contrast, well diffracting protein crystals were obtained for the truncated N-terminal fragment of endoNF (5.2.2.4) as shown in Figure 24.

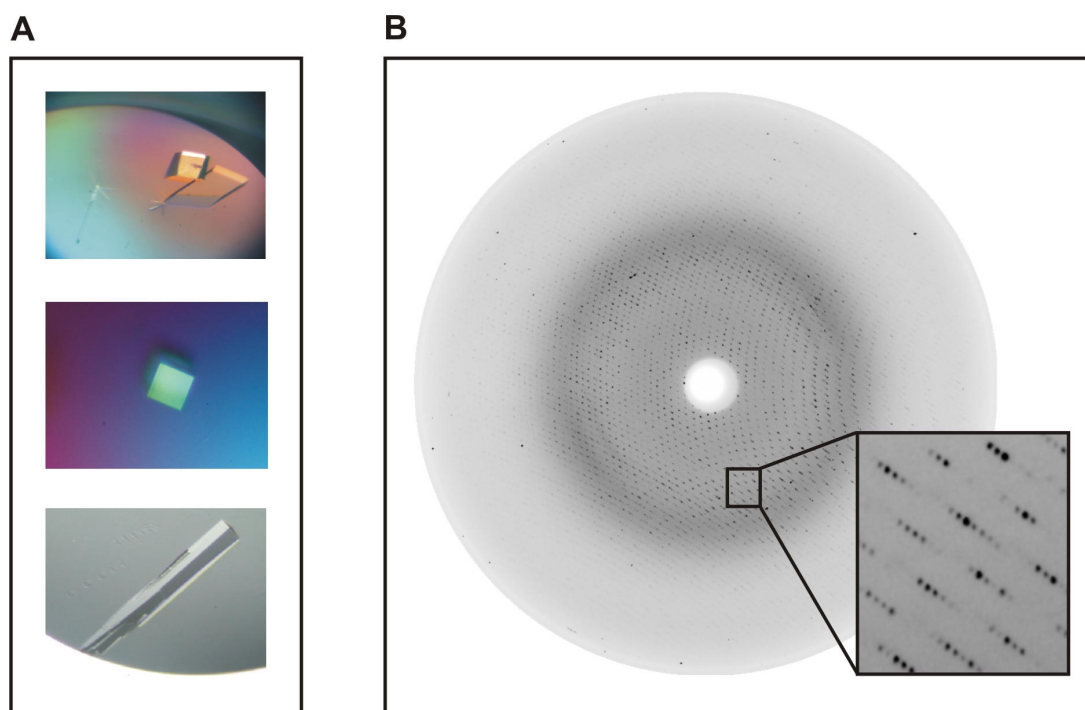


**Figure 24: Crystallization of  $\Delta 245$ -endoNF** (A) Crystals of the truncated (by 245 amino acids) catalytically active N-terminal fragment of endoNF. Colouring of the upper two pictures results from the use of a polarization filter. (B) Diffraction pattern of the crystals. The magnified panel illustrates the tight packing of the spots, which is due to the long axis of the unit cell ( $c = 346.7 \text{ \AA}$ ). The resolution at the edge of the image is 1.8  $\text{\AA}$ .

Crystals were grown at 20°C in 4 µl droplets composed of 2 µl protein solution (10 mg/ml) and 2 µl crystallization reagent (14 % PEG3350, 0.2M LiSO<sub>4</sub>, 0.1 M Tris/HCl pH 7.5, 4 mM DTT). The crystals appeared after one week and reached a maximum size of 100 x 100 x 1000 µm<sup>3</sup> within four weeks. The crystals belonged to the space group P222<sub>1</sub> with unit cell dimensions of  $a = 99.7 \text{ \AA}$ ,  $b = 131.3 \text{ \AA}$  and  $c = 346.7 \text{ \AA}$ . For data collection the crystals were soaked for 1 min in reservoir solution containing a cryoprotectant, mounted in cryo-loops and flash frozen in the nitrogen stream at 100 K. After careful optimisation of the cryoconditions (reservoir solution containing 10% 2,3-butanediol) native data to 1.9 Å were collected at the EMBL beamline 7B (DESY, Hamburg). Phase information necessary to solve the structure was obtained by multiwavelength anomalous dispersion (MAD). Therefore a three-wavelength dataset of a selenomethionine derivatized endoNF crystal was collected to 3.1 Å at the EMBL beamline 7A (DESY, Hamburg). The selenomethionine derivative was expressed and purified as described in chapter (5.2.2.5) and crystallized in analogy to the native Δ245-endoNF. To understand the molecular basis for the highly specific binding and cleavage properties of endosialidases it was necessary to analyse complexes with bound substrate. Crystals of the Δ245-endoNF-sialic acid complex were obtained by soaking native crystals in precipitant solution containing 3 mM pentameric α2,8-linked sialic acid (Calbiochem) for 48 h at 20°C. Data of the complex were collected to 2.6 Å at the BESSY BL2-Beamline in Berlin.

The collected data were processed and scaled either with DENZO/SCALEPACK (HKL Research) or MOSFLM (Powell, 1999) and SCALA (Bailey, 1994). The data statistics are summarized in Table 1.

### Data statistics

Data set	MAD			Native	(Di)sialic acid
Wavelength [Å]:	0.9800 (Peak)	0.9802 (Inflection)	0.9736 (Remote)	0.8416	0.9195
Space group:	P222 <sub>1</sub>			P222 <sub>1</sub>	P222 <sub>1</sub>
Cell dimensions [Å]:	$a = 100.1$ $b = 131.8$ $c = 348.3$			$a = 99.7$ $b = 131.3$ $c = 346.7$	$a = 99.5$ $b = 131.4$ $c = 346.0$
resolution [Å]:	3.15			1.90	2.55
No. of reflections:	150407	149441	152359	335241	130540
Completeness [%]:	98.7 (98.0)	97.1 (89.1)	99.9 (99.8)	93.7 (96.0)	88.4 (79.8)
Rmerge:	0.066 (0.128)	0.062 (0.125)	0.079 (0.127)	0.103 (0.352)	0.107 (0.303)

**Table 1: Data statistics** summarized for the three collected data sets.  $R_{\text{merge}} = \frac{\sum_{\text{hkl}} \sum_i |I_{\text{hkl}}^i - \langle I_{\text{hkl}}^i \rangle|}{\sum_{\text{hkl}} \sum_i \langle I_{\text{hkl}}^i \rangle}$  where the sum  $i$  is over all separate measurements of the unique reflections  $\text{hkl}$ .

#### 5.2.4 Phasing, density improvement, and model building

The crystal structure of  $\Delta 245$ -endoNF was solved by the multiwavelength anomalous dispersion (MAD) method. As the asymmetric unit of the crystals contained six monomers of  $\Delta 245$ -endoNF each providing 13 selenomethionine residues a total of 78 selenium sites had to be found. All selenium atoms were located using the program SHELX-D (Sheldrick, 2001) and initial phases were calculated in SHELX-E (Sheldrick, 2001). Density modification by solvent flattening, histogram matching and phase extension was performed in DM (Cowtan and Zhang, 1999). The resulting map showed molecular boundaries and allowed the recognition of secondary structural elements but could be significantly further improved by noncrystallographic symmetry (ncs) averaging. The ncs-operators symmetry relating the six monomers in the asymmetric unit were derived from the selenium sites using PROFESS (Bailey, 1994) while for the averaging again the program DM was used. The resulting map at 1.9 Å was of good quality and interpreted by cycles of model building in O (Jones *et al.*, 1991) and Xtalview (McRee, 1992) and refinement using REFMAC (Bailey, 1994). To interpret the asymmetric unit first an initial C $\alpha$ -trace for one monomer was built in O that was then used to generate also the C $\alpha$ -traces of the remaining five monomers by symmetry transformations using the ncs-operators in MOLEMAN2 (Kleywegt, 1997). After rigid-body refinement in REFMAC the C $\alpha$ -traces were converted into poly-alanine models and the amino acid side chains were built in XFIT (McRee, 1992). Again only one monomer was manually built, while the others were obtained by symmetry transformations. The model was refined using the maximum-likelihood algorithm implemented in REFMAC applying ncs-restraints and individual isotropic B-factor refinement. After three additional cycles of manual model building and refinement water molecules were included using ARP/wARP cycled with REFMAC. In later stages also TLS-refinement was used where each monomer was defined as one TLS-group. The final model contained all endoNF residues except the very C-terminal serine and one additional N-terminal serine that is part of the affinity tag. This results in 3996 Protein residues in the asymmetric unit that also contained 3075 water molecules and six phosphate ions. The final model refined to an R-factor of 16.6 % with a corresponding R<sub>free</sub> of 20.2 % over a 5 % test set of the reflections and good stereochemical quality. The refinement statistics are summarized in Table 2.

---

**Refinement statistics**


---

Data set	Native	(Di)sialic acid
R-factor [%]:	16.6	18.0
R <sub>free</sub> [%]:	20.2	23.1
No. protein atoms:	31380	31380
No. of water molecules:	3075	926
No. ligand atoms:	30	279
Average protein B-value [Å <sup>2</sup> ]:	14.2	21.0
Average ligand B-value [Å <sup>2</sup> ]:	36.9	40.3
Average water B-value [Å <sup>2</sup> ]:	27.3	28.1

---

**Ramachandran plot of non-glycine and non-proline residues**


---

most favourable regions:	2885 (85.1 %)	2857 (84.3 %)
additionally allowed regions:	472 (13.9 %)	494 (14.6 %)
generously allowed regions:	27 (0.8 %)	28 (0.8 %)
disallowed regions:	6 (0.2 %)	11 (0.3 %)

---

**r.m.s. deviations from ideal values**


---

Bond distances [Å]:	0.012	0.015
Angles [°]:	1.43	1.57

---

**Table 2: Refinement statistics**

$$R\text{-factor} = \frac{\sum_{hkl} |F_{obs}| - |F_{calc}|}{\sum_{hkl} |F_{obs}|}$$

R<sub>free</sub> as R-factor but summed over a 5 % test set of reflections.

For the Δ245-endoNF complexed with sialic acid the structure factors calculated from the processed data of the complex were merged with the native model-phases. After refinement in REFMAC clear additional electron density for monomeric and dimeric sialic acid moieties bound to the enzyme was observed in the F<sub>O</sub>-F<sub>C</sub>-map. The ligands were build in O and the final model refined to an R-factor of 18.0 % with a corresponding R<sub>free</sub> of 23.1 % over a 5 % test set of the reflections. It included 3996 protein residues, 3075 water molecules, 6 phosphate ions and six monomeric as well as three dimeric sialic acid ligands. The refinement statistics are summarized in Table 2.

The coordinates of Δ245-endoNF as apoenzyme and in complex with substrate have been submitted to the Protein Data Bank (PDB). The accession codes are 1v0e for the apoenzyme and 1v0f for Δ245-endoNF complexed with sialic acid.

## 5.2.5 Structure description

### 5.2.5.1 Overall structure of the catalytic fragment of endoNF ( $\Delta 245$ -endoNF)

The asymmetric unit of the crystals obtained from  $\Delta 245$ -endoNF contains six monomers. In agreement with the protein analytical studies (5.2.1) the monomers are arranged in two trimers. As shown in Figure 25A the trimers exhibit an overall mushroom-like outline that can be clearly separated in a stalk and a head region. Maximum dimensions are 100 Å in width and 115 Å in length.

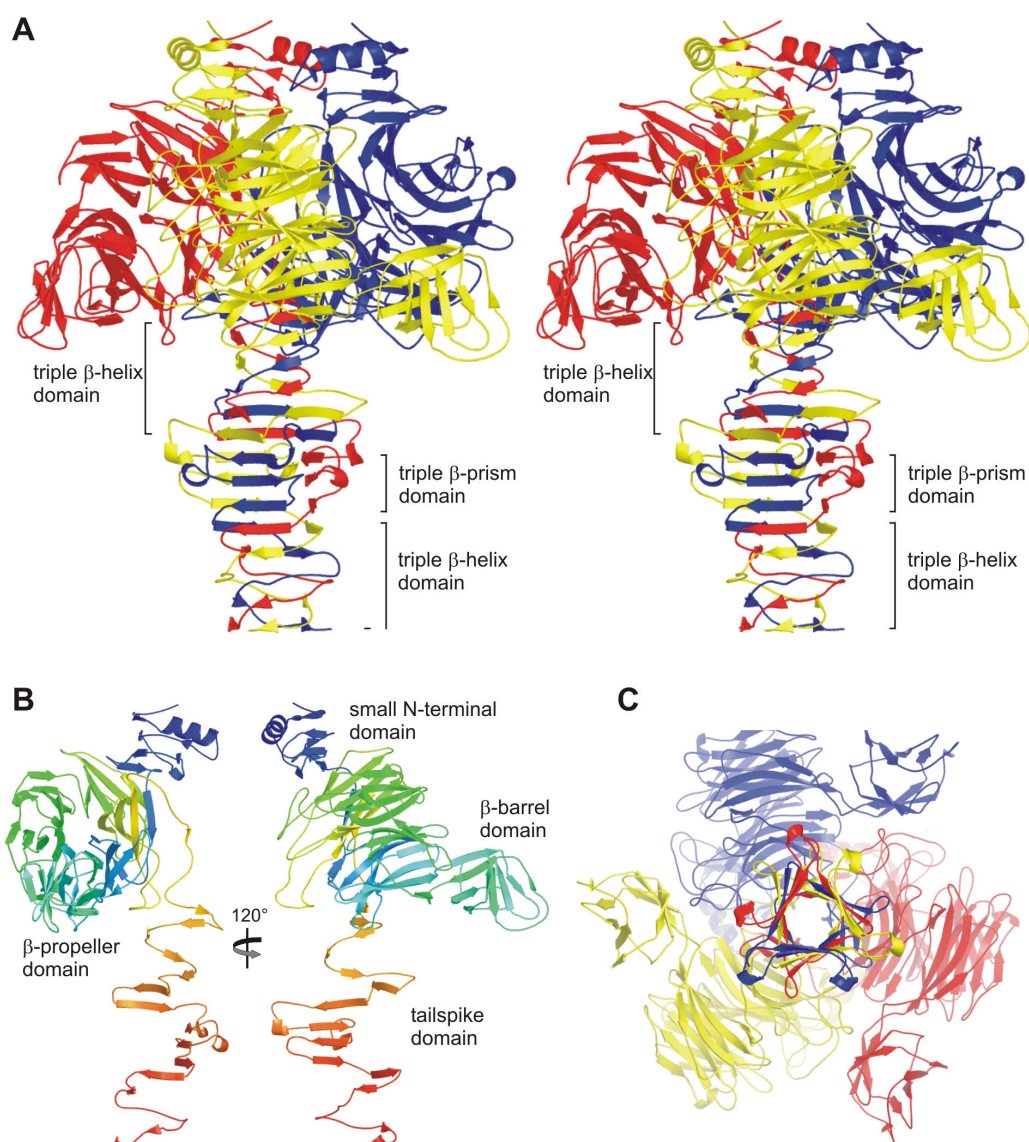


**Figure 25: Structure of  $\Delta 245$ -endoNF** (A) Ribbon stereo diagram of one of the  $\Delta 245$ -endoNF homotrimers present in the asymmetric unit. The three monomers are coloured red, blue and yellow. (B) Structure of the  $\Delta 245$ -endoNF monomer. The four domains that can be discerned in the monomer are indicated. The chain is coloured from blue at the N-terminus through to red at the C-terminus. (C) Bottom view of the homotrimer with cross-section through its triangular tail domain. Ribbon diagrams were drawn with PYMOL (DeLano, 2002).

Each monomer folds into four distinct domains (Figure 25B). The three N-terminal domains assemble in the compact head whereas the C-terminal domain forms an extended tail-like structure. In the trimer the three tails intertwine to build an elongated stalk of 60 Å in length with triangular cross-section (Figure 25A, C).

The mushroom head is dominated by a six-bladed  $\beta$ -propeller typical for sialidases (Taylor, 1996). From the third blade of the  $\beta$ -propeller a nine-stranded  $\beta$ -barrel is branching off, which shows structural homology to the  $\beta$ -barrel domains of elongation factors and flavoproteins. Although the primary sequence identity is only 11%, the  $\beta$ -barrel structures of the *E. coli* elongation factor EF-Tu (PDB-entry 1EFC) and of endoNF can be superimposed with an r.m.s.d. fit of 2.6 Å.

The very N-terminal part of the head structure (residues 246-322) holds the only  $\alpha$ -helix of the entire 666 amino acid spanning protein. This is presumably the residual part of the deleted N-terminal domain (residues 1-245) proposed to be the head binding domain, which attaches the endosialidase to the phage tail (Petter *et al.*, 1993; Pajunen *et al.*, 2000).

#### 5.2.5.2 The head region: active site and polySia binding

The six bladed  $\beta$ -propeller is known to be a characteristic structural feature of exosialidases. The structure is found in all bacterial, viral, and eukaryotic exosialidases solved so far. The propeller blades, each build by a four-stranded antiparallel  $\beta$ -sheet, are assembled around a central axis that passes through the active site cleft. While this overall topology is similar, the loop regions and the length of the  $\beta$ -strands differ between the respective exosialidases. The sialidase  $\beta$ -propeller of endoNF shows higher structural similarity to bacterial (Crennell *et al.*, 1993; Crennell *et al.*, 1994; Gaskell *et al.*, 1995) and eukaryotic (Luo *et al.*, 1998; Buschiazzo *et al.*, 2000) than to viral sialidases (Varghese *et al.*, 1991; Tulip *et al.*, 1991; Burmeister *et al.*, 1992). The  $\beta$ -propeller domains of endoNF and a *Trypanosoma rangeli* sialidase (Buschiazzo *et al.*, 2000) can be superimposed with an r.m.s.d. of 3.0 Å between 280 equivalent C $\alpha$ -atoms, indicating significant structural similarity. Common to all non-viral exosialidases are the short 'Asp-box' motifs (SXDXGXTW) forming conformationally well conserved  $\beta$ -hairpins. The two Asp-box motifs found in endoNF are located between sheet three and four of the second and the fifth propeller blade. Superposition of the two  $\beta$ -hairpins including all main- and sidechains atoms of the eight residues results in an r.m.s.d. of 0.8 Å, illustrating their structural similarity.



However, the active site clefts located around the hub of the propeller differ between exosialidases and endoNF. Only three out of the six amino acids conserved in all known exosialidases are present in endoNF (Figure 26).

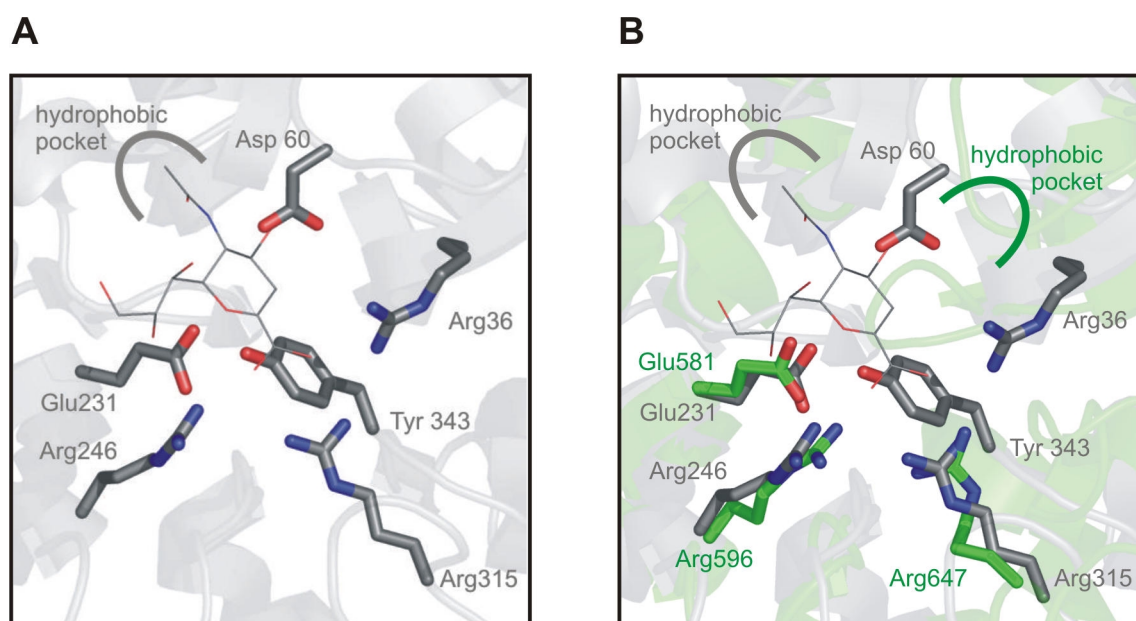


**Figure 26: Overlay of conserved active site features of exosialidases with the active site of endoNF.** (A) Highly conserved active site residues of exosialidases are indicated and shown in grey stick representation. Exemplary a sialidase from *Trypanosoma rangeli* (PDB-entry 1mz6) is depicted with bound inhibitor DANA. The hydrophobic pocket accommodating the N-acetyl group of DANA is depicted as grey cartoon. (B) Overlay with the corresponding residues preserved in endoNF (green). The displaced hydrophobic pocket of endoNF is shown as green cartoon.

Conserved are two arginines (Arg596, Arg647) and one glutamic acid (Glu581) residue. In exosialidases, the respective arginines are part of a conserved arginine triad involved in binding to the carboxylate group of sialic acid. The conserved glutamic acid together with a conserved tyrosine (missing in endoNF) is believed to stabilize the sialosylation transition-state intermediate proposed for the exosialidase reaction (Chong *et al.*, 1992). Superposition of the conserved residues provides strong evidence that the substrate orientation in the active site of endo- and exosialidases is considerably different. Interestingly, the hydrophobic pocket accommodating the N-acetyl group of sialic acid is displaced by a rotation of 90° (Figure 26B). This finding explains why trials to incorporate 2,3-dehydro-3-deoxy-N-acetylneuraminic acid (DANA), a common active site ligand in exosialidase structures, into endoNF crystals either by soaking or in co-crystallization experiments failed.

Soaking endoNF crystals with pentameric  $\alpha$ 2,8-linked sialic acid and subsequent crystal structure analysis revealed that the nine-stranded  $\beta$ -barrel domain extending from the sialidase propeller is involved in polySia binding (Figure 27). A clear additional electron density corresponding to a disialic acid moiety identified a specific binding site within the  $\beta$ -barrel domain (Figure 27B). Due to differing accessibilities of the binding sites within the crystal lattice, bound disialic acid was observed for only three out of six monomers present in the asymmetric unit.

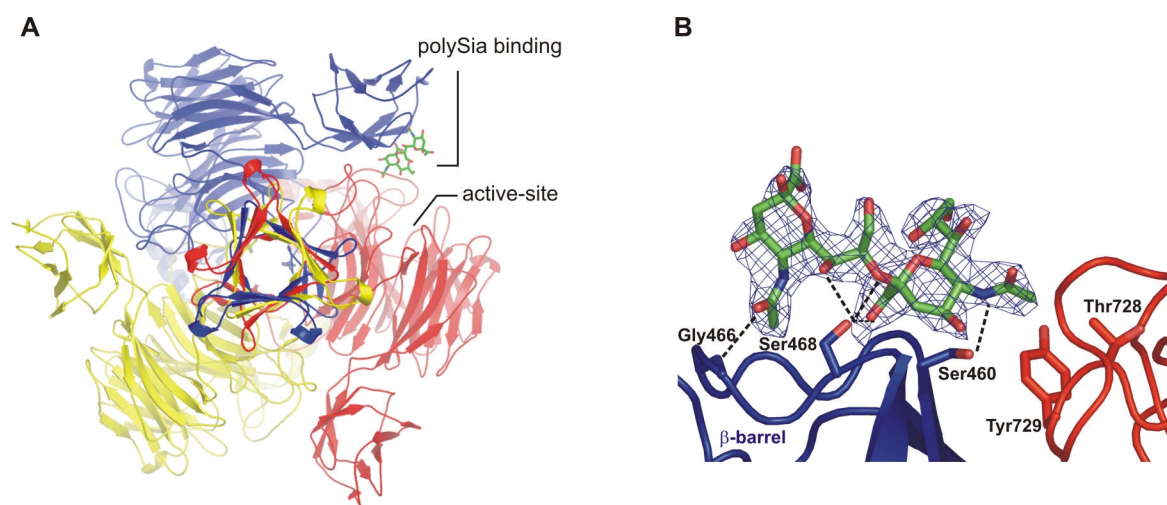


**Figure 27: PolySia bound to the  $\beta$ -barrel of endoNF** (A) Bottom view of the homotrimer with cross-section through its triangular tail domain. An  $\alpha$ 2,8- linked sialic acid dimer bound to the blue  $\beta$ -barrel domain is shown in stick representation (B) Details of the disialic acid binding. Residues involved in sugar binding are labelled and according to the respective subunit coloured in blue or red. Dotted lines indicate hydrogen bonding interactions. The ligand is depicted in green sticks while the final electron density observed in a refined 2F0-Fc map contoured at 1  $\sigma$  is represented as blue mesh.

The bound disialic acid points with the non-reducing end towards the core of the trimer and the two  $\alpha$ 2,8-linked sialic acid moieties are anticlockwise twisted by 57°. Interaction is mainly mediated by Ser468 forming hydrogen bonds to one of the carboxylate oxygens of the sialic acid residue at the non-reducing end, to the oxygen of the glycosidic linkage, and to the 7-hydroxyl oxygen of the sialic acid at the reducing end. Additional hydrogen bonds are established between the main chain nitrogen of Gly466 and the N-acetyl carbonyl oxygen of the reducing sugar as well as between Ser460 and the nitrogen in position C-5 of the sialic acid at the non reducing end, while the methyl function of the N-acetyl group is in hydrophobic contact with Thr728 and Tyr729. Both residues belong to the  $\beta$ -propeller of the

adjacent monomer, indicating that oligomerisation of endoNF is essential for enzymatic activity. This is further supported by the fact that the 22 Å distant active site cleft of the involved  $\beta$ -propeller could be reached by a pentameric substrate.

The functional trimer is a rigid structure with low flexibility. In the trimeric head region (residues 246-786), contacts between the three monomers are mediated by more than 90 intermolecular hydrogen bonds, mostly provided by the linkers connecting  $\beta$ -propeller and the tailspike domains, burying 25% of the monomer's solvent accessible surface upon trimerisation. The mainly hydrophobic interface between  $\beta$ -barrel and  $\beta$ -propeller buries a total of  $\sim 920$  Å<sup>2</sup>, corresponding to 17.5 % of the  $\beta$ -barrel and contains three interdomain hydrogen bonds. Thus, the catalytic domain of endoNF is assembled by stable intermolecular interactions between the polySia binding and cleaving domains of two adjacent monomers (Figure 28).

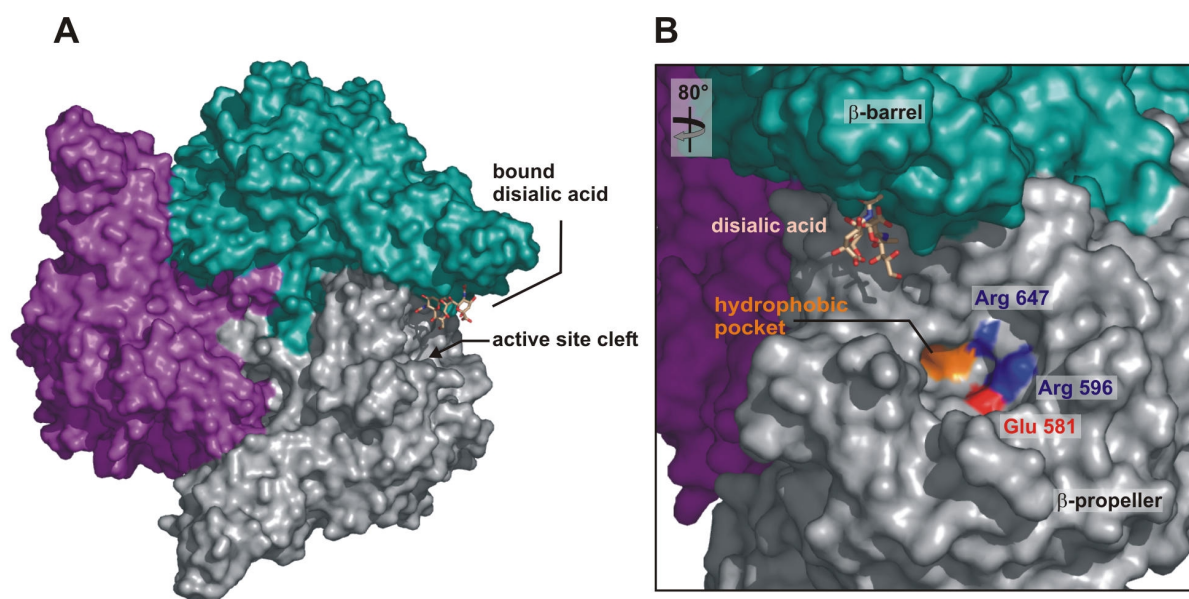


**Figure 28: EndoNF is a functional trimer** (A) Surface representation of the trimeric head domain of endoNF. Bottom view with deleted trimeric stalk. The bound disialic acid and the position of the active site cleft are indicated. (B) The magnified picture is rotated by 80° to illustrate the orientation of dimeric sialic acid towards the active site cleft in more detail. Conserved active site residues and the hydrophobic pocket are indicated.

As illustrated in Figure 28 the topology of the active site cleft suggests the introduction of a sharp kink into the polySia chain upon binding. This would first of all favour the planar transition state proposed for the sialidase reaction (Chong *et al.*, 1992). Besides that the introduced kink could move the carboxyl group of a vicinal sialic acid residue into a favourable position to substitute the carboxylate function of the missing aspartic acid residue

(Figure 26) that initialises the hydrolysis of the glycosidic linkage in exosialidases. This substrate-assisted catalysis could explain the strict substrate specificity of endosialidases for polysialic acid. The potential reaction mechanism of endoNF is discussed in more detail in chapter 6.2.

### 5.2.5.3 The stalk region: intertwined subunits and sialic acid binding

Intermonomeric interactions established already in the head region are further intensified in the trimeric stalk (residues 784-910) where the three C-terminal tailspike domains intertwine. Here a total of 62% of the monomer's solvent accessible surface is buried in the trimer highlighting the intense intersubunit interactions in this domain. The stalk region folds in a triple  $\beta$ -helix that is interrupted by a small triple  $\beta$ -prism domain (Figure 25A). Both folds have recently been described for three bacteriophage tail proteins (Steinbacher *et al.*, 1994; van Raaij *et al.*, 2001; Kanamaru *et al.*, 2002) and especially the triple  $\beta$ -helix has been accounted for the unusually stable trimers of these proteins. The trimeric stalk of endoNF exhibits an overall twisted appearance with a total twist of 120°. The triangular shaped interior contains no ordered waters and is exclusively hydrophobic except for one histidine (His874) involved in an interchain hydrogen bond to tyrosine 869. The inwardly pointing residues build six hydrophobic stacks extending over the whole length of the domain (Figure 29B-C). Substantial networks of hydrogen bonds, intrachain in the prism-domain or interchain in the intertwined  $\beta$ -helical domains, additionally stabilize the stalk region.

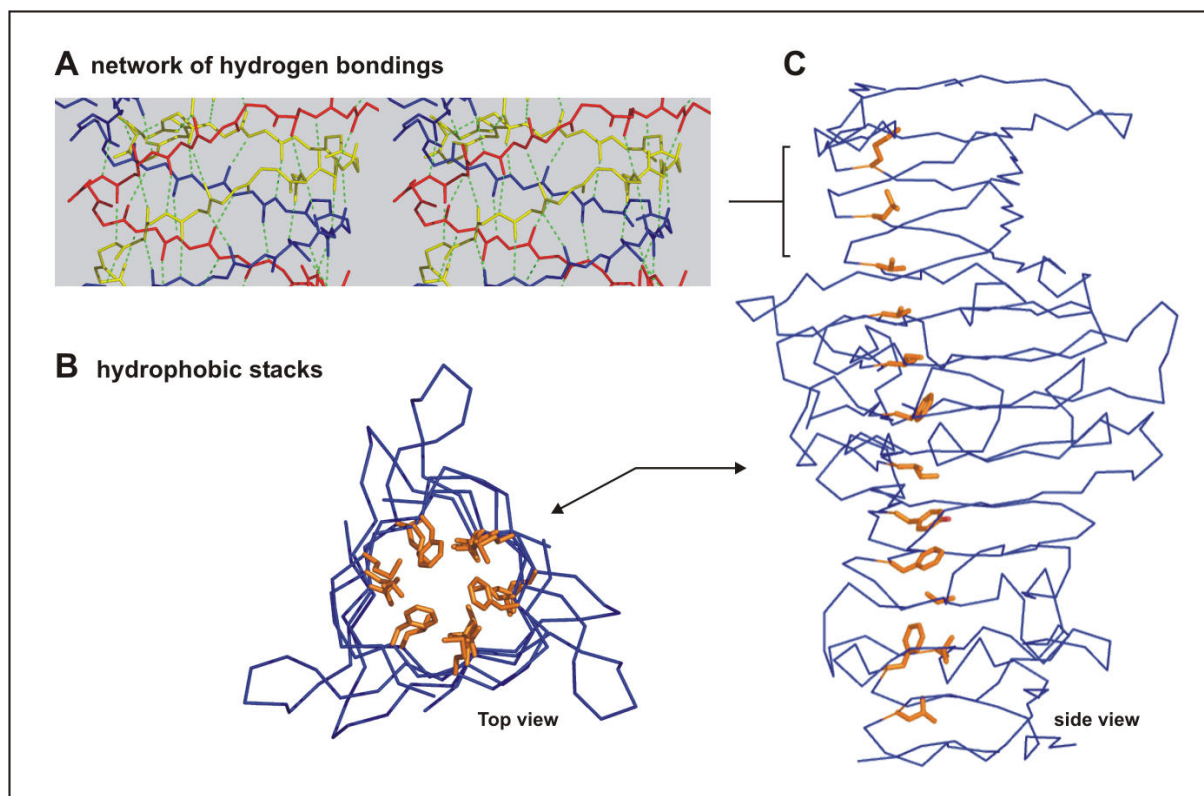


**Figure 29: Stabilizing interactions of the stalk region** (A) Stereo ribbon diagram illustrating the network of interchain hydrogen bondings established in the triple  $\beta$ -helix domain. Hydrogen bonds are shown as green dotted lines while the main chain atoms of the three intertwined subunits are shown in red, blue and yellow, respectively. The depicted fragment of the stalk is indicated in panel C. (B) Top view showing the six hydrophobic stacks in the interior of the stalk. Hydrophobic side-chains are coloured in orange. (C) Side view of the stalk domain. The hydrophobic site chains of one of the stacks (indicated with an arrow) are shown in orange.

The first  $\beta$ -helical turn (residues 784-799) is similar to the  $\beta$ -helix domain found in the short tail fibre of bacteriophage T4 (van Raaij *et al.*, 2001). Superposition of these sixteen equivalent  $C\alpha$  atoms results in an r.m.s.d. of 2.7 Å. The second helical turn (residues 800-826), however, differs significantly from the first. The length of the  $\beta$ -strands increases from three to six residues and additionally a twist of  $50^\circ$  is introduced into the stalk. Both changes are mainly mediated by the more extended loop regions of this turn. The  $\beta$ -helical domain in the C-terminal region of the stalk (residues 871-910) appears less regular than the two N-terminal turns. The faces of the triple  $\beta$ -helix are inwardly curved and the length of the  $\beta$ -strands decreases from five to only two residues at the C-terminal end. In parallel, also the surface area of the triangular cross section decreases by 50 % and again a twist of  $50^\circ$  is introduced into the trimeric stalk. The small triple  $\beta$ -prism domain (residues 827-870) interrupting the two intertwined  $\beta$ -helix domains contains three antiparallel  $\beta$ -strands of five



residues each. The loop connecting the first  $\beta$ -helix to the  $\beta$ -prism domain and the loop between the first two strands of the  $\beta$ -prism both contain a three residue spanning 3/10-helix and expand vertically over the face of the  $\beta$ -sheet creating a shallow groove. Remarkably, this groove could be identified as second sialic acid binding site, for which well defined electron density of a bound single sialic acid molecule in  $\beta$ -conformation was observed for all six monomers in the asymmetric unit.

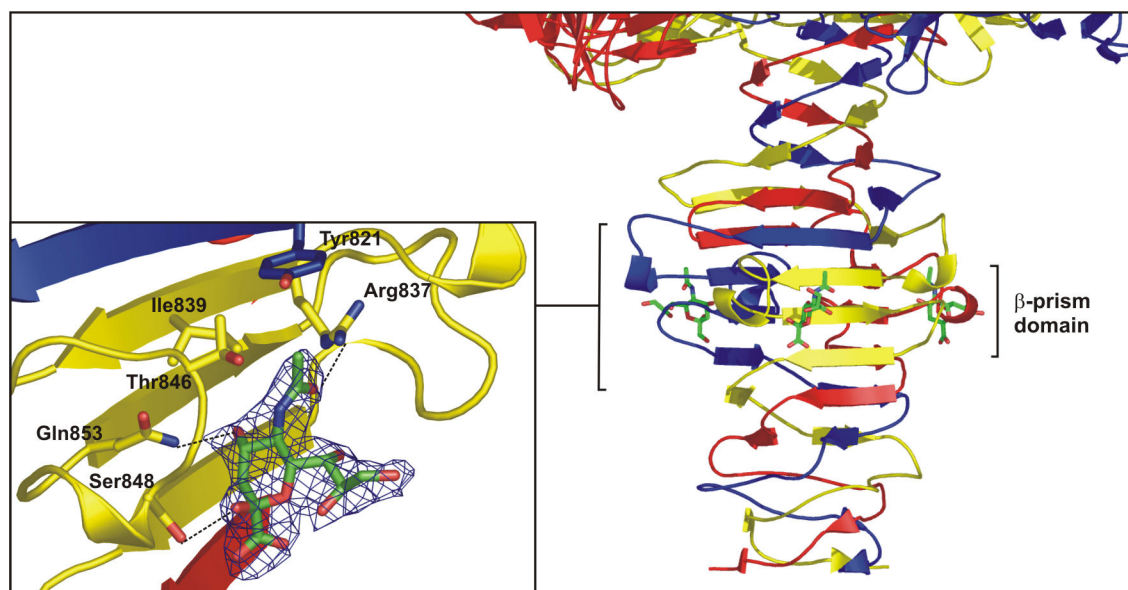


**Figure 30: Sialic acid binding site of the stalk region** Side view of the stalk region with sialic acid residues shown in stick representation (green) bound to the three  $\beta$ -prism domains. The three monomers are coloured red, blue and yellow, respectively. Details of sialic binding are illustrated in the insert panel showing a magnified slightly rotated view of one binding site. Residues involved in sialic acid binding are labelled and according to the respective subunit coloured in blue or yellow. Dotted lines indicate hydrogen bonding interactions. The final electron density of the ligand observed in a refined 2F<sub>0</sub>-F<sub>c</sub> map contoured at 1  $\sigma$  is represented as blue mesh.

This carbohydrate-protein interaction is mediated by hydrogen bonds of Gln853 to the 4-hydroxyl oxygen and by main and side chain atoms of Ser848 to the 2-hydroxyl oxygen of the sugar. Furthermore the carbonyl oxygen of the sialic acid N-acetyl group hydrogen bonds to Arg837 while the methyl group is involved in hydrophobic interactions with Thr846 and Ile839 as well as Tyr821 that comes from a second subunit. Thus the trimeric stalk region of endoNF has not just dominant influence on the stability of the functional trimer, but is also directly involved in substrate binding.

### 5.2.6 Site directed mutagenesis of conserved active site residues of endoNF

As shown in Figure 26 three active site residues of endoNF, a glutamic acid (Glu525) and two arginines (Arg596, Arg647), are conserved in all sialidases analysed so far. In initial mutagenesis studies, the conserved residues were exchanged to alanine by site-directed mutagenesis as described in chapter 4.2.12 and the mutant enzymes were expressed in *E. coli* BL21(DE3) (4.4.8). Soluble fractions of the bacterial lysates were analysed by SDS-PAGE (4.4.2) and Western blot analysis (4.4.5) and enzymatic activity was assayed using the ELISA-based endosialidase activity assay (4.4.18). The assay principle does not allow quantitative comparison of the enzyme activity but enables qualitative comparison at the basis of endpoint dilution.

As depicted in Figure 31 all mutant enzymes are proteolytically cleaved and form SDS-resistant trimers. The expression levels are comparable to the wild-type with exception of the mutant R647A that is expressed at detectable lower level.

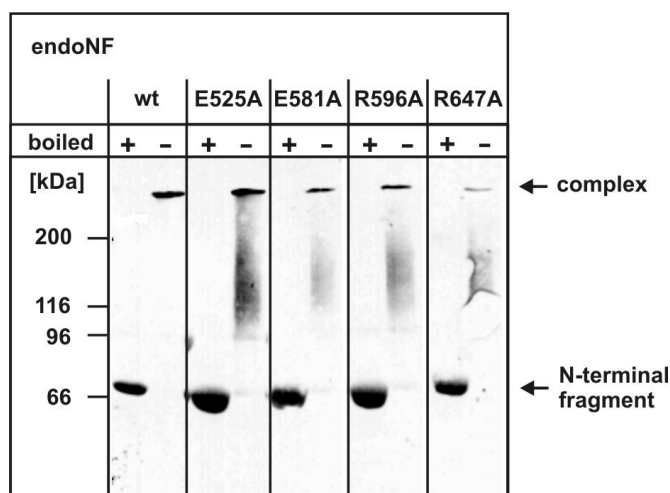


**Figure 31: Site directed mutagenesis of conserved active site residues of endoNF** (A) Wild type and mutant forms of endoNF were expressed in *E. coli* BL21(DE3). Soluble fractions of the bacterial lysates were analysed by 8 % SDS-PAGE and Western blot developed with StrepTactin directed against the StrepII-tag.

Mutagenesis of the conserved active site residues decreased the activity of the mutant enzymes significantly (Figure 32). The wild-type fraction could be diluted at least 100 fold further than the three mutants E581A, R596A and R647A. In contrast mutation of the glutamic acid in position 525, which is located at the bottom of the active site cleft as direct neighbour of E581, had no influence on the enzymatic activity.

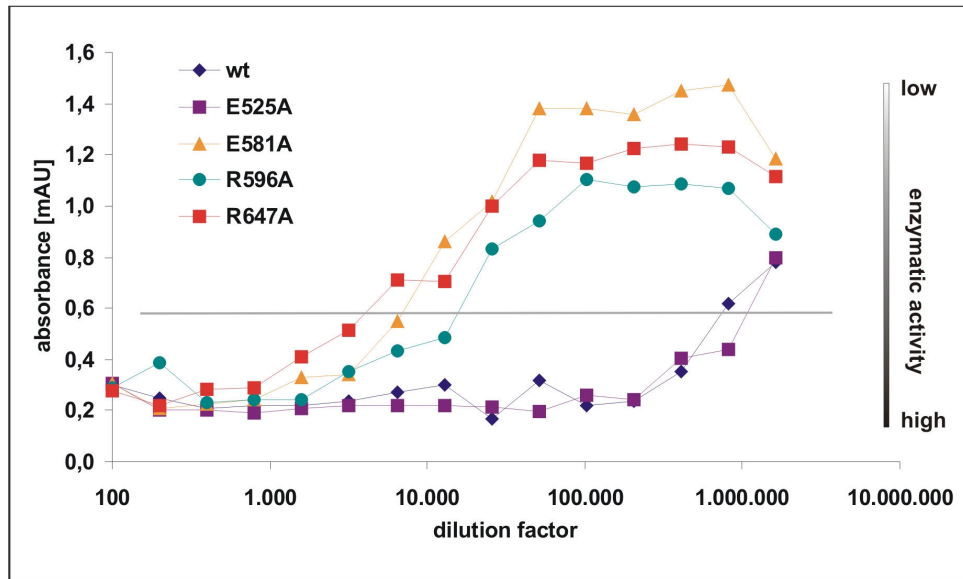


**Figure 32: Enzymatic activity of mutant endosialidases (A)** ELISA based endosialidase activity assay. Microplate wells coated with polySia were incubated with serial dilutions of the soluble fractions as indicated. The remaining non-cleaved substrate was afterwards detected by immunostaining using the polySia specific mAb 735. High absorbance values correspond to low enzymatic activity of the sample.

In summary these data allow to conclude, that the three conserved active site residues are important for the enzyme reaction of endoNF, but none of the residues is essential, since all the mutant enzymes clearly exhibit activity.



## 6 Discussion

### 6.1 The eukaryotic polysialyltransferase ST8SiaIV: Large scale expression, purification and crystallisation trials

The presence of  $\alpha$ 2,8-linked polysialic acid (polySia) on the neural cell adhesion molecule (NCAM) modulates the cell-cell interactions during developmental processes and oncogenesis. The polySia expression of some human tumours of neuroectodermal origin could recently be directly correlated with high metastatic potential and poor prognosis (Daniel *et al.*, 2001). Modulating polySia expression in the tumour situation is therefore an important goal and has moved the polysialyltransferases ST8SiaII and ST8SiaIV, the key enzymes in polySia synthesis, into the centre of therapeutic interest. However, although extensively studied there is only limited knowledge about the biochemical properties of these enzymes and no structural information is available so far. The detailed analysis of structure function relationships in polysialyltransferases is mainly hampered by the lack of expression systems capable to supply sufficient amounts of active enzymes. The mammalian polysialyltransferases ST8SiaII and ST8SiaIV are glycoproteins, containing six and five N-glycan attachment sites, respectively, and it has been shown that N-glycosylation plays a pivotal role for the catalytic functions of the enzymes (Mühlenhoff *et al.*, 1996a; Close *et al.*, 2000; Mühlenhoff *et al.*, 2001). Thus, trials to express the mammalian enzymes in protein-glycosylation deficient organisms like *E. coli* resulted in the production of inactive proteins. On the other hand trials to express polysialyltransferases in glycosylation competent mammalian cell systems have so far been confronted with the problem of low yields. Therefore, the goal of this study was to evaluate the insect cell line established from *Spodoptera frugiperda* (*Sf9* cells) as expression system for the mammalian polysialyltransferases. Hamster ST8SiaIV was used as a model protein in these studies.

In insect cells high expression rates of recombinant proteins can be obtained, in particular in combination with baculovirus expression vectors. Insect cell are glycosylation competent (for review see (Altmann *et al.*, 1999) though the produced glycan structures differ from the complex mammalian type N-glycans; for example, no terminal sialic acid residues and only very little, if any, galactose residues are found.

Active polysialyltransferases can be expressed as secreted soluble proteins when the N-terminal transmembrane domain is replaced by a secretion signal (Mühlenhoff *et al.*, 1996a).

Therefore a recombinant baculovirus was constructed encoding the N-terminally truncated ST8SiaIV $\Delta$ 25 downstream of the honeybee melittin secretion signal (Figure 7). As shown in Figure 8, catalytically active ST8SiaIV was expressed and secreted to the culture medium of infected *Sf9* cells. By ELISA-based activity assay the capability of the recombinant enzyme to perform NCAM- and autopolysialylation was clearly demonstrated (Figure 9B). The finding that ST8SiaIV expressed in insect cells was able to perform autopolysialylation was surprising, because earlier studies with polysialyltransferases expressed in CHO-cells had shown that autopolysialylation requires the presence of terminal galactose residues (Mühlenhoff *et al.*, 1996a). Initial lectin analyses of *Sf9* cell lysates and of recombinant ST8SiaIV expressed in these cells gave no indication for the presence of sialic acid or galactose (data not shown). Hence N-acetylglucosamine or potentially mannose might be the acceptors for the transferred sialic acid. However, the lectin analysis is not sufficiently sensitive to completely exclude that a minor fraction of ST8SiaIV is galactosylated and represents the autocatalytically active enzyme. More detailed glycan analysis by mass spectrometry will be necessary to characterize the polySia acceptor structures of insect cell expressed ST8SiaIV.

As the ST8SiaIV $\Delta$ 25 was secreted in good quantities, a procedure to purify the recombinant enzyme from the culture medium of infected *Sf9* cells was established. Though pioneering small-scale purifications of ST8SiaIV $\Delta$ 25 by myc-affinity chromatography (mAb 9E10) were promising (Figure 9A), the protein turned out to be unstable under the pH-conditions needed for elution from the myc-affinity column during the up-scaling studies. Purified protein fractions started to form precipitates shortly after elution and all trials to avoid the formation of insoluble precipitates failed. To circumvent these problems an alternative purification via His<sub>6</sub>-affinity chromatography was established. This technique avoids the acidic steps, which, by all likelihood, were responsible for protein denaturation. Instead His<sub>6</sub>-tagged proteins bound to a Ni<sup>2+</sup>-affinity column are eluted by increasing imidazole concentrations. As the binding affinity of the His<sub>6</sub>-epitope to the Ni<sup>2+</sup>-matrix is significantly lower than the myc-9E10-affinity, trials to bind recombinant ST8SiaIV $\Delta$ 25 to the affinity matrix directly from the harvested supernatant failed. Careful optimisation steps were necessary to improve the binding conditions. The major problem in the loading step resulted from low molecular weight components of the insect cell culture media. These compounds competitively interfere with the His<sub>6</sub>-tagged protein for binding to the column. Therefore the harvested supernatant was concentrated ten fold and simultaneously the buffer was exchanged by tangential cross-

flow filtration. This treatment allowed efficient binding of the recombinant protein to the affinity column and resulted in almost homogeneously purified protein in a single step (5.1.2.2). The resulting protein fractions could be concentrated to 10 mg/ml without detectable precipitate, indicating the higher stability compared to myc-affinity purified ST8SiaIV. Furthermore, the isolated enzyme was active. Additional purification by gel filtration resulted in homogeneously purified ST8SiaIV (Figure 14).

To compare processivity between CHO and insect cell expressed ST8SiaIV $\Delta$ 25 polySia chains produced by the respective enzymes were visualized in a radioactive polysialyltransferase assay. To visualize the chain length of the synthesized polySia, purified ST8SiaIV $\Delta$ 25 was analysed in a radioactive polysialyltransferase assay where the synthesized radiocarbon labelled polySia is detected by autoradiography after separation by SDS-PAGE. As shown in Figure 13 the pattern of the observed radioactive signals are similar for ST8SiaIV $\Delta$ 25 expressed in *Sf9* insect cells and in CHO cells, indicating that both enzymes synthesize polySia chains of comparable length. After specific degradation of polySia by endoneuraminidase, two distinct bands corresponding to formerly polysialylated NCAM and enzyme appeared, demonstrating NCAM- and autopolysialylation. Yet, to detect autopolysialylation of the insect cell expressed ST8SiaIV in the absence of NCAM, the amount of enzyme used in the radioactive assay had to be increased ten fold. Thus the autopolysialylation activity appears to be enhanced in the presence of NCAM. A similar phenomenon is described for some point mutants of ST8SiaVI after expression in CHO-cells. These mutants, which were inactive at the cellular level, could be transferred into active enzymes under *in vitro* conditions, if tested in the presence of NCAM. All enzyme forms that were active *in vitro* showed both NCAM- and autopolysialylation (Windfuhr *et al.*, 2000).

The mechanism of autopolysialylation is not understood and it is not clear at the moment, whether the visible automodification in fact represents a monomolecular real auto-catalytic or a bimolecular process. Thus, no more than a model view of how the automodification can be influenced by NCAM can be discussed (Figure 33). In case of a monomolecular self-polysialylation reaction the enhancing effect of NCAM could be explained by a conformational change introduced into ST8SiaIV upon binding to NCAM that increases the transferase activity of the enzyme. Considering instead a bimolecular reaction mechanism for autopolysialylation, NCAM could have a stabilizing influence on the active homodimeric complex.

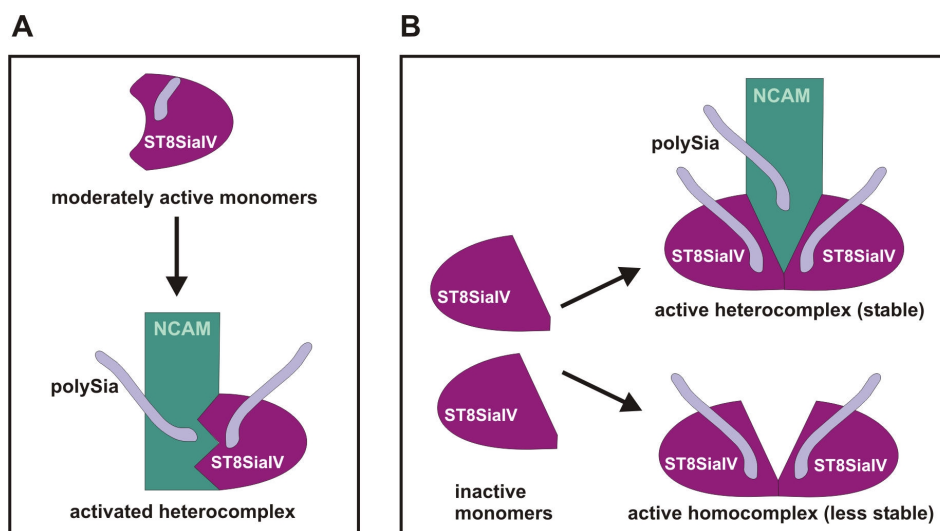


**Figure 33: Model view on the enhancing influence of NCAM on the autopolysialylation reaction.** (A) In case of a monomolecular autopolysialylation reaction: binding to NCAM (green) activates the moderately active ST8SiaIV monomers (purple). (B) In case of a bimolecular autopolysialylation reaction: binding to NCAM stabilizes the active homodimeric complex.

In the ELISA-based polysialyltransferase assay, autopolysialylation activity can be detected without NCAM even if very diluted samples are used as enzyme source (e.g. supernatant of infected cell cultures). This may result from a higher sensitivity of the detection system, but could also be due to the solid phase fixation of the enzyme. The fixation forces a close and prolonged interaction between the bound molecules and could thereby stabilize oligomeric ST8SiaIV complexes. This would argue for a bimolecular rather than a monomolecular self-modification reaction. However, additional data of kinetic studies are required to understand the enhancing effect of NCAM on the autopolysialylation activity of ST8SiaIV in more detail.

Of major importance for the understanding of the polysialyltransferase reaction mechanism are detailed structural information as provided by a crystal structure. The expression and purification procedure established in this study yielded up to 2 mg of purified ST8SiaIV $\Delta$ 25 per litre if *Sf9*-cell culture and therefore enabled the production of sufficient amounts of recombinant protein for crystallization trials. Crystallisation trials were performed with the homogeneously purified enzyme obtained after gel-filtration (see Figure 14) and with the near homogenous enzyme fraction obtained by His<sub>6</sub>-affinity chromatography (see Figure 10). However, for more than 1000 conditions tested in the course of this study no protein crystals of ST8SiaIV were obtained. Sparse matrix screenings were performed either with the enzyme alone or together with the competitive inhibitor CMP. For future screenings also CDP, Neu5Ac, CMP-Neu5Ac or derivatives of those compounds could be added as crystallization

ligands. The recently crystallized bacterial sialyltransferase from *Camphylobacter jejuni* was crystallized in the presence of CMP-3FNeu5Ac (Chiu *et al.*, 2004). The electronegative fluorine atom at position C3' prevents hydrolysis by inductively destabilizing the oxocarbenium ion-like transition state postulated for the reaction (Burkart *et al.*, 2000). Moreover further truncated or engineered forms of recombinant ST8SiaIV could be tested. Recent studies in CHO-cells revealed that the N-terminus could be truncated by 60 amino acids without effecting enzymatic activity. The residual part of the stem region present in ST8SiaIV $\Delta$ 25 may be disordered and thus hamper crystallization. Also the five N-glycans attached to ST8SiaIV might interfere with the crystallization of the protein. It is known from parallel studies carried out in our laboratory that the engineered protein with only one residual N-glycan at position Asn74 (Figure 7) is active (Mühlenhoff *et al.*, 2001). Initial trials to express the engineered enzyme in *Sf9* cells indicated, however, significantly reduced expression levels compared to the wild type (data not shown). Still current efforts in the laboratory concentrate at up-scaling the production of this mutant.

In summary, the effective two-step purification of polysialyltransferases from baculovirus-infected insect cells (*Sf9*) facilitates the isolation of large quantities of homogeneously purified and enzymatically active polysialyltransferases. This forthcoming source of enzyme should enable structural studies that will provide valuable information regarding the molecular basis for substrate specificity and activity of the polysialyltransferases and support the search for polysialyltransferase inhibitors that are promising compounds for the treatment of polySia expressing tumours.

## 6.2 Crystal structure of the polysialic acid degrading endosialidase cloned from bacteriophage K1F

Endosialidases (endo-N-acetylneuraminidases) are polysialic acid degrading tail spike proteins of bacteriophages infecting the human pathogen *E. coli* K1, which is encapsulated in a thick protective layer of polySia. To access the bacterial cell wall for infection K1 specific bacteriophages penetrate the polySia barrier using the depolymerising activity of their tailspikes (Figure 34). Endosialidases are the only known enzymes that bind and degrade polySia and are due to their high substrate specificity for polysialic acid essential and widely used tools in polySia research. The use of endosialidases enabled analysis of the biological functions of polySia in vertebrates without interfering with abundant mono- or disialylated structures. Recent studies in animal model systems demonstrated that endoneuraminidases interfere with the pathomechanism of polysialic acid encapsulated tumour cells (Daniel *et al.*, 2001). Thus the enzymes may also find use as diagnostic or therapeutic tool in the treatment of polySia bearing tumours. In contrast to exosialidases, where the catalytic mechanism is well described and several crystal structures are available (Varghese *et al.*, 1991; Tulip *et al.*, 1991; Burmeister *et al.*, 1991; Crennell *et al.*, 1993; Crennell *et al.*, 1994; Gaskell *et al.*, 1995) no structural data exist for endosialidases. The aim of this study was to analyse structure and function relationships in this group of polySia degrading enzymes.

Several endosialidases have been cloned in the laboratory (Gerardy-Schahn *et al.*, 1995; Mühlenhoff *et al.*, 2003) and comparative protein expression studies carried out for the different enzymes demonstrated best yields for the endosialidase derived from bacteriophage K1 F. Therefore further studies concentrated on this protein.

In the course of the protein expression studies the large tailspike protein (1064 amino acid residues) was found to undergo proteolytic cleavage into a large N-terminal (residues 1-911) and a small C-terminal fragment (residues 912-1064). The N-terminal fragment harbours the enzymatic activity and forms unusually stable SDS-resistant trimers. Although the C-terminal fragment is released and not part of the active complex, the presence of this domain in the nascent protein chain was shown to be essential. While uncleaved proteins with mutated cleavage sites remained active and able to form trimers, trimer formation and enzymatic activity was completely abolished in C-terminally truncated proteins (Mühlenhoff *et al.* 2003). Together these studies argue for an implication of the C-terminal domain in either folding or oligomerisation of the large N-terminal domain. Towards structural analysis the

expression of recombinant endoNF and the establishment of purification methods for both fragments were the first goals (Figure 18).

The full-length endoNF - epitope tagged with a His<sub>6</sub>-tag at the C-terminal end and a StrepII-tag at the N-terminal end - was expressed and proteolytically cleaved in *E. coli* BL21(DE3). For affinity purification of the C-terminal fragment the bacterial lysate was passed over a Ni<sup>2+</sup>-affinity column. Unexpectedly, also the N-terminal fragment bound quantitatively and eluted highly enriched at low imidazole concentrations (Figure 19). The fragment could be purified to homogeneity in a subsequent StrepII-affinity step (Figure 20) and was shown to be highly stable throughout the purification procedure by analysing the specific enzymatic activity of the obtained fractions (Figure 20). The pool containing the C-terminal fragment after Ni<sup>2+</sup>-affinity was contaminated with full-length uncleaved endoNF and the N-terminal fragment (Figure 19C). Bacterial lysates always contained a minor fraction of endoNF that is not proteolytically processed and copurifies due to its His<sub>6</sub>-tag. The unexpected coelution of the N-terminal fragment results most probably from complex formation with the uncleaved protein. The C-terminal fragment was purified to homogeneity by size exclusion chromatography. Though the small fragment could be separated from the larger endoNF species, the separation was less pronounced than the difference in molecular masses implied. This finding strongly suggests that also the C-terminal fragment forms stable oligomers. The observed retention volume of the eluted protein in the gel filtration suggests trimeric or tetrameric complexes of the C-terminal fragment.

The expression and purification procedure for endoNF was efficient, yielding 35 mg of homogeneously purified N-terminal and 2.5 mg of the C-terminal fragment from one liter of expression culture. Both recombinant proteins were used in crystallization trials, however, so far no protein crystals were obtained.

From crystallization studies carried out with the P22 tailspike protein was known, that the full-length protein did not produce crystals. In this case it was necessary to remove the N-terminal part known to function as head-binding domain attaching the tailspike to the phage baseplate. The flexibility of the linker region connecting head-binding and spike domain in the P22 tailspike protein seemed to hamper the crystallization process. Because primary sequence analyses revealed a similar head-binding domain in endoNF, N-terminal truncations of endoNF were generated to define the minimal catalytically active unit. As shown in chapter 5.2.1 up to 245 amino acids could be deleted from the N-terminus without severely affecting expression, enzymatic activity or trimer formation of the endosialidase. The truncated protein

(endoNF $\Delta$ 245) was purified as described for the wild-type and used in crystallization screenings. Well diffracting crystals were obtained after optimization of the initial crystallization conditions. The large unit cells dimension, in particular the length of the c-axis (346 Å), required careful optimization of the cryoconditions to obtain optimal diffraction patterns and separated spots. Yet high resolution data had to be limited to 1.9 Å to ensure sufficient spot separation.

The endosialidase monomers (see Figure 25) exhibit a modular domain architecture. Four domains can be clearly distinguished: (i) a six-bladed  $\beta$ -propeller, (ii) a nine-stranded  $\beta$ -barrel, (iii) the residual part of the head-binding domain and finally (iiii) an extended tail-like C-terminal domain. In agreement with the biochemical data (Mühlenhoff *et al.*, 2003) the monomers assemble into a stable trimer (two trimers were found in the asymmetric unit). The C-terminal tail-like domains build the remarkable elongated stalk of the trimer, whereas the N-terminal domains assemble to its compact head.

The six bladed  $\beta$ -propeller is a characteristic structural feature of exosialidases, found in enzymes of bacterial, viral or eukaryotic origin (Taylor, 1996). The sialidase  $\beta$ -propeller of endoNF shows higher structural similarity to bacterial (Crennell *et al.*, 1993; Crennell *et al.*, 1994; Gaskell *et al.*, 1995) and eukaryotic (Luo *et al.*, 1998; Buschiazzo *et al.*, 2000) than to viral sialidases (Varghese *et al.*, 1991; Tulip *et al.*, 1991; Burmeister *et al.*, 1991) and contains to Asp-box motifs. The biological function of the conserved 'Asp-box' motifs (SXDXGXTW) found in all non-viral exosialidases is unclear. As they are located on the propeller surface remote from the active site, contributions to the catalytic reaction are unlikely. Moreover Asp-boxes have been identified in at least eight distinct protein families in different structural contexts (Copley *et al.*, 2001). The evolution of short conserved peptide sequences, including also P-loop and helix-hairpin-helix motif, is not yet understood. Under discussion are either divergent or convergent evolution of the motifs or a possible function as ancient peptide ancestors for proteins with otherwise different folds (Copley *et al.*, 2001).

The nine-stranded  $\beta$ -barrel extending from the sialidase propeller is involved in polysialic acid binding. In endoNF crystals soaked with pentameric sialic acid, a dimer of  $\alpha$ 2,8-linked sialic acid was found bound to this domain. The presence of a sialic acid dimer rather than a pentamer seems to be a consequence of enzymatic cleavage in the crystal. Though endosialidases most effectively cleave sialic acid polymers longer than seven residues, for high enzyme to substrate ratios and prolonged incubation times cleavage of shorter fragments has been reported (Hallenbeck *et al.*, 1987; Pelkonen *et al.*, 1989).



The substrate complex revealed that endoNF is a catalytic trimer. Already the binding of the dimeric sugar involved two subunits of the trimer (Figure 27). Furthermore, the arrangement of binding ( $\beta$ -barrel) and cleaving ( $\beta$ -propeller) units within the monomer excludes a direct interaction of a bound ligand with both domains. Instead interactions with the respective domains belonging each to adjacent subunits of the trimer are very likely. Though also for viral exosialidases the formation of dimeric or tetrameric oligomers is described, oligomerisation is most likely not of functional relevance as substrate binding and hydrolysis occur within one subunit.

The functional trimer is stabilized by numerous intersubunit interactions. Already in the head region intersubunit hydrogen bonds and hydrophobic interactions are established and a total of 25 % of the solvent accessible surface is buried upon trimerisation. However, dominant influence on the remarkable stability of the endoNF homotrimer has the trimeric stalk region folding in a triple  $\beta$ -helix that is interrupted by a small triple  $\beta$ -prism domain (Figure 25A). Here a total of 62 % of the solvent accessible surface area is buried upon trimerisation and extensive networks of hydrogen bondings as well as stacking interactions of the hydrophobic interior of the stalk stabilize the trimer. The triple  $\beta$ -helix motif where the three intertwining subunits wind around the three-fold rotation axis of the trimer, has so far been described exclusively for proteins associated with the tail apparatus of bacteriophages. The tailspike of the salmonella phage P22 contains one tight  $\beta$ -helical turn (Steinbacher *et al.*, 1994) whereas the protease stable fragment of the short tail fiber of the T4-phage crystallized by Raaij revealed two full turns of a triple  $\beta$ -helix (van Raaij *et al.*, 2001). The longest  $\beta$ -helix motif is described for the tail lysozyme complex of the T4-phage with seven full turns. The extended needle like prism is supposed to act as cell puncturing device that penetrates the bacterial cell wall and functions as injection needle for the phage DNA. A similar function of the endoNF stalk domain is unlikely as the stalk is exclusively hydrophobic and in contrast to the T4-complex not hollow. Common to all three proteins is their ability to form unusually stable trimers. The trimer stability is most likely to a large extent mediated by the intertwined chains of the triple  $\beta$ -helix motifs as they enable extensive hydrogen bonding between the chains and the formation of a hydrophobic core common to all three chains. However, the intertwined topology and the many interchain interactions stabilizing the triple  $\beta$ -helix fold, raise the question how these homotrimers assemble from their monomeric subunits. For the P22 tailspike is known, that partly folded monomers associate into pro-trimer intermediates, which then undergo further conformational changes to form the SDS-resistant trimers. In contrast, the short T4-tail fiber, which has a more extended triple  $\beta$ -helix than P22, needs the

phage encoded chaperone gp57 for folding *in vivo* (King and Laemmli, 1973) and *in vitro* (Burda and Miller, 1999). Correct folding of endoNF requires the presence of the C-terminal domain in the nascent protein chain (Mühlenhoff *et al.*, 2003), that might have a similar function as the gp57 and act as intramolecular chaperone or oligomerisation domain. Homologous regions to the C-terminal domain of endoNF were identified also in several other bacteriophage tail fiber proteins (Mühlenhoff *et al.*, 2003), indicating that the concept of an intramolecular C-terminal chaperone or oligomerisation domain might be commonly used for the folding of phage tail fibers.

Besides the triple  $\beta$ -helix found in bacteriophage tail associated proteins, another motif of intertwined  $\beta$ -strands has been described for fibrous proteins of two human viruses. The fiber of adenovirus Ad2 (van Raaij *et al.*, 1999) and the attachment protein  $\sigma 1$  of reovirus T3D (Chappell *et al.*, 2002) both contain a triple  $\beta$ -spiral motif. Also this motif mediates the formation of stable trimers. For the reovirus attachment protein  $\sigma 1$  it is additionally known that the host chaperone hsp70 is essential for correct folding of its triple  $\beta$ -spiral domain (Leone *et al.*, 1996).

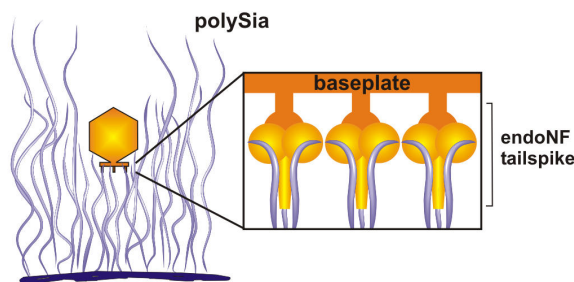
Moreover, the  $\sigma 1$  protein contains a sialic acid binding site in its fibrous tail as has been shown by mutagenesis studies (Chappell *et al.*, 1997). Structural data for the sialic acid binding part of  $\sigma 1$  are not available to date. Most interestingly also the endoNF stalk domain functions not only as stabilizing unit for the functional trimer but is directly involved in sialic acid binding. The substrate complex revealed a sialic acid monomer bound to the stalk region of endoNF. The shallow binding pocket is provided by the small triple  $\beta$ -prism domain interrupting the two triple  $\beta$ -helix domains of the stalk.

Recognition and processing of oligomeric substrates by enzymes frequently involves extended binding sites that can be considered as a series of subsites each binding to a single substrate moiety. Hence, the observed sialic acid binding sites in the  $\beta$ -barrel and the stalk region of endoNF can be regarded as high affinity subsites able to bind short dimeric or even monomeric sialic acid. Although the sialic acid bound to the stalk binding site is in  $\beta$ -chair conformation, the favored conformation of sialic acids in solution, the structure suggests that also  $\alpha$ -conformation would fit into the binding site, implying that a polysialic acid molecule could simultaneously interact with the stalk, the  $\beta$ -barrel, and the catalytic pocket of endoNF. Considering this aspect, polySia binding by endoNF involves a large portion of the protein and all three subunits of the homotrimer. Moreover, the polySia-endoNF interactions could be further stabilized by contacts to low affinity subsites not capable of binding short polySia

fragments. This multivalent binding would establish stable interactions between the phage and the host capsule, in particular because probably six of the trimeric endoNF tailspikes are attached to the bacteriophage baseplate.

The interactions between the endoNF tailspike and polySia are not only necessary for the depolymerization of the capsule, but apparently also crucial for the infection process of bacteriophage K1F: capsule-negative mutants of *E. coli* K1 are resistant against bacteriophage infection (Whitfield *et al.*, 1984; Pelkonen *et al.*, 1992). Starting from this observation it can be hypothesized that the short oligosialic acid remnants left after capsule depolymerisation are important for fixation of the phage particle to the host membrane. It is most likely that the stalk region of endoNF, being closest to the bacterial membrane, mediates this binding (Figure 34). The trimeric stalk domain seems to have developed as a most efficient device in the host recognition, attachment and infection process. Studies are planned to directly analyze the impact of the spike domain on the enzymatic activity and kinetic properties of endoNF.

#### A) Capsule depolymerization



#### B) Adhesion

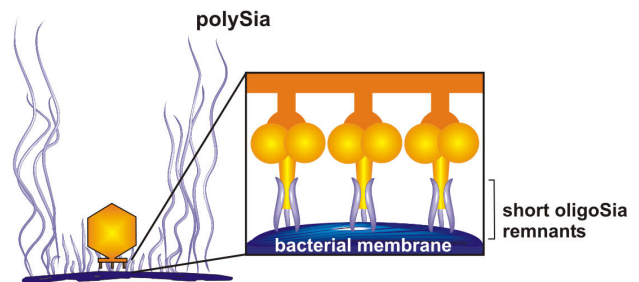


**Figure 34: Functions of the endoNF tailspike** (A) The bacteriophage (orange) penetrates the polySia capsule of *E. coli* K1 using the depolymerising activity of its endoNF tailspike. Each of the six tailspikes (three are depicted) can bind and degrade three polySia chains. (B) The short oligoSia remnants left after capsule depolymerisation are bound by the stalk region of the tailspike thereby ensuring tight fixation of the phage to the bacterial membrane.

All exosialidases crystallized so far, share conserved active site features Figure 26. In particular six amino acids are strictly conserved and have been implicated in the reaction mechanism proposed by Chong and colleagues. An arginine triad is binding to the carboxylate function of sialic acid. The interaction distorts the chair conformation of the pyranose ring that is preferred in solution into an  $\alpha$ -boat conformation. Due to this strained conformation, where the ring atoms C2, C3 and O6 are coplanar, the cleavage of the glycosidic linkage and

the formation of a planar oxocarbenium ion that has been identified by kinetic isotope effect experiments are favored (Chong *et al.*, 1992). Hydrolysis of the glycosidic linkage is proposed to be initiated by a conserved aspartic acid acting as proton donor. Two conserved residues at the bottom of the active site cleft, a glutamic acid and a tyrosine, are believed to stabilize the cationic transition state. Hydroxylation of the oxocarbenium ion is then mediated by a water molecule, which is activated by the conserved aspartic acid now acting as general base. However, for the *Trypanosoma cruzi* trans-sialidase and the exosialidase of *Micromonospora viridifaciens* an alternative mechanism involving a covalent sialyl-enzyme intermediate has been postulated (Watts *et al.*, 2003). According to that mechanism, the conserved Glu/Tyr couple at the bottom of the active site cleft acts as catalytic nucleophile. The tyrosine is relaying charge from the glutamic acid residue and by attacking the C2 atom breaks the glycosidic linkage to form the covalent intermediate. The sialyl-enzyme intermediate is then hydrolyzed by the nucleophilic attack of a water molecule activated by the conserved aspartic residue. All exosialidases analyzed so far are retaining glycosidases keeping the anomeric conformation in the primary hydrolysis product, which then undergoes mutarotation to the favored  $\beta$ -conformation. In case of the proposed  $S_N1$ -mechanism including the sialosylation intermediate, retention of the configuration is mediated by the tyrosine residue that shields the  $\beta$ -face of the sialosyl-moiety from water. Also the postulated double displacement mechanism involving two subsequent  $S_N2$ -reactions, the first with nucleophilic attack from the  $\beta$ -face and the second with attack from the  $\alpha$ -face retains conformation.

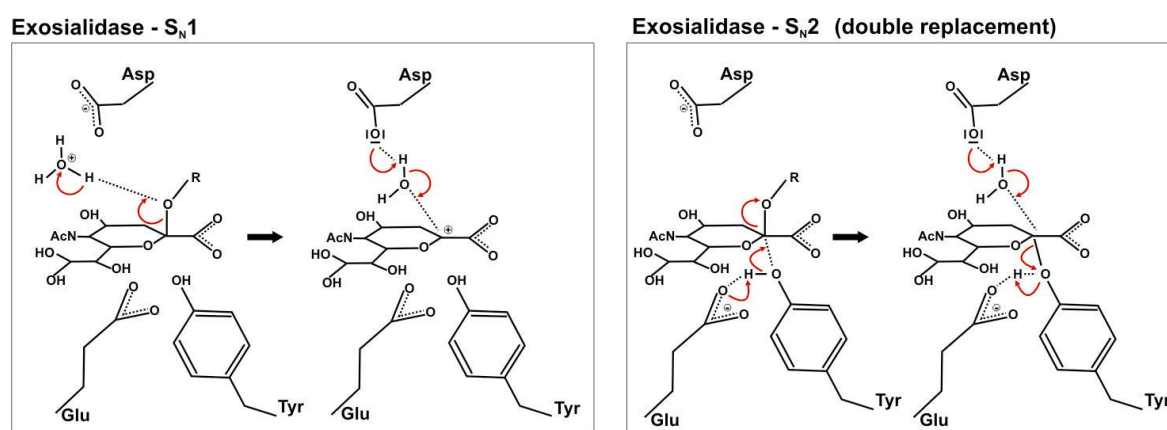


**Figure 35: Proposed reaction mechanism of exosialidases** (A) Generalized two-step  $S_N1$ -mechanism proposed for most exosialidases. The indicated conserved tyrosine and glutamic acid stabilize the sialosylation intermediate. The catalytic aspartic residue acts as general base. (B) Double replacement mechanism including a covalent sialyl-enzyme intermediate proposed for *T.cruzi* trans-sialidase and *M.viridifaciens* sialidase. The conserved tyrosine acts as nucleophile.

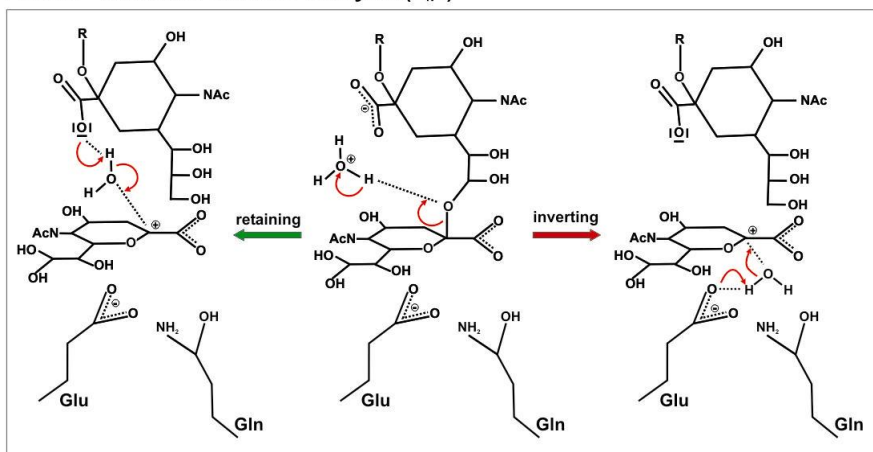
Remarkably only the conserved glutamic acid (Glu581) and two of the arginines (Arg596, Arg647) are preserved in endoNF. In contrast to exosialidases that cleave off terminal sialic acid residues (*exo*), endosialidases cleave within a polymeric sialic acid chain (*endo*). The topology of the active site clearly indicates, that a sharp kink needs to be introduced into the polySia chain to fit the polymer into the active cleft. This kink would be formed by a distorted  $\alpha$ -boat conformation of the residue bound to the active site that would additionally favor the planar sialosyl transition state. In contrast to exosialidases, stabilizing protein-carbohydrate interactions can be established to neighboring sugar residues on either side of the cleavage point. This might explain why the arginine triad, presumed to enforce the unfavorable planar transition state in exosialidases, is not fully conserved in endoNF. Mutation of either of the two remaining arginine residues resulted in a decrease though not a complete loss of enzymatic activity (5.2.6).

Most importantly the aspartic acid and the tyrosine, both critical residues in either of the two proposed exosialidase mechanisms, are not conserved in endoNF. Mutagenesis of the tyrosine residue resulted for the analyzed viral sialidases and trans-sialidases either in misfolded proteins or enzymes with dramatically decreased activity (Lentz *et al.*, 1987; Cremona *et al.*, 1995; Ghate and Air, 1998). For the *Clostridium perfringens small* sialidase, mutation of this tyrosine to phenylalanine resulted in inactive enzyme (Kleineidam *et al.*, 2001), while mutation to isoleucine retained the active protein. A recent study carried out with *Micromonospora viridifaciens* sialidase has demonstrated that mutants whose critical tyrosine residue is replaced by alanine, aspartic acid, or glycine exhibit residual activity (Watson *et al.*, 2003). However, these mutants were no longer retaining but became inverting sialidases. The authors discuss that the replacement of tyrosine with smaller amino acids results in additional free space at the  $\beta$ -face of the bound sialic acid that can be occupied by a water molecule acting as nucleophile in either an  $S_N2$  or  $S_N1$  reaction. In case of the  $S_N2$  reaction the conserved glutamic acid would function as general base and activate the hydrolyzing water. Considering an  $S_N1$  reaction the conserved aspartic acid would initialize the formation of the sialosylation that could then be trapped by a water molecule located at the  $\beta$ -face.

In the active site of endoNF the position of the missing tyrosine is occupied by a glutamine residue. The glutamine residue and the conserved glutamic acid do indeed hydrogen bond to an ordered water molecule (clearly visible in the final Fo-Fc-map) that could act as nucleophile. In a mutagenesis approach the conserved glutamic acid residue was changed to alanine. The resulting mutant exhibits decreased but clearly detectable enzymatic activity.

The catalytic aspartic residue acting as acid catalyst in a potential  $S_N1$  reaction is missing in endoNF. Considering the kicked acidic polySia substrate is it, however, possible that instead the carboxyl function of an adjacent sialic acid residue substitutes for the missing acidic amino acid. As it is not known to date if endosialidases are retaining or inverting glycosidases, the oxocarbenium intermediate could be hydroxylized by a water molecule from the  $\beta$ -face or the  $\alpha$ -face of sialic acid. This model of a substrate assisted catalysis of endosialidases would also explain the lack of detectable exosialidase activity and the strict polySia specificity observed for endosialidases.

EndoNF- substrate assisted catalysis ( $S_N1$ )



EndoNF- ( $S_N2$ )

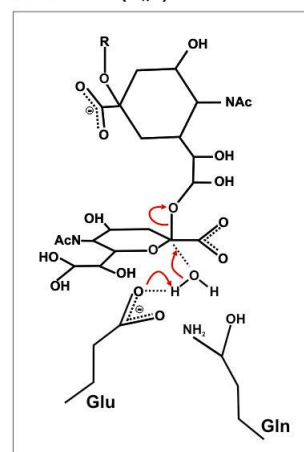


**Figure 38: Two possible catalytic mechanism for endoNF** (A) Substrate assisted catalysis model for endoNF ( $S_N1$ ) The carboxyl group of a sialic acid residue functions as acid-catalyst and initialises the hydrolysis of the glycosidic linkage. (B) Concerted ( $S_N2$ ) reaction with general base catalysis of the conserved glutamic acid.

Even though the detectable catalytic activity of the mutant Glu581Ala might argue against the role of this residue as general base and put forward the substrate assisted  $S_N1$  mechanism, none of the described potential mechanisms can be ruled out. For a more detailed view on the enzymatic mechanism of endoNF additional kinetic and NMR-based studies are necessary. Valuable information could also be gained by a crystal structure of endoNF with bound active-site ligand. Soaking and cocrystallization experiments with the exosialidase inhibitor DANA were not successful so far, but a variety of sialidase inhibitors are available that can be testes for inhibitory effect on endoNF and used as crystallization ligands.

The modular architecture of endoNF impressively reflects the evolution of this mutidomain enzyme by shuffling whole domains into a new protein context. Structural similarity and

---

presence of the conserved Asp-box motifs suggest a bacterial origin of the endoNF sialidase  $\beta$ -propeller. Its functional combination with a  $\beta$ -barrel domain and a triple intertwined spike domain, characteristic for bacteriophage tail-fibres, lead to an enzyme with unique and novel substrate specificity. As tailspikes are main determinants of the bacteriophage host range, the novel polySia degrading tailspike provided the basis for the evolution of a new group of bacteriophages, able to infect also protected polySia encapsulated *E. coli* K1 bacteria.

## 7 References

- Altmann,F., Staudacher,E., Wilson,I.B., and Marz,L. (1999). Insect cells as hosts for the expression of recombinant glycoproteins. *Glycoconj. J.*, **16**, 109-123.
- Altschul,S.F., Madden,T.L., Schaffer,A.A., Zhang,J., Zhang,Z., Miller,W., and Lipman,D.J. (1997). Gapped BLAST and PSI-BLAST: a new generation of protein database search programs. *Nucleic. Acids. Res.*, **25**, 3389-3402.
- Angata,K., Nakayama,J., Fredette,B., Chong,K., Ranscht,B., and Fukuda,M. (1997). Human STX polysialyltransferase forms the embryonic form of the neural cell adhesion molecule. Tissue-specific expression, neurite outgrowth, and chromosomal localization in comparison with another polysialyltransferase, PST. *J. Biol. Chem.*, **272**, 7182-7190.
- Angata,K., Suzuki,M., and Fukuda,M. (1998). Differential and cooperative polysialylation of the neural cell adhesion molecule by two polysialyltransferases, PST and STX. *J. Biol. Chem.*, **273**, 28524-28532.
- Angata,K., Suzuki,M., and Fukuda,M. (2002). ST8Sia II and ST8Sia IV Polysialyltransferases Exhibit Marked Differences in Utilizing Various Acceptors Containing Oligosialic Acid and Short Polysialic Acid. The Basis for cooperative Polysialylation by two Enzymes., *J. Biol. Chem.*, **277**, 36808-36817.
- Angata,K., Suzuki,M., McAuliffe,J., Ding,Y., Hindsgaul,O., and Fukuda,M. (2000). Differential biosynthesis of polysialic acid on neural cell adhesion molecule (NCAM) and oligosaccharide acceptors by three distinct alpha 2,8-sialyltransferases, ST8Sia IV (PST), ST8Sia II (STX), and ST8Sia III. *J. Biol. Chem.*, **275**, 18594-18601.
- Angata,K., Yen,T.Y., El Battari,A., Macher,B.A., and Fukuda,M. (2001). Unique disulfide bond structures found in ST8Sia IV polysialyltransferase are required for its activity. *J. Biol. Chem.*, **276**, 15369-15377.
- Bailey,S. (1994). The Ccp4 Suite - Programs for Protein Crystallography. *Acta Crystallogr. D*, **50**, 760-763.
- Barrow,P., Lovell,M., and Berchieri,A., Jr. (1998). Use of lytic bacteriophage for control of experimental Escherichia coli septicemia and meningitis in chickens and calves. *Clin. Diagn. Lab Immunol.*, **5**, 294-298.
- Barthels,D., Santoni,M.J., Wille,W., Ruppert,C., Chaix,J.C., Hirsch,M.R., Fontecilla-Camps,J.C., and Goridis,C. (1987). Isolation and nucleotide sequence of mouse NCAM cDNA that codes for a Mr 79,000 polypeptide without a membrane-spanning region. *EMBO J.*, **6**, 907-914.
- Becker,C.G., Artola,A., Gerardy-Schahn,R., Becker,T., Welzl,H., and Schachner,M. (1996). The polysialic acid modification of the neural cell adhesion molecule is involved in spatial learning and hippocampal long-term potentiation. *J. Neurosci. Res.*, **45**, 143-152.
- Beggs,H.E., Baragona,S.C., Hemperly,J.J., and Maness,P.F. (1997). NCAM140 interacts with the focal adhesion kinase p125(fak) and the SRC-related tyrosine kinase p59(fyn). *J. Biol. Chem.*, **272**, 8310-8319.



- Bonfanti,L., Olive,S., Poulain,D.A., and Theodosios,D.T. (1992). Mapping of the distribution of polysialylated neural cell adhesion molecule throughout the central nervous system of the adult rat: an immunohistochemical study. *Neuroscience*, **49**, 419-436.
- Brisson,J.R., Baumann,H., Imberty,A., Perez,S., and Jennings,H.J. (1992). Helical epitope of the group B meningococcal alpha(2-8)-linked sialic acid polysaccharide. *Biochemistry*, **31**, 4996-5004.
- Burda,M.R. and Miller,S. (1999). Folding of coliphage T4 short tail fiber in vitro. Analysing the role of a bacteriophage-encoded chaperone. *Eur. J. Biochem.*, **265**, 771-778.
- Burkart,M.D., Vincent,S.P., Duffels,A., Murray,B.W., Ley,S.V., and Wong,C.H. (2000). Chemo-enzymatic synthesis of fluorinated sugar nucleotide: useful mechanistic probes for glycosyltransferases. *Bioorg. Med. Chem.*, **8**, 1937-1946.
- Burmeister,W.P., Daniels,R.S., Dayan,S., Gagnon,J., Cusack,S., and Ruigrok,R.W. (1991). Sequence and crystallization of influenza virus B/Beijing/1/87 neuraminidase. *Virology*, **180**, 266-272.
- Burmeister,W.P., Ruigrok,R.W., and Cusack,S. (1992). The 2.2 Å resolution crystal structure of influenza B neuraminidase and its complex with sialic acid. *EMBO J.*, **11**, 49-56.
- Buschiazzo,A., Tavares,G.A., Campetella,O., Spinelli,S., Cremona,M.L., Paris,G., Amaya,M.F., Frasch,A.C., and Alzari,P.M. (2000). Structural basis of sialyltransferase activity in trypanosomal sialidases. *EMBO J.*, **19**, 16-24.
- Chappell,J.D., Gunn,V.L., Wetzel,J.D., Baer,G.S., and Dermody,T.S. (1997). Mutations in type 3 reovirus that determine binding to sialic acid are contained in the fibrous tail domain of viral attachment protein sigma 1. *J. Virol.*, **71**, 1834-1841.
- Chappell,J.D., Prota,A.E., Dermody,T.S., and Stehle,T. (2002). Crystal structure of reovirus attachment protein sigma 1 reveals evolutionary relationship to adenovirus fiber. *EMBO J.*, **21**, 1-11.
- Chen,B. and King,J. (1991). Thermal unfolding pathway for the thermostable P22 tailspike endorhamnosidase. *Biochemistry*, **30**, 6260-6269.
- Chiu,C.P., Watts,A.G., Lairson,L.L., Gilbert,M., Lim,D., Wakarchuk,W.W., Withers,S.G., and Strynadka,N.C. (2004). Structural analysis of the sialyltransferase CstII from *Campylobacter jejuni* in complex with a substrate analog. *Nat. Struct. Mol. Biol.*, **11**, 163-170.
- Chong,A.K.J., Pegg,M.S., Taylor,N.R., and Vonitzstein,M. (1992). Evidence for A Sialosyl Cation Transition-State Complex in the Reaction of Sialidase from Influenza-Virus. *Eur. J. Biochem.*, **207**, 335-343.
- Close,B.E. and Colley,K.J. (1998). In Vivo Autopolysialylation and Localization of the Polysialyltransferases PST and STX. *J. Biol. Chem.*, **273**, 34586-34593.
- Close,B.E., Mendiratta,S.S., Geiger,K.M., Broom,L.J., Ho,L.L., and Colley,K.J. (2003). The minimal structural domains required for neural cell adhesion molecule polysialylation by PST/ST8Sia IV and STX/ST8Sia II. *J. Biol. Chem.*, **278**, 30796-30805.

- Close,B.E., Tao,K., and Colley,K.J. (2000). Polysialyltransferase-1 autopolysialylation is not requisite for polysialylation of neural cell adhesion molecule. *J. Biol. Chem.*, **275**, 4484-4491.
- Close,B.E., Wilkinson,J.M., Bohrer,T.J., Goodwin,C.P., Broom,L.J., and Colley,K.J. (2001). The polysialyltransferase ST8Sia II/STX: posttranslational processing and role of autopolysialylation in the polysialylation of neural cell adhesion molecule. *Glycobiology*, **11**, 997-1008.
- Cole,G.J., Loewy,A., Cross,N.V., Akeson,R., and Glaser,L. (1986). Topographic localization of the heparin-binding domain of the neural cell adhesion molecule N-CAM. *J. Cell Biol.*, **103**, 1739-1744.
- Copley,R.R., Russell,R.B., and Ponting,C.P. (2001). Sialidase-like Asp-boxes: sequence-similar structures within different protein folds. *Protein Sci.*, **10**, 285-292.
- Cowtan,K.D. and Zhang,K.Y. (1999). Density modification for macromolecular phase improvement. *Prog. Biophys. Mol. Biol.*, **72**, 245-270.
- Cremer,H., Lange,R., Christoph,A., Plomann,M., Vopper,G., Roes,J., Brown,R., Baldwin,S., Kraemer,P., and Scheff,S. (1994). Inactivation of the N-CAM gene in mice results in size reduction of the olfactory bulb and deficits in spatial learning. *Nature*, **367**, 455-459.
- Cremona,M.L., Sanchez,D.O., Frasch,A.C., and Campetella,O. (1995). A single tyrosine differentiates active and inactive Trypanosoma cruzi trans-sialidases. *Gene*, **160**, 123-128.
- Crennell,S., Garman,E., Laver,G., Vimr,E., and Taylor,G. (1994). Crystal structure of Vibrio cholerae neuraminidase reveals dual lectin- like domains in addition to the catalytic domain. *Structure.*, **2**, 535-544.
- Crennell,S., Takimoto,T., Portner,A., and Taylor,G. (2000). Crystal structure of the multifunctional paramyxovirus hemagglutinin-neuraminidase. *Nat. Struct. Biol.*, **7**, 1068-1074.
- Crennell,S.J., Garman,E.F., Laver,W.G., Vimr,E.R., and Taylor,G.L. (1993). Crystal structure of a bacterial sialidase (from Salmonella typhimurium LT2) shows the same fold as an influenza virus neuraminidase. *Proc. Natl. Acad. Sci. U. S. A.*, **90**, 9852-9856.
- Cunningham,B.A., Hemperly,J.J., Murray,B.A., Prediger,E.A., Brackenbury,R., and Edelman,G.M. (1987). Neural cell adhesion molecule: structure, immunoglobulin-like domains, cell surface modulation, and alternative RNA splicing. *Science*, **236**, 799-806.
- Daniel,L., Durbec,P., Gautherot,E., Rouvier,E., Rougon,G., and Figarella-Branger,D. (2001). A nude mice model of human rhabdomyosarcoma lung metastases for evaluating the role of polysialic acids in the metastatic process. *Oncogene*, **20**, 997-1004.
- Datta,A.K. and Paulson,J.C. (1995). The sialyltransferase "sialylmotif" participates in binding the donor substrate CMP-NeuAc. *J. Biol. Chem.*, **270**, 1497-1500.
- Datta,A.K., Sinha,A., and Paulson,J.C. (1998). Mutation of the sialyltransferase S-sialylmotif alters the kinetics of the donor and acceptor substrates. *J. Biol. Chem.*, **273**, 9608-9614.
- DeLano,W.L. (2002). *Pymol User's manual*. DeLano Scientific, San Carlos.

- Doherty,P., Fruns,M., Seaton,P., Dickson,G., Barton,C.H., Sears,T.A., and Walsh,F.S. (1990). A threshold effect of the major isoforms of NCAM on neurite outgrowth. *Nature*, **343**, 464-466.
- Drickamer,K. (1993). A conserved disulphide bond in sialyltransferases. *Glycobiology*, **3**, 2-3.
- Eckhardt,M., Bukalo,O., Chazal,G., Wang,L., Goridis,C., Schachner,M., Gerardy-Schahn,R., Cremer,H., and Dityatev,A. (2000). Mice deficient in the polysialyltransferase ST8SiaIV/PST-1 allow discrimination of the roles of neural cell adhesion molecule protein and polysialic acid in neural development and synaptic plasticity. *J. Neurosci.*, **20**, 5234-5244.
- Eckhardt,M., Mühlenhoff,M., Bethe,A., and Gerardy-Schahn,R. (1996). Expression cloning of the Golgi CMP-sialic acid transporter. *Proc. Natl. Acad. Sci. U. S. A.*, **93**, 7572-7576.
- Eckhardt,M., Mühlenhoff,M., Bethe,A., Koopman,J., Frosch,M., and Gerardy-Schahn,R. (1995). Molecular characterization of eukaryotic polysialyltransferase-1. *Nature*, **373**, 715-718.
- Evans,S.V., Sigurskjold,B.W., Jennings,H.J., Brisson,J.R., To,R., Tse,W.C., Altman,E., Frosch,M., Weisgerber,C., and Kratzin,H.D. (1995). Evidence for the extended helical nature of polysaccharide epitopes. The 2.8 Å resolution structure and thermodynamics of ligand binding of an antigen binding fragment specific for alpha-(2-->8)-polysialic acid. *Biochemistry*, **34**, 6737-6744.
- Figarella-Branger,D.F., Durbec,P.L., and Rougon,G.N. (1990). Differential spectrum of expression of neural cell adhesion molecule isoforms and L1 adhesion molecules on human neuroectodermal tumors. *Cancer Res.*, **50**, 6364-6370.
- Finne,J., Finne,U., Deagostini-Bazin,H., and Goridis,C. (1983). Occurrence of alpha 2-8 linked polysialosyl units in a neural cell adhesion molecule. *Biochem. Biophys. Res. Commun.*, **112**, 482-487.
- Finne,J. and Makela,P.H. (1985). Cleavage of the polysialosyl units of brain glycoproteins by a bacteriophage endosialidase. Involvement of a long oligosaccharide segment in molecular interactions of polysialic acid. *J. Biol. Chem.*, **260**, 1265-1270.
- Franceschini,I., Angata,K., Ong,E., Hong,A., Doherty,P., and Fukuda,M. (2001). Polysialyltransferase ST8Sia II (STX) polysialylates all of the major isoforms of NCAM and facilitates neurite outgrowth. *Glycobiology*, **11**, 231-239.
- Frosch,M., Gorgen,I., Boulnois,G.J., Timmis,K.N., and Bitter-Suermann,D. (1985). NZB mouse system for production of monoclonal antibodies to weak bacterial antigens: isolation of an IgG antibody to the polysaccharide capsules of Escherichia coli K1 and group B meningococci. *Proc. Natl. Acad. Sci. U. S. A.*, **82**, 1194-1198.
- Gaskell,A., Crennell,S., and Taylor,G. (1995). The 3 Domains of A Bacterial Sialidase - A Beta-Propeller, An Immunoglobulin Module and A Galactose-Binding Jelly-Roll. *Structure*, **3**, 1197-1205.
- Gerardy-Schahn,R., Bethe,A., Brennecke,T., Mühlenhoff,M., Eckhardt,M., Ziesing,S., Lottspeich,F., and Frosch,M. (1995). Molecular cloning and functional expression of bacteriophage PK1E- encoded endoneuraminidase Endo NE. *Mol. Microbiol.*, **16**, 441-450.

- Geremia,R.A., Harduin-Lepers,A., and Delannoy,P. (1997). Identification of two novel conserved amino acid residues in eukaryotic sialyltransferases: implications for their mechanism of action. *Glycobiology.*, **7**, v-vii.
- Ghate,A.A. and Air,G.M. (1998). Site-directed mutagenesis of catalytic residues of influenza virus neuraminidase as an aid to drug design. *Eur. J. Biochem.*, **258**, 320-331.
- Glass,J.D., Shen,H., Fedorkova,L., Chen,L., Tomaszewicz,H., and Watanabe,M. (2000). Polysialylated neural cell adhesion molecule modulates photic signaling in the mouse suprachiasmatic nucleus. *Neurosci. Lett.*, **280**, 207-210.
- Glüer,S., Schelp,C., Madry,N., von Schweinitz,D., Eckhardt,M., and Gerardy-Schahn,R. (1998). Serum polysialylated neural cell adhesion molecule in childhood neuroblastoma. *Br. J. Cancer*, **78**, 106-110.
- Gross,R.J., Cheasty,T., and Rowe,B. (1977). Isolation of bacteriophages specific for the K1 polysaccharide antigen of Escherichia coli. *J. Clin. Microbiol.*, **6**, 548-550.
- Hallenbeck,P.C., Vimr,E.R., Yu,F., Bassler,B., and Troy,F.A. (1987). Purification and properties of a bacteriophage-induced endo-N- acetylneuraminidase specific for poly-alpha-2,8-sialosyl carbohydrate units. *J. Biol. Chem.*, **262**, 3553-3561.
- He,H.T., Finne,J., and Goridis,C. (1987). Biosynthesis, membrane association, and release of N-CAM-120, a phosphatidylinositol-linked form of the neural cell adhesion molecule. *J. Cell Biol.*, **105**, 2489-2500.
- Henderson,T.J., Venable,R.M., and Egan,W. (2003). Conformational flexibility of the group B meningococcal polysaccharide in solution. *J. Am. Chem. Soc.*, **125**, 2930-2939.
- Hildebrandt,H., Becker,C., Murau,M., Gerardy-Schahn,R., and Rahmann,H. (1998). Heterogeneous expression of the polysialyltransferases ST8Sia II and ST8Sia IV during postnatal rat brain development. *J. Neurochem.*, **71**, 2339-2348.
- Hirn,M., Ghandour,M.S., Deagostini-Bazin,H., and Goridis,C. (1983). Molecular heterogeneity and structural evolution during cerebellar ontogeny detected by monoclonal antibody of the mouse cell surface antigen BSP-2. *Brain Res.*, **265**, 87-100.
- Horstkorte,R., Schachner,M., Magyar,J.P., Vorherr,T., and Schmitz,B. (1993). The fourth immunoglobulin-like domain of NCAM contains a carbohydrate recognition domain for oligomannosidic glycans implicated in association with L1 and neurite outgrowth. *J. Cell Biol.*, **121**, 1409-1421.
- Inoue,S., Lin,S.L., and Inoue,Y. (2000). Chemical analysis of the developmental pattern of polysialylation in chicken brain. *J. Biol. Chem.*, **275**, 29968-29979.
- Jennings,H.J., Roy,R., and Michon,F. (1985). Determinant specificities of the groups B and C polysaccharides of Neisseria meningitidis. *J. Immunol.*, **134**, 2651-2657.
- Jones,T.A., Zou,J.Y., Cowan,S.W., and Kjeldgaard,M. (1991). Improved Methods for Building Protein Models in Electron-Density Maps and the Location of Errors in These Models. *Acta Cryst. Section A*, **47**, 110-119.

- Kadmon,G., Kowitz,A., Altevogt,P., and Schachner,M. (1990a). Functional cooperation between the neural adhesion molecules L1 and N- CAM is carbohydrate dependent. *J. Cell Biol.*, **110**, 209-218.
- Kadmon,G., Kowitz,A., Altevogt,P., and Schachner,M. (1990b). The neural cell adhesion molecule N-CAM enhances L1-dependent cell-cell interactions. *J. Cell Biol.*, **110**, 193-208.
- Kanamaru,S., Leiman,P.G., Kostyuchenko,V.A., Chipman,P.R., Mesyanzhinov,V.V., Arisaka,F., and Rossmann,M.G. (2002). Structure of the cell-puncturing device of bacteriophage T4. *Nature*, **415**, 553-557.
- Kibbelaar,R.E., Moolenaar,C.E., Michalides,R.J., Bitter-Suermann,D., Addis,B.J., and Mooi,W.J. (1989). Expression of the embryonal neural cell adhesion molecule N-CAM in lung carcinoma. Diagnostic usefulness of monoclonal antibody 735 for the distinction between small cell lung cancer and non-small cell lung cancer. *J. Pathol.*, **159**, 23-28.
- King,J. and Laemmli,U.K. (1973). Bacteriophage T4 tail assembly: structural proteins and their genetic identification. *J. Mol. Biol.*, **75**, 315-337.
- Kiss,J.Z. and Rougon,G. (1997). Cell biology of polysialic acid. *Curr. Opin. Neurobiol.*, **7**, 640-646.
- Kitazume-Kawaguchi,S., Kabata,S., and Arita,M. (2001). Differential biosynthesis of polysialic or disialic acid Structure by ST8Sia II and ST8Sia IV. *J. Biol. Chem.*, **276**, 15696-15703.
- Kleineidam,R.G., Kruse,S., Roggentin,P., and Schauer,R. (2001). Elucidation of the role of functional amino acid residues of the small sialidase from *Clostridium perfringens* by site-directed mutagenesis. *Biol. Chem.*, **382**, 313-319.
- Komminoth,P., Roth,J., Lackie,P.M., Bitter-Suermann,D., and Heitz,P.U. (1991). Polysialic acid of the neural cell adhesion molecule distinguishes small cell lung carcinoma from carcinoids. *Am. J. Pathol.*, **139**, 297-304.
- Kwiatkowski,B., Boschek,B., Thiele,H., and Stirm,S. (1982). Endo-N-acetylneuraminidase associated with bacteriophage particles. *J. Virol.*, **43**, 697-704.
- Kwiatkowski,B., Boschek,B., Thiele,H., and Stirm,S. (1983). Substrate specificity of two bacteriophage-associated endo-N- acetylneuraminidases. *J. Virol.*, **45**, 367-374.
- Laemmli,U.K. (1970). Cleavage of structural proteins during the assembly of the head of bacteriophage T4. *Nature*, **227**, 680-685.
- Leggate,D.R., Bryant,J.M., Redpath,M.B., Head,D., Taylor,P.W., and Luzio,J.P. (2002). Expression, mutagenesis and kinetic analysis of recombinant K1E endosialidase to define the site of proteolytic processing and requirements for catalysis. *Mol. Microbiol.*, **44**, 749-760.
- Lentz,M.R., Webster,R.G., and Air,G.M. (1987). Site-directed mutation of the active site of influenza neuraminidase and implications for the catalytic mechanism. *Biochemistry*, **26**, 5351-5358.

- Leone, G., Coffey, M.C., Gilmore, R., Duncan, R., Maybaum, L., and Lee, P.W. (1996). C-terminal trimerization, but not N-terminal trimerization, of the reovirus cell attachment protein is a posttranslational and Hsp70/ATP-dependent process. *J. Biol. Chem.*, **271**, 8466-8471.
- Liedtke, S., Geyer, H., Wuhler, M., Geyer, R., Frank, G., Gerardy-Schahn, R., Zahringer, U., and Schachner, M. (2001). Characterization of N-glycans from mouse brain neural cell adhesion molecule. *Glycobiology*, **11**, 373-384.
- Livingston, B.D., Jacobs, J.L., Glick, M.C., and Troy, F.A. (1988). Extended polysialic acid chains (n greater than 55) in glycoproteins from human neuroblastoma cells. *J. Biol. Chem.*, **263**, 9443-9448.
- Livingston, B.D. and Paulson, J.C. (1993). Polymerase chain reaction cloning of a developmentally regulated member of the sialyltransferase gene family. *J. Biol. Chem.*, **268**, 11504-11507.
- Long, G.S., Bryant, J.M., Taylor, P.W., and Luzio, J.P. (1995). Complete nucleotide sequence of the gene encoding bacteriophage E endosialidase: implications for K1E endosialidase structure and function. *Biochem. J.*, **309 ( Pt 2)**, 543-550.
- Luckow, V.A., Lee, S.C., Barry, G.F., and Olins, P.O. (1993). Efficient generation of infectious recombinant baculoviruses by site-specific transposon-mediated insertion of foreign genes into a baculovirus genome propagated in *Escherichia coli*. *J. Virol.*, **67**, 4566-4579.
- Luo, Y., Li, S.C., Chou, M.Y., Li, Y.T., and Luo, M. (1998). The crystal structure of an intramolecular trans-sialidase with a NeuAc alpha2-->3Gal specificity. *Structure.*, **6**, 521-530.
- Machida, Y., Miyake, K., Hattori, K., Yamamoto, S., Kawase, M., and Iijima, S. (2000). Structure and function of a novel coliphage-associated sialidase. *FEMS Microbiol. Lett.*, **182**, 333-337.
- Miragall, F., Kadmon, G., Faissner, A., Antonicek, H., and Schachner, M. (1990). Retention of J1/tenascin and the polysialylated form of the neural cell adhesion molecule (N-CAM) in the adult olfactory bulb. *J. Neurocytol.*, **19**, 899-914.
- Miyake, K., Muraki, T., Hattori, K., Machida, Y., Watanabe, M., Kawase, M., Yoshida, Y., and Iijima, S. (1997). Screening of bacteriophages producing endo-N-acetylneuraminidase. *J. Ferm. Bioeng.*, **84**, 90-93.
- Mühlenhoff, M., Eckhardt, M., Bethe, A., Frosch, M., and Gerardy-Schahn, R. (1996a). Autocatalytic polysialylation of polysialyltransferase-1. *EMBO J.*, **15**, 6943-6950.
- Mühlenhoff, M., Eckhardt, M., Bethe, A., Frosch, M., and Gerardy-Schahn, R. (1996b). Polysialylation of NCAM by a single enzyme. *Curr. Biol.*, **6**, 1188-1191.
- Mühlenhoff, M., Eckhardt, M., and Gerardy-Schahn, R. (1998). Polysialic acid: three-dimensional structure, biosynthesis and function. *Curr. Opin. Struct. Biol.*, **8**, 558-564.
- Mühlenhoff, M., Manegold, A., Windfuhr, M., Gotza, B., and Gerardy-Schahn, R. (2001). The impact of N-glycosylation on the functions of polysialyltransferases. *J. Biol. Chem.*, **276**, 34066-34073.

- Mühlenhoff,M., Stummeyer,K., Grove,M., Sauerborn,M., and Gerardy-Schahn,R. (2003). Proteolytic processing and oligomerization of bacteriophage-derived endosialidases. *J. Biol. Chem.*, **278**, 12634-12644.
- Muller,D., Wang,C., Skibo,G., Toni,N., Cremer,H., Calaora,V., Rougon,G., and Kiss,J.Z. (1996). PSA-NCAM is required for activity-induced synaptic plasticity. *Neuron*, **17**, 413-422.
- Nakayama,J., Fukuda,M.N., Fredette,B., Ranscht,B., and Fukuda,M. (1995). Expression cloning of a human polysialyltransferase that forms the polysialylated neural cell adhesion molecule present in embryonic brain. *Proc. Natl. Acad. Sci. U. S. A.*, **92**, 7031-7035.
- Nelson,R.W., Bates,P.A., and Rutishauser,U. (1995). Protein determinants for specific polysialylation of the neural cell adhesion molecule. *J. Biol. Chem.*, **270**, 17171-17179.
- Ong,E., Nakayama,J., Angata,K., Reyes,L., Katsuyama,T., Arai,Y., and Fukuda,M. (1998). Developmental regulation of polysialic acid synthesis in mouse directed by two polysialyltransferases, PST and STX. *Glycobiology*, **8**, 415-424.
- Ono,K., Tomasiwicz,H., Magnuson,T., and Rutishauser,U. (1994). N-CAM mutation inhibits tangential neuronal migration and is phenocopied by enzymatic removal of polysialic acid. *Neuron*, **13**, 595-609.
- Pajunen,M., Kiljunen,S., and Skurnik,M. (2000). Bacteriophage phiYeO3-12, specific for *Yersinia enterocolitica* serotype O:3, is related to coliphages T3 and T7. *J. Bacteriol.*, **182**, 5114-5120.
- Paratcha,G., Ledda,F., and Ibanez,C.F. (2003). The neural cell adhesion molecule NCAM is an alternative signaling receptor for GDNF family ligands. *Cell*, **113**, 867-879.
- Pelkonen,S., Aalto,J., and Finne,J. (1992). Differential activities of bacteriophage depolymerase on bacterial polysaccharide: binding is essential but degradation is inhibitory in phage infection of K1-defective *Escherichia coli*. *J. Bacteriol.*, **174**, 7757-7761.
- Pelkonen,S., Pelkonen,J., and Finne,J. (1989). Common cleavage pattern of polysialic acid by bacteriophage endosialidases of different properties and origins. *J. Virol.*, **63**, 4409-4416.
- Petter,J.G. and Vimr,E.R. (1993). Complete nucleotide sequence of the bacteriophage K1F tail gene encoding endo-N-acylneuraminidase (endo-N) and comparison to an endo-N homolog in bacteriophage PK1E. *J. Bacteriol.*, **175**, 4354-4363.
- Pollerberg,G.E., Burridge,K., Krebs,K.E., Goodman,S.R., and Schachner,M. (1987). The 180-kD component of the neural cell adhesion molecule N-CAM is involved in a cell-cell contacts and cytoskeleton-membrane interactions. *Cell Tissue Res.*, **250**, 227-236.
- Pollerberg,G.E., Schachner,M., and Davoust,J. (1986). Differentiation state-dependent surface mobilities of two forms of the neural cell adhesion molecule. *Nature*, **324**, 462-465.
- Powell,H.R. (1999). The Rossmann Fourier autoindexing algorithm in MOSFLM. *Acta Crystallogr. D*, **55 ( Pt 10)**, 1690-1695.
- Rao,Y., Wu,X.F., Garipey,J., Rutishauser,U., and Siu,C.H. (1992). Identification of a peptide sequence involved in homophilic binding in the neural cell adhesion molecule NCAM. *J. Cell Biol.*, **118**, 937-949.

- Rohr, T.E. and Troy, F.A. (1980). Structure and biosynthesis of surface polymers containing polysialic acid in *Escherichia coli*. *J. Biol. Chem.*, **255**, 2332-2342.
- Roth, J., Zuber, C., Wagner, P., Blaha, I., Bitter-Suermann, D., and Heitz, P.U. (1988). Presence of the long chain form of polysialic acid of the neural cell adhesion molecule in Wilms' tumor. Identification of a cell adhesion molecule as an oncodevelopmental antigen and implications for tumor histogenesis. *Am. J. Pathol.*, **133**, 227-240.
- Rutishauser, U. (1996). Polysialic acid and the regulation of cell interactions. *Curr. Opin. Cell Biol.*, **8**, 679-684.
- Rutishauser, U. and Landmesser, L. (1996). Polysialic acid in the vertebrate nervous system: a promoter of plasticity in cell-cell interactions. *Trends. Neurosci.*, **19**, 422-427.
- Saffell, J.L., Williams, E.J., Mason, I.J., Walsh, F.S., and Doherty, P. (1997). Expression of a dominant negative FGF receptor inhibits axonal growth and FGF receptor phosphorylation stimulated by CAMs. *Neuron*, **18**, 231-242.
- Santoni, M.J., Barthels, D., Barbas, J.A., Hirsch, M.R., Steinmetz, M., Goridis, C., and Wille, W. (1987). Analysis of cDNA clones that code for the transmembrane forms of the mouse neural cell adhesion molecule (NCAM) and are generated by alternative RNA splicing. *Nucleic Acids Res.*, **15**, 8621-8641.
- Santoni, M.J., Barthels, D., Vopper, G., Boned, A., Goridis, C., and Wille, W. (1989). Differential exon usage involving an unusual splicing mechanism generates at least eight types of NCAM cDNA in mouse brain. *EMBO J.*, **8**, 385-392.
- Scheidegger, E.P., Lackie, P.M., Papay, J., and Roth, J. (1994). In vitro and in vivo growth of clonal sublines of human small cell lung carcinoma is modulated by polysialic acid of the neural cell adhesion molecule. *Lab. Invest.*, **70**, 95-106.
- Scheidegger, E.P., Sternberg, L.R., Roth, J., and Lowe, J.B. (1995). A human STX cDNA confers polysialic acid expression in mammalian cells. *J. Biol. Chem.*, **270**, 22685-22688.
- Scholl, D., Rogers, S., Adhya, S., and Merrill, C.R. (2001). Bacteriophage K1-5 encodes two different tail fiber proteins, allowing it to infect and replicate on both K1 and K5 strains of *Escherichia coli*. *J. Virol.*, **75**, 2509-2515.
- Seki, T. and Arai, Y. (1991). The persistent expression of a highly polysialylated NCAM in the dentate gyrus of the adult rat. *Neurosci. Res.*, **12**, 503-513.
- Sheldrick, G.M. (2001). *in Crystallography of Biological Macromolecules International Tables for Crystallography Vol. F*. Kluwer Academic, Dordrecht.
- Shen, H., Watanabe, M., Tomasiewicz, H., Rutishauser, U., Magnuson, T., and Glass, J.D. (1997). Role of neural cell adhesion molecule and polysialic acid in mouse circadian clock function. *J. Neurosci.*, **17**, 5221-5229.
- Skoza, L. and Mohos, S. (1976). Stable thiobarbituric acid chromophore with dimethyl sulphoxide. Application to sialic acid assay in analytical de-O-acetylation. *Biochem. J.*, **159**, 457-462.



- Smith,H.W. and Huggins,M.B. (1982). Successful treatment of experimental Escherichia coli infections in mice using phage: its general superiority over antibiotics. *J. Gen. Microbiol.*, **128**, 307-318.
- Soler,A.P., Johnson,K.R., Wheelock,M.J., and Knudsen,K.A. (1993). Rhabdomyosarcoma-derived cell lines exhibit aberrant expression of the cell-cell adhesion molecules N-CAM, N-cadherin, and cadherin-associated proteins. *Exp. Cell Res.*, **208**, 84-93.
- Steinbacher,S., Seckler,R., Miller,S., Steipe,B., Huber,R., and Reinemer,P. (1994). Crystal-Structure of P22 Tailspike Protein - Interdigitated Subunits in A Thermostable Trimer. *Science*, **265**, 383-386.
- Steven,A.C., Trus,B.L., Maizel,J.V., Unser,M., Parry,D.A., Wall,J.S., Hainfeld,J.F., and Studier,F.W. (1988). Molecular substructure of a viral receptor-recognition protein. The gp17 tail-fiber of bacteriophage T7. *J. Mol. Biol.*, **200**, 351-365.
- Stummeyer,K. (2000). Struktur-Funktionsanalyse der eukaryontischen Polysialyltransferasen ST8SiaII und ST8SiaIV. Diploma thesis, Med. Mikrobiologie, Medizinische Hochschule Hannover
- Sunshine,J., Balak,K., Rutishauser,U., and Jacobson,M. (1987). Changes in neural cell adhesion molecule (NCAM) structure during vertebrate neural development. *Proc. Natl. Acad. Sci. U. S. A.*, **84**, 5986-5990.
- Tanaka,F., Otake,Y., Nakagawa,T., Kawano,Y., Miyahara,R., Li,M., Yanagihara,K., Nakayama,J., Fujimoto,I., Ikenaka,K., and Wada,H. (2000). Expression of polysialic acid and STX, a human polysialyltransferase, is correlated with tumor progression in non-small cell lung cancer. *Cancer Res.*, **60**, 3072-3080.
- Taylor,G. (1996). Sialidases: Structures, biological significance and therapeutic potential. *Curr. Opin. Struct. Biol.*, **6**, 830-837.
- Theodosios,D.T., Rougon,G., and Poulain,D.A. (1991). Retention of embryonic features by an adult neuronal system capable of plasticity: polysialylated neural cell adhesion molecule in the hypothalamo-neurohypophysial system. *Proc. Natl. Acad. Sci. U. S. A.*, **88**, 5494-5498.
- Tomlinson,S. and Taylor,P.W. (1985). Neuraminidase associated with coliphage E that specifically depolymerizes the Escherichia coli K1 capsular polysaccharide. *J. Virol.*, **55**, 374-378.
- Troy,F.A. (1992). Polysialylation: from bacteria to brains. *Glycobiology*, **2**, 5-23.
- Tulip,W.R., Varghese,J.N., Baker,A.T., vanDonkelaar,A., Laver,W.G., Webster,R.G., and Colman,P.M. (1991). Refined Atomic Structures of N9 Subtype Influenza-Virus Neuraminidase and Escape Mutants. *J. Mol. Biol.*, **221**, 487-497.
- van Raaij,M.J., Mitraki,A., Lavigne,G., and Cusack,S. (1999). A triple beta-spiral in the adenovirus fibre shaft reveals a new structural motif for a fibrous protein. *Nature*, **401**, 935-938.
- van Raaij,M.J., Schoehn,G., Burda,M.R., and Miller,S. (2001). Crystal structure of a heat and protease-stable part of the bacteriophage T4 short tail fibre. *J. Mol. Biol.*, **314**, 1137-1146.

- Varghese, J.N. and Colman, P.M. (1991). 3-Dimensional Structure of the Neuraminidase of Influenza Virus-A/Tokyo/3/67 at 2.2-Å Resolution. *J. Mol. Biol.*, **221**, 473-486.
- Vimr, E.R., McCoy, R.D., Vollger, H.F., Wilkison, N.C., and Troy, F.A. (1984). Use of prokaryotic-derived probes to identify poly(sialic acid) in neonatal neuronal membranes. *Proc. Natl. Acad. Sci. U. S. A.*, **81**, 1971-1975.
- Von der Ohe, M., Wheeler, S.F., Wuhler, M., Harvey, D.J., Liedtke, S., Mühlenhoff, M., Gerardy-Schahn, R., Geyer, H., Dwek, R.A., Geyer, R., Wing, D.R., and Schachner, M. (2002). Localization and characterization of polysialic acid-containing N-linked glycans from bovine NCAM. *Glycobiology*, **12**, 47-63.
- Vutskits, L., Djebbara-Hannas, Z., Zhang, H., Paccaud, J.P., Durbec, P., Rougon, G., Muller, D., and Kiss, J.Z. (2001). PSA-NCAM modulates BDNF-dependent survival and differentiation of cortical neurons. *Eur. J. Neurosci.*, **13**, 1391-1402.
- Walsh, F.S., Putt, W., Dickson, J.G., Quinn, C.A., Cox, R.D., Webb, M., Spurr, N., and Goodfellow, P.N. (1986). Human N-CAM gene: mapping to chromosome 11 by analysis of somatic cell hybrids with mouse and human cDNA probes. *Brain Res.*, **387**, 197-200.
- Watson, J.N., Dookhun, V., Borgford, T.J., and Bennet, A.J. (2003). Mutagenesis of the conserved active-site tyrosine changes a retaining sialidase into an inverting sialidase. *Biochemistry*, **42**, 12682-12690.
- Watts, A.G., Damager, I., Amaya, M.L., Buschiazzi, A., Alzari, P., Frasch, A.C., and Withers, S.G. (2003). Trypanosoma cruzi trans-sialidase operates through a covalent sialyl-enzyme intermediate: tyrosine is the catalytic nucleophile. *J. Am. Chem. Soc.*, **125**, 7532-7533.
- Whitfield, C., Vimr, E.R., Costerton, J.W., and Troy, F.A. (1984). Protein synthesis is required for in vivo activation of polysialic acid capsule synthesis in Escherichia coli K1. *J. Bacteriol.*, **159**, 321-328.
- Williams, E.J., Furness, J., Walsh, F.S., and Doherty, P. (1994). Activation of the FGF receptor underlies neurite outgrowth stimulated by L1, N-CAM, and N-cadherin. *Neuron*, **13**, 583-594.
- Windfuhr, M., Manegold, A., Mühlenhoff, M., Eckhardt, M., and Gerardy-Schahn, R. (2000). Molecular defects that cause loss of polysialic acid in the complementation group 2A10. *J. Biol. Chem.*, **275**, 32861-32870.
- Yabe, U., Sato, C., Matsuda, T., and Kitajima, K. (2003). Polysialic acid in human milk. CD36 is a new member of mammalian polysialic acid-containing glycoprotein. *J. Biol. Chem.*, **278**, 13875-13880.
- Yang, P., Yin, X., and Rutishauser, U. (1992). Intercellular space is affected by the polysialic acid content of NCAM. *J. Cell Biol.*, **116**, 1487-1496.
- Yoshida, Y., Kojima, N., and Tsuji, S. (1995). Molecular cloning and characterization of a third type of N-glycan alpha 2,8-sialyltransferase from mouse lung. *J. Biochem. (Tokyo)*, **118**, 658-664.

---

Zhang,H., Miller,R.H., and Rutishauser,U. (1992). Polysialic acid is required for optimal growth of axons on a neuronal substrate. *J. Neurosci.*, **12**, 3107-3114.

Zuber,C., Lackie,P.M., Catterall,W.A., and Roth,J. (1992). Polysialic acid is associated with sodium channels and the neural cell adhesion molecule N-CAM in adult rat brain. *J. Biol. Chem.*, **267**, 9965-9971.

## 8 Abbreviations

ABTS	2,2'-Azino-di-(3-ethylenbethiazolin-sulphate)
AP	Alkaline phosphatase
APS	Ammonium peroxidisulphate
ATP	Adenosine triphosphate
BCA	Bichionic acid
BCIP	5-Brom-4-chlor-3-indolyl-phosphate
bp	Base pairs
BSA	Bovine serum albumin
CMP	Cytidine 5'-monophosphat
Da	Dalton
DMEM	'Dulbecco's Modified Eagle's medium'
DMF	Dimethylformamide
DMSO	Dimethylsulfoxide
DNA	Desoxyribonucleic acid
DTT	Dithiothreito
EDTA	Ethylendiamine-N,N,N',N'-tetraacetic acid
ELISA	Enzyme linked immono sorbant assay
endoNE	Endoneuraminidase NE
IPTG	Isopropyl-beta-D-thiogalactopyranoside
kb	kilobase
kDa	Kilodalton
Kdn	2-Keto-3-doexy-D-glycero-D-galacto-nonususonic acid
LB	Luria-Bertani
mAb	Monoclonal antibody
MAD	Multiwavelength anomalous dispersion
MES	2-(N-Morpholino)ethanesulphonic acid
NBT	Nitrotetrazolium-blue chloride
NCAM	Neural cell adhesion molelcule
Neu5Ac	5-N-acetyl-neuraminic acid
OD	Optical density
PAGE	Polyacrylamide gelectrophoresis
PBS	Phosphate buffered saline
PCR	Polymerase chain reaction
PEG	Polyethyleneglycol
PMSF	Phenylmethansulfonylflouride
polySia	Polysialic acid
POX	Peroxidase
rmsd	Root mean square deviation
RT	Room temperature
SDS	Sodium dodecyl-sulphate
TCA	Trichloroacetic acid
TEMED	N,N,N',N'-Tetramethyl-ethylendiamin
TRIS	Tris(hydroxymethyl)-aminomethan)

## 9 Curriculum vitae and publications

### Personal Data

---

Home address	Katharina Stummeyer Hülshagen 108 31714 Lauenhagen
email	Stummeyer.Katharina@mh-hannover.de
Date of birth/place	20.12.1975 in Stadthagen
Nationality	German

### Education

---

1982 - 1995	Gerda-Philippsohn-Schule (Grundschule) in Sachsenhagen
1996 - 1988	Magister-Nothold-Schule (Orientierungsstufe) in Lindhorst
1988 – 1995	Wilhem-Busch-Gymnasiums in Stadthagen
Juni 1995	Abitur

### Scientific education

---

1995-2000	Studies in biochemistry at the university and ‚Medizinischen Hochschule‘ in Hanover
2000	Diploma thesis at ‚Institut für Medizinische Mikrobiologie‘ of the ‚Medizinischen Hochschule Hannover‘ Titel: ‚Studien zu Struktur und Funktion der eukaryotischen Polysialyltransferasen ST8SiaIV (PST) und ST8SiaII (STX)‘
2000-2004	Doctorial thesis at the ‚Abteilung für Zelluläre Chemie‘ of the ‚Medizinischen Hochschule Hannover‘ Titel: ‚Enzymes involved in biosynthesis and degradation of poly- $\alpha$ 2,8-sialic acid: structure-function-relationships‘

---

## Publications

---

Mühlenhoff,M., **Stummeyer,K.**, Grove,M., Sauerborn,M., and Gerardy-Schahn,R. (2003). Proteolytic Processing and Oligomerization of Bacteriophage-derived Endosialidases. *J. Biol. Chem.* 278, 12634-12644.

Strandberg,Y.C., **Stummeyer,K.**, Mühlenhoff,M., Gerardy-Schahn,R., and Halliday,J.A. (2004). Expression and purification of catalytically active mammalian polysialyltransferases ST8SiaII and ST8SiaIV in baculovirus-infected insect cells (*Sf9*), submitted for publication.

**Stummeyer,K.**, Dickmanns,A., Mühlenhoff,M., Gerardy-Schahn,R. and Ficner,R. (2004). Crystal structure of the polysialic acid specific EndoNF, submitted for publication.

---

## Abstract and Posterpresentations

---

Speidel,D., Böck,N., Meyer,G., **Stummeyer,K.**, Zühlke,H. (1998). Expression of neuronal Nos and PIN (protein inhibitor of neuronal NOS) in rat insulinoma cell lines. *Herbsttagung der GBM*, Jena, Deutschland

**Stummeyer,K.**, Gerardy-Schahn,R., Mühlenhoff, M. (2001). Expression of recombinant polysialyltransferase ST8SiaIV using a baculovirus expression system. *'International Symposium on Protein traffic, Glycosylation, and Human Health'*, Interlaken, Schweiz

**Stummeyer,K.**, Gerardy-Schahn,R., Mühlenhoff, M. (2001). Expression of recombinant polysialyltransferase ST8SiaIV in insect cells using a baculovirus expression system. *'GLYCO XVI'*, Den Haag, Niederlande

**Stummeyer,K.**, Mackensen,A.C., Gerardy-Schahn,R., Mühlenhoff ,M. (2002). Purification of catalytically active polysialyltransferase ST8SiaIV from baculovirus-infected insect cells. *13<sup>th</sup> Joint Meeting of the 'Nederlandse Vereniging voor Glycobiologie', the 'Studiengruppe Glykokonjugate der GB' and the 'Groupe Lilloise de Glycobiologie'*, Münster, Deutschland

**Mühlenhoff,M.**, Stummeyer,K., Grove,M., Sauerborn,M., Gerardy-Schahn,R. (2002). Proteolytic cleavage and complex formation of endosialidases. *13<sup>th</sup> Joint Meeting of the 'Nederlandse Vereniging voor Glycobiologie', the 'Studiengruppe Glykokonjugate der GB' and the 'Groupe Lilloise de Glycobiologie'*, Münster, Deutschland

**Stummeyer,K.**, Mackensen,A.C., Gerardy-Schahn,R., Mühlenhoff ,M. (2002). Expression and purification of recombinant polysialyltransferase ST8SiaIV using a baculovirus expression system. *'GlycoT – 3<sup>rd</sup> International Symposium on Glycosyltransferases'*, Stockholm, Schweden

**Mühlenhoff,M.**, Stummeyer,K., Grove,M., Schwarzer,D., Gerardy-Schahn,R. (2003). Homo- and Heteromeric complex formation of endosialidases. *14<sup>th</sup> Joint Meeting of the 'Nederlandse Vereniging voor Glycobiologie', the 'Studiengruppe Glykokonjugate der GB' and the 'Groupe Lilloise de Glycobiologie'*, Lille, Frankreich

**Stummeyer,K.**, Dickmanns,A., Mühlenhoff,M., Gerardy-Schahn,R., Ficner,R. (2004). Crystal structure of EndosialidaseNF – a Polysialic Acid degrading enzyme. *Jahrestagung der DGK und DGKK*, Jena, Deutschland.

**Stummeyer,K.**, Dickmanns,A., Mühlenhoff,M., Gerardy-Schahn,R., Ficner,R. (2004). Crystal structure of endoneuraminidase EndoNF. Publiziert in *EMBL HASYLAB – Annual Report 2003*

## Acknowledgements

I would like to thank all of those who have contributed to this work.

In particular I would like to thank Professor Rita Gerardy-Schahn for giving me the opportunity to work on this project and for her continuous support and interest in my work and me.

I am also grateful to Professor Walter Müller and Professor Ralf Ficner for cosupervising this thesis.

Many thanks to Dr. Martina Mühlenhoff for her friendship, for very helpful discussions, for numerous valuable hints and tips and for cloning the Endoneuraminidase NF.

A big thank goes also to Dr. Achim Dickmanns and again to Professor Ralf Ficner for a great collaboration and for introducing me into the secrets of protein crystallography as well as to Antje Dickmanns for her great hospitality.

Thanks also to the complete RGS-team Angel Ashikov, Andrea Bethe, Hans Backer, Jutta Fuhlrott, Melanie Grove, Roland Kabuss, Barbara Kleczka, Anne Mackensen, Martina Mühlenhoff, Anja Münster, Astrid Oberbeck, Imke Oltmann, Melanie Oschlies, Uli Peters, Françoise Routier, David Schwarzer and Birgit Weinhold for a great time and many tasty cakes.

In addition I would like to thank Dr. Detlev Suckau from Bruker Daltonik for doing the ESI-TOF analysis.

Finally I would like to thank my family for their love and support and in particular my husband Thomas for sharing all the little pleasures and disappointments of every days life with me and for stubbornly insisting that there is also life outside the Lab.

## **Erklärung**

Hiermit versichere ich an Eides statt, dass ich die vorliegende Dissertation selbständig und nur unter Verwendung der angegebenen Quellen und Hilfsmittel angefertigt habe. Außerdem versichere ich an Eides statt, dass die zugrunde liegenden Ergebnisse nicht für eine andere Prüfungsarbeit verwendet worden sind.

Hannover, 28.04.04